



---

**Forschungszentrum Karlsruhe**  
in der Helmholtz-Gemeinschaft

---

**Wissenschaftliche Berichte**  
FZKA 7373

# **Behaviour of Oxide Layer of Zirconium-Based Fuel Rod Cladding under Steam Starvation Conditions**

**J. Stuckert, M. S. Veshchunov**

**Institut für Materialforschung  
Programm Nukleare Sicherheitsforschung**

**April 2008**



**Forschungszentrum Karlsruhe**

In der Helmholtz-Gemeinschaft

Wissenschaftliche Berichte

FZKA 7373

Behaviour of oxide layer of zirconium-based fuel  
rod cladding under steam starvation conditions

J. Stuckert, M. S. Veshchunov\*

Institut für Materialforschung

Programm Nukleare Sicherheitsforschung

\*Nuclear Safety Institute

Russian Academy of Sciences, Moscow

Für diesen Bericht behalten wir uns alle Rechte vor

Forschungszentrum Karlsruhe GmbH  
Postfach 3640, 76021 Karlsruhe

Mitglied der Hermann von Helmholtz-Gemeinschaft  
Deutscher Forschungszentren (HGF)

ISSN 0947-8620

urn:nbn:de:0005-073735

# **Das Verhalten der Oxidschicht von Zirkonium-basierten Brennstabhüllrohren unter Dampfmangelbedingungen**

## **Zusammenfassung**

Es werden die Ergebnisse von Dauerglühversuchen mit voroxidierten Zircaloy-Hüllrohren in Inertgasatmosphäre bei Glühtemperaturen zwischen 1250 und 1500 °C und ein entsprechendes Modell dargestellt. Ziel der Tests war die Untersuchung der Kinetik der Oxidschichtreduzierung während der Dampfmangelphase bei der Trockenlegung des Reaktorkerns während eines schweren Störfalles. Neben der Abnahme der Oxidschichtstärke wurden die homogene Entwicklung von  $\alpha$ -Zr(O) Ausscheidungen innerhalb der Oxidschicht und die Entwicklung einer  $\alpha$ -Zr(O) Schicht an der äußeren Oberfläche des Hüllrohres nachgewiesen. Das Phänomen sollte einen starken Einfluss auf die intensive Wasserstofffreisetzung während der folgenden Abschreckphase haben.

## **Abstract**

This report presents the results of tests relating to the long-term annealing of pre-oxidised Zircaloy cladding tubes in an inert atmosphere at annealing temperatures between 1250 and 1500 °C and a corresponding model. The tests were aimed at investigating the reduction kinetics of the oxide layer in the steam starvation phase by the progression of core drying during a severe accident. Homogeneous formation of  $\alpha$ -Zr(O) precipitations inside the oxide layer and formation of  $\alpha$ -Zr(O) scale on the outer cladding surface were detected in addition to a decrease in the oxide layer thickness. This phenomenon is supposed to have a strong influence on intensive hydrogen release during the following quench phase.

# Contents

|   |    |
|---|----|
| 1. INTRODUCTION .....   | 1  |
| 2. EXPERIMENTS WITH SINGLE RODS UNDER NON-ISOTHERMAL<br>CONDITIONS .....  | 1  |
| 2.1. Test rig and experimental procedure for single rod tests .....   | 1  |
| 2.2. Results of single rod tests.....   | 3  |
| 2.2.1. <i>First series in 2002 at annealing temperatures of 1400..1500°C</i> .....                              | 3  |
| 2.2.2. <i>Experimental series in 2003 at annealing temperatures of 1400..1500°C</i>                             | 4  |
| 2.2.3. <i>Experimental series in 2004 at annealing temperatures of 1300 °C</i> .....                            | 5  |
| 3. DEVELOPMENT OF A NEW MODEL OF THE ZRO <sub>2</sub> BEHAVIOUR UNDER<br>STEAM STARVATION CONDITIONS.....       | 6  |
| 3.1. Mechanism driving the $\alpha$ -Zr(O) phase growth in ZrO <sub>2</sub> scale.....                          | 6  |
| 3.2. Mass transfer in the two-phase zone.....   | 6  |
| 3.2.1. <i>Flux matches at the two-phase zone interfaces</i> .....   | 8  |
| 3.2.2. <i>Mass balances</i> .....   | 10 |
| 3.3. Analysis of $\alpha$ -Zr(O) growth kinetics.....   | 10 |
| 3.4. Conclusions with respect to model development.....   | 12 |
| 4. EXPERIMENTS WITH SMALL TUBE PROBES UNDER QUASI-ISOTHERMAL<br>CONDITIONS .....                                | 13 |
| 4.1. Test rig and experimental procedure for isothermal tests .....   | 13 |
| 4.2. Results of quasi-isothermal tests .....  | 13 |
| 4.2.1. <i>Experimental series in 2003-2004 with single-sided oxidation</i> .....                                | 13 |
| 4.2.2. <i>Experimental series in 2006 with double-sided oxidation of different<br/>cladding materials</i> ..... | 14 |
| CONCLUSIONS .....   | 16 |
| REFERENCES.....   | 17 |

## List of Tables

|   |    |
|---|----|
| Table 1. 2002 experiments in the Quench test rig at ~1450°C with an annealing duration of ~3h: test parameters and some measurement results.....    | 18 |
| Table 2. 2002 experiments in the Quench test rig at ~1450°C with an annealing duration of ~3h: results of metallographic investigations. ....       | 18 |
| Table 3. 2003 experiments in the Quench test rig at ~1450°C with a pre-oxidation duration of ~660 s: results of metallographic investigations. .... | 19 |
| Table 4. 2003 experiments in the Quench test rig at ~1450°C with a pre-oxidation duration of~1080 s: results of metallographic investigations. .... | 19 |
| Table 5. Comparison of the SVECHA calculation results with experimental data.....   | 20 |
| Table 6. Two series of 2004 experiments in the Quench test rig at 1270 °C...1320 °C. ....   | 21 |
| Table 7. 2003 and 2004 BOX experiments at 1400°C and 1450 °C, respectively, with different oxidation and annealing durations. ....                  | 22 |
| Table 8. 2003 and 2004 BOX experiments at 1400°C and 1450 °C, respectively: results of metallographic investigations. ....                          | 22 |
| Table 9. 2006 isothermal BOX experiments at 1350 °C with an oxidation of ~12 min in steam (60 g/h) and annealing of 150 min in argon (50 l/h).....  | 23 |
| Table 10. 2006 isothermal BOX experiments at 1350 °C: results of metallographic investigations.....   | 23 |

## List of Figures

|  |    |
|--|----|
| Fig. 1. Schematic representation of the QUENCH-SR test rig.....  | 24 |
| Fig. 2. Typical test conduct.....  | 24 |
| Fig. 3. Sample in the inductive furnace at different temperatures.....   | 25 |
| Fig. 4. 2002 experiments in the Quench test rig with different pre-oxidation durations and an annealing time of ~3 h: pyrometer ( $\epsilon=0.7$ ), steam supply, and hydrogen release diagrams (mass spectrometer data) .....   | 26 |
| Fig. 5. 2002 experiments in the Quench test rig with different pre-oxidation durations and an annealing time of ~3 h: external view of the Zry-4 claddings pre-oxidised in steam and then annealed in argon at a temperature of ~1475 °C measured with a pyrometer on the cladding surface. .... | 27 |

|   |    |
|---|----|
| Fig. 6. Cross-sections at middle elevation of the Zry-4 specimens pre-oxidised at ~1475 °C for 250 s (upper photo) and pre-oxidised at ~1475 °C for 250 s and then annealed at ~1475 °C for 10800 s (lower photo). .....  | 28 |
| Fig. 7. Cross-sections at middle elevation of the Zry-4 specimens pre-oxidised at ~1475 °C for 750 s (upper photo) and pre-oxidised at ~1475 °C for 750 s and then annealed at ~1475 °C for 10800 s (lower photo). .....  | 29 |
| Fig. 8. Cross-sections at middle elevation of the Zry-4 specimens pre-oxidised at ~1475 °C for 2000 s (upper photo) and pre-oxidised at ~1475 °C for 2000 s and then annealed at ~1475 °C for 10800 s (lower photo). .....  | 30 |
| Fig. 9. 2003 experiments in the Quench test rig with a pre-oxidation duration of 660 s and different annealing durations: pyrometer ( $\epsilon=0.65$ ), middle thermocouples (inside TCi and outside TCo), and steam supply diagrams. ....   | 31 |
| Fig. 10. 2003 experiments in the Quench test rig with a pre-oxidation of ~11 min. and different annealing durations: outer view of the Zry-4 claddings pre-oxidised in steam and then annealed in argon at a temperature of ~1475 °C measured with a TC fixed to the cladding. .... | 32 |
| Fig. 11. 2003 experiments in the Quench test rig with a pre-oxidation of ~11 min. and different annealing durations: cladding cross-section. ....   | 33 |
| Fig. 12. 2003 experiments in the Quench test rig with a pre-oxidation of ~11 min. and different annealing durations: oxide layer structure. Coagulation of $\alpha$ -Zr(O) precipitates and formation of the outer $\alpha$ -Zr(O) surface layer. ....                              | 34 |
| Fig. 13. 2003 experiments in the Quench test rig: test with an annealing duration of 3600 s and an initial oxide layer of ~200 $\mu$ m. EDX analysis of outer layers on the cladding. ....  | 35 |
| Fig. 14. 2003 experiments in the Quench test rig with a pre-oxidation duration of 1080 s and different annealing durations: pyrometer ( $\epsilon=0.65$ ), middle thermocouples (inside TCi and outside TCo), and steam supply diagrams .....                                       | 36 |
| Fig. 15. 2003 experiments in the Quench test rig with a pre-oxidation of ~18 min. and different annealing durations: outer view of the Zry-4 claddings pre-oxidised in steam and then annealed in argon at a temperature of ~1475 °C measured with a TC fixed to the cladding. .... | 37 |
| Fig. 16. 2003 experiments in the Quench test rig with a pre-oxidation of ~18 min. and different annealing durations: cladding cross-section. ....   | 38 |
| Fig. 17. 2003 experiments in the Quench test rig with a pre-oxidation of ~18 min. and different annealing durations: oxide layer structure. Coagulation of $\alpha$ -Zr(O) precipitates. ....   | 39 |

|   |    |
|---|----|
| Fig. 18. 2003 experiments in the Quench test rig: test with an annealing duration of 5400 s and an initial oxide layer of ~320 $\mu\text{m}$ . EDX analysis of outer layers on the cladding. ....   | 40 |
| Fig. 19. 2004 experiments in the Quench test rig with a pre-oxidation duration of 720 s and different annealing durations: pyrometer ( $\varepsilon=0.7$ ), middle thermocouples (inside of sample), and steam supply diagrams.....   | 41 |
| Fig. 20. 2004 experiments in the Quench test rig with a pre-oxidation of ~12 min. and different annealing durations: outer view of the Zry-4 claddings pre-oxidised in steam and then annealed in argon at a temperature of ~1300 $^{\circ}\text{C}$ measured with the internal centre TC located inside the specimen at the middle elevation. .... | 42 |
| Fig. 21. 2004 experiments in the Quench test rig with a pre-oxidation of ~12 min. and different annealing durations at ~1300 $^{\circ}\text{C}$ : cladding cross-section. ....  | 43 |
| Fig. 22. 2004 experiments in the Quench test rig with a pre-oxidation of ~12 min. and different annealing durations at ~1300 $^{\circ}\text{C}$ : oxide layer structure. Development of $\alpha\text{-Zr(O)}$ precipitates and formation of the outer $\alpha\text{-Zr(O)}$ surface layer. ....   | 44 |
| Fig. 23. 2004 experiments in the Quench test rig with a pre-oxidation duration of 20 min. and different annealing durations: pyrometer ( $\varepsilon=0.7$ ), middle thermocouples (inside of sample), and steam supply diagrams. ....  | 45 |
| Fig. 24. 2004 experiments in the Quench test rig with a pre-oxidation of ~20 min. and different annealing durations: outer view of the Zry-4 claddings pre-oxidised in steam and then annealed in argon at a temperature of ~1300 $^{\circ}\text{C}$ measured with the internal centre TC located in the specimen at the middle elevation.....      | 46 |
| Fig. 25. 2004 experiments in the Quench test rig with a pre-oxidation of ~20 min. and different annealing durations at ~1300 $^{\circ}\text{C}$ : cladding cross-section. ....  | 47 |
| Fig. 26. 2004 experiments in the Quench test rig with a pre-oxidation of ~20 min. and different annealing durations at ~1300 $^{\circ}\text{C}$ : oxide layer structure. Development of $\alpha\text{-Zr(O)}$ precipitates and formation of the outer $\alpha\text{-Zr(O)}$ surface layer. ....   | 48 |
| Fig. 27. Measurement of the surface's electrical resistance demonstrates the presence of a metallic surface layer after a relatively short duration of annealing. ....  | 49 |
| Fig. 28. Equilibrium Zr-O binary phase diagram according to Ruh and Garret [8]. ...   | 50 |
| Fig. 29. Oxygen concentration profiles (schematic) in the saturated oxide phase with a zero and non-zero temperature gradient under steam starvation conditions... ..   | 50 |
| Fig. 30. Oxygen concentration profiles (schematic) in different layers of the oxidised Zry cladding after saturation (equilibration) of the oxide phase under steam starvation conditions.....  | 50 |
| Fig. 31. BOX rig for oxidation experiments under quasi-isothermal conditions.....   | 51 |

|  |    |
|--|----|
| Fig. 32. Time schedule of the BOX tests in 2003..2004 with rods and sealed tubes.  | 51 |
| Fig. 33. Overview of samples after the BOX tests with Zry-4 rods and Zry-4 sealed tubes filled with air (1 <sup>st</sup> tube) or argon (2 <sup>nd</sup> and 3 <sup>rd</sup> tubes).   | 52 |
| Fig. 34. BOX tests in 2003..2004: layer structure.   | 53 |
| Fig. 35. BOX tests in 2003..2004: structure of outer oxide layer.  | 54 |
| Fig. 36. Isothermal BOX test: EDX analysis of the outer layers on the surface of a sample pre-oxidised at 1400°C for 660 s and annealed for 5400 s.  | 55 |
| Fig. 37. BOX rig: movable sample holder allows for the fast sample positioning in the furnace and the fast sample removal from the furnace.  | 56 |
| Fig. 38. Time schedule of the 2006 isothermal BOX tests with open tubes inserted into the furnace and withdrawn from the furnace at work temperature.  | 56 |
| Fig. 39. Annealing series 2006; mass-spectrometer measurements of gas concentrations during annealing of the Zry-4 sample.   | 57 |
| Fig. 40. Isothermal BOX tests in 2006 with different cladding materials: overview of samples oxidised in steam for 720 s without annealing (left column) and with annealing for 9000 s in argon at 1350 °C (right column).   | 58 |
| Fig. 41. Isothermal BOX tests in 2006 (1350 °C) with different cladding materials: cladding cross-sections.  | 59 |
| Fig. 42. Isothermal BOX tests in 2006 (1350 °C): cracked structure of oxide layer without annealing (left column) and development of outer metallic scale on surface of annealed samples (right column).   | 60 |
| Fig. 43. Isothermal BOX tests 2006 (1350 °C): development of $\alpha$ -Zr(O) film at surface of external oxide layer (left column) and absence of $\alpha$ -Zr(O) film at surface of internal oxide layer (right column).  | 61 |
| Fig. 44. Outer view of ZrO <sub>2</sub> crucibles used for the tests relating to the dissolution of ZrO <sub>2</sub> with molten Zircaloy under Ar: formation of an $\alpha$ -Zr(O) metallic strip with the height corresponding to the melt height inside the crucible. | 62 |



## 1. Introduction

Steam starvation conditions may occur on fuel rod surfaces during a severe accident due to the dry-out of the reactor core and blockage formation. The oxide layer of the cladding tube surface will be reduced under these conditions. Hence, knowledge about the oxide layer reduction processes is important for severe accident management measures. Up to now, detailed experimental investigations have been performed only for the description of the oxide layer *growth* during cladding oxidation under isothermal conditions [1] and non-isothermal conditions [2].

Oxide layer *reduction* processes under non-isothermal conditions were investigated at FZK from 2002 to 2003 in the temperature range between 1400°C and 1490°C (temperature drift between these values during the test) [3, 4]. These tests relating to the degradation of the oxide layer during annealing in an argon atmosphere unexpectedly revealed the formation of  $\alpha$ -Zr(O) *precipitates* that were quasi homogeneously distributed inside the oxide layer. Other tests were performed in 2004 at a significantly lower temperature (1250...1350 °C) and nevertheless showed bulk precipitate formation as well as the development of *metallic scale* on the outer surface of the oxide layer during annealing [5]. Furthermore, results of tests at 1350, 1400 and 1450 °C under isothermal conditions [13] demonstrated the weak development of bulk metallic precipitates and expressed growth of outer metallic scale.

## 2. Experiments with single rods under non-isothermal conditions

Twenty four annealing tests with cladding tube segments were performed under the influence of a strong temperature gradient across the tube wall. In addition, eight reference oxidation tests were performed without subsequent annealing.

### 2.1. Test rig and experimental procedure for single rod tests

The IMF experimental QUENCH-SR rig [2] was used for the pre-oxidation of the samples and subsequent annealing of some oxidised samples. The design of the QUENCH-SR rig is shown in [Fig. 1](#).

The specimens used in the tests were segments of PWR fuel rod cladding tubes (Zry-4) with a length of 150 mm, an outer diameter of 10.75 mm, and a wall thickness of 0.725 mm. The top and bottom of the tube were sealed with Zircaloy plugs. The specimen was suspended inside a quartz tube on a thin Zry capillary tube, which connected the specimen interior with the atmosphere. Heating was provided by an

induction coil around the section of the quartz tube. Power was supplied to the coil from a 20 kW generator at a frequency of 700 kHz, which induced currents in the bulk of the metal with subsequent Joule heating. The feedback control of the generator was performed by means of a pyrometer focusing on the specimen surface in the centre of the rod.

Besides the pyrometer, the measurements of which are relative rough due to the changing probe emissivity during the test, thermocouples were used for precise temperature measurement. The temperature at the outer surface of the cladding was measured by thermocouples at an elevation of 75 mm. The Pt/Rh thermocouple was fixed to the outer pre-oxidised tube surface by a Pt/Rh wire. The other Pt/Rh thermocouple was used as centreline thermocouple and measured the temperature at elevation of 75 mm inside the rod.

Prior to the tests, the specimens were pre-oxidised to a small extent to prevent eutectic interactions between the outer thermocouple and cladding surface. This thin oxide scale had also been formed in the QUENCH-SR rig by exposing specimens to argon/oxygen atmosphere for one minute at a temperature 1200°C. The resulting protective oxide layer thickness was 20 - 30 µm.

The test conduct is represented schematically in [Fig. 2](#). The following phases of the test sequence can be distinguished. First, an initial phase, during which the facility was prepared for the actual test. The specimen was heated up to 1000°C under constant argon flow with the addition of 20% oxygen to prevent dissolution of the oxide protection layer. After establishing the thermal equilibrium, the steam was injected at a constant rate of 0.028 g/s. Secondly, during the enhanced pre-oxidation period, the specimen was heated up to work temperature (1250 – 1450 °C) under a constant flow of argon and steam through the test section. The specimen was kept ([Fig. 3](#)) at this temperature until the desired oxide layer thickness was reached. Finally, the specimen was annealed in argon at work temperature, while the steam flow was shut down. The test was completed by switching off the inductive heating.

The out-coming gas composition was measured by a “Balzers GAM-300” mass spectrometer (MS). GAM-300 is an entirely computer-controlled quadrupole MS with an 8 mm rod system which allows for the quantitative measurement of gas concentrations down to about 10 vppm. To prevent steam condensation, the whole off-gas system was heated to about 150°C. During the whole test, argon was supplied as carrier and reference gas for quantitative analysis. The main task of the MS was to measure the hydrogen release rate and the concentrations of the outgoing steam.

After the tests, detailed metallographic analyses of the cladding structures at elevations corresponding to the TC locations (half of the sample height) were

performed. 1 cm long tube segments were embedded, ground, lapped, and finally polished by means of STRUER's equipment. The microphotographs were taken by means of a "Reichert-Jung" metallographic light microscope that was coupled to the computer via the "SensiCam" 12-bit CCD camera. The "analySIS" software was applied for the measurements. Also the SEM/EDX analysis was performed for some selected samples.

## 2.2. Results of single rod tests

### 2.2.1. First series in 2002 at annealing temperatures of 1400..1500°C

The first series of the tests in the inductive furnace were performed in 2002 at a temperature of about 1450 °C. After different oxidation durations (Table 1), the sample was annealed for about 3 hours. The measurement of the hydrogen produced during cladding oxidation in steam corresponds very well to the sample mass gain resulting from oxygen uptake.

The temperature was controlled by a pyrometer with a fixed emissivity of  $\varepsilon=0.7$  (maximum emissivity of the  $ZrO_2$  layer [6]) without use of thermocouples. The pyrometer readings (Fig. 4) are results of calculations on the basis of the Stefan–Boltzmann law for thermal radiation  $j$ :

$$j = \varepsilon \cdot \sigma \cdot T^4,$$

where  $\sigma$  is the Stefan-Boltzmann constant.

Since emissivity  $\varepsilon$  can vary during oxide layer growth, the real temperature  $T$  may also deviate from the constant level depicted in Fig. 4. The later experiments with a simultaneous use of thermocouples showed that the tube temperature may rise up to 1480 °C during such tests.

The oxidised samples showed a typical black surface (Fig. 5). The samples, which were annealed after oxidation, exhibited a brighter surface. The sample with an initial oxide layer thickness of about 130  $\mu\text{m}$  even showed a metallic surface, i.e. the oxide layer had been dissolved completely during annealing. This observation was confirmed by the metallographic examinations (Fig. 6): the cross-section exhibited a homogeneous distribution of the  $\alpha$ -Zr(O) phase across the annealed sample. A completely unexpected layer structure was found in annealed samples with initially thicker oxide layers ( $\delta_{\text{ox}} > 200 \mu\text{m}$ ). The oxide layer thickness (Table 2) either decreased negligibly (Fig. 7) or even increased by more than 25% for very thick ( $\sim 400 \mu\text{m}$ ) initial oxide layers (Fig. 8). At the same time, the new effect of developing *metallic precipitates* could be observed inside the oxide layer. The precipitates had a stretched form oriented in radial direction corresponding to the columnar structure of the oxide layer. The fraction of precipitates was measured by means of computer

image analysis and did not reveal any dependence on the initial oxide layer thickness (Table 2).

### **2.2.2. Experimental series in 2003 at annealing temperatures of 1400..1500°C**

The next series of experiments with empty Zircaloy rods was aimed at investigating the oxide layer structure variation as a function of the annealing duration. Two initial oxide layer thicknesses were used: ~200  $\mu\text{m}$  and ~300  $\mu\text{m}$ .

The experiments were performed with a more accurate temperature measurement. The outer surface Pt/Rh thermocouple TCo was installed at the middle elevation of the sample. Some of samples were also equipped with centreline thermocouples TCi, which were inserted into the sample through an upper capillary tube. As a consequence of the variation of the electrical generator power during the test, both kinds of thermocouples showed temperature deviations that were controlled by the monochrome pyrometer. The latter, however, does not respond to the variation of cladding surface emissivity during the transformation of the oxide layer and shows a constant temperature. The readings of the pyrometers and both thermocouples for six samples pre-oxidised to 200  $\mu\text{m}$  are depicted in [Fig. 9](#). It is obvious that the real temperature measured with the inner thermocouple increased continuously during the test, with the values being more than 50 K higher than the readings of the outer thermocouple influenced by the steam.

The outer surface of annealed samples was grey and sometimes coloured with metallic glitter ([Fig. 10](#)). Metallographic investigation did not reveal a clear dependence of the oxide layer thickness on the annealing duration ([Table 3](#), [Fig. 11](#)) due to a rather complicated temperature history. The oxide layer included metallic precipitates ([Fig. 12](#)), the fraction of which varied between 12% and 22%, but also did not show any clear dependence on the annealing duration. It was only possible to observe the coagulation of small dispersed precipitates into widely spaced large-scale precipitates with increasing annealing duration. Furthermore, the concentration of precipitates was higher at the outer surface of the samples. This trend of increasing precipitate concentration in the direction towards the outer sample surface is clearly illustrated by the SEM in [Fig. 13](#). At the same time, the EDX analysis shows an increase of the oxygen content inside the metallic precipitates towards the inner  $\alpha$ -layer of the cladding.

Experiments with a thicker initial oxide layer (about 300  $\mu\text{m}$ ) also have a complicated temperature history ([Fig. 14](#)) and show not a clear dependence of oxide layer thickness on the annealing duration ([Table 4](#)). The outer surface of annealed samples was coloured with metallic glitter ([Fig. 15](#)). The metallic precipitates inside the oxide layer have a more dispersed small-scale structure in comparison with

precipitates formed inside the initially thin oxide layer (compare [Fig. 16](#) and [Fig. 11](#)). The density of precipitates is higher inside the outer part of the oxide layer ([Fig. 17](#)), whereas the oxygen content is higher in metallic precipitates inside the inner part of the oxide layer. This trend of increasing precipitate concentration in the direction towards the outer sample surface is illustrated by the SEM in [Fig. 18](#). This distribution of metallic precipitates correlates with distribution of the micro cracks in oxide layer of oxidised Zry-4 tubes: numerous observations show that the cracks concentration is higher in outer region of the oxide layer.

To consider the influence of the complicated temperature history (typical for all experiments), detailed computer simulations of each experiment were performed with the SVECHA code [7]. The test and calculation results are combined in [Table 5](#). Analysis of the results obtained shows that the current version of the SVECHA oxidation model correctly describes oxygen redistribution in the alpha layer (trend to the upper boundary concentration) that leads to oxide layer thinning. However, the model does not account for the decreasing oxygen concentration in the oxide layer below the boundary value and the appearance of alpha-phase precipitates. Consequently, the long annealing experiments with an observed displacement of the inner oxide boundary into the alpha layer cannot be described by the conventional oxidation model.

### **2.2.3. Experimental series in 2004 at annealing temperatures of 1300 °C**

To exclude the influence of the potential development of the high-temperature  $ZrO_{2-x}$  cubic phase at the inner boundary of the oxide layer, another series of annealing tests were conducted at lower temperature. The test parameters and results of post-test measurements are presented in [Table 6](#). Two series were conducted under variable initial oxidation conditions to investigate the influence of the initial pre-oxidation time on the annealing processes. The measurement of temperature ([Fig. 19](#) and [Fig. 23](#)) was performed with the inner thermocouple, which appeared more reliable in comparison with the outer surface thermocouple. Each series consisted of three annealing tests and one reference oxidation test. The first series ([Fig. 20](#), [Fig. 21](#)) with pre-oxidation for 12 minutes (and initially thick metal layers) shows a higher rate of oxide layer thinning than the second series ([Fig. 24](#), [Fig. 25](#)) with a pre-oxidation for 20 minutes (and initially thinner metal layers). At the same time, the development of  $\alpha$ -Zr(O) precipitates is *more pronounced* in the first series ([Fig. 22](#) and [Fig. 26](#)) *with a thinner initial oxide layer*. Furthermore, the growth of the  $\alpha$ -Zr(O) layer on the surface of the oxide layer was typical for both test layers. The corresponding measurements ([Fig. 27](#)) revealed the electrical properties of the metal-coated outer surface.

### 3. Development of a New Model of the ZrO<sub>2</sub> Behaviour under Steam Starvation Conditions

#### 3.1. Mechanism driving the $\alpha$ -Zr(O) phase growth in ZrO<sub>2</sub> scale

Analysis with the SVECHA/QUENCH code [2] of the high-temperature tests performed in the QUENCH-SR rig with induction heating shows that the temperature gradient across the ZrO<sub>2</sub> scale of the Zry tube is significant and attains a value of  $\sim 0.2$  K/ $\mu\text{m}$  in the new FZK tests [3] relating to the ZrO<sub>2</sub> behaviour under steam starvation conditions.

In accordance with the binary Zr-O phase diagram, [Fig. 28](#), this temperature gradient induces the oxygen concentration gradient and finite oxygen flux from the ZrO<sub>2</sub> layer to the inner  $\alpha$ -Zr(O) layer after equilibration (“saturation”) of the oxide phase. Indeed, the minimum oxygen concentration in the oxide phase is determined by the equilibrium line separating the tetragonal oxide phase from the two-phase region (ZrO<sub>2</sub> +  $\alpha$ -Zr(O)) in the binary phase diagram [8] (in the temperature range of the FZK tests, 1200-1400 °C). This minimum oxygen concentration is temperature dependent and, thus, determines the oxygen concentration gradient during equilibration of the oxide phase in the case of a temperature gradient across the ZrO<sub>2</sub> scale, [Fig. 29](#).

After equilibration of the oxide phase, however, this concentration gradient induces a corresponding non-vanishing diffusion flux, which causes further reduction of the oxygen content in the ZrO<sub>2</sub> layer beyond the saturation limit. This may lead to a precipitation of the  $\alpha$ -Zr(O) phase in the oxide layer and formation of the two-phase zone (ZrO<sub>2-x</sub> +  $\alpha$ -Zr(O)), [Fig. 30](#).

Besides, oxygen flux in the oxide layer does not match a zero oxygen flux at the gas/solid interface in the inert atmosphere. In order to sustain such a flux match, an  $\alpha$ -Zr(O) layer with a flat oxygen profile has to be formed at the outer surface of the oxide layer.

Both processes of two-phase zone growth and outer  $\alpha$ -Zr(O) layer growth were observed in the FZK tests.

#### 3.2. Mass transfer in the two-phase zone

Mass transfer through a two-phase zone in a binary system under a temperature gradient is described by Flemings’ approach [9, 10]. This approach is mainly based on the assumption that the two phases are in local equilibrium with each other in the entire bulk of the two-phase layer. For the binary system, this condition of local

equilibrium can be fulfilled when concentration gradients are formed inside both phases (stimulating diffusion mass transfer) subjected to the temperature gradient.

In this approach the equation for mass transfer in the two-phase zone has the form:

$$\frac{\partial}{\partial t}[c_o(x,t)f(x,t) + \rho_o(x,t)(1-f(x,t))] = \frac{\partial}{\partial x} \left[ D_o^{(ox)}(1-f) \frac{\partial \rho_o}{\partial x} + D_o^{(\alpha)} f \frac{\partial c_o}{\partial x} \right], \quad (1)$$

where  $c_o(x,t)$  and  $\rho_o(x,t)$  are oxygen concentration profiles in the  $\alpha$ -Zr(O) and ZrO<sub>2</sub> phases of the two-phase mixture, respectively;  $f(x,t)$  is the volume fraction of the  $\alpha$ -Zr(O) precipitates in the ZrO<sub>2</sub> matrix;  $D_o^{(ox)}$ ,  $D_o^{(\alpha)}$  are the oxygen diffusion coefficients in the  $\alpha$ -Zr(O) and ZrO<sub>2</sub> phases, respectively.

The one-dimensional Eq. (1) is obtained after averaging in the direction perpendicular to  $x$ . This averaging procedure is valid for the reaction zone with a macroscopic inhomogeneity in one direction ( $x$ ) only, i.e. for the layered structure. After this procedure, the function  $f(x,t)$  becomes smooth and continuous even when the second phase is discontinuous and forms separate precipitates in the first-phase matrix [11].

In addition, it is assumed that local equilibrium occurs at each axial position  $x$  of the two-phase zone due to rapid diffusion at relatively short distances  $\sim l$  between the second-phase precipitates in the direction perpendicular to  $x$ ,  $l \ll L$ , where  $L$  is the thickness of the two-phase zone (in the axial direction  $x$ ). This assumption is valid when the variation of the two-phase zone thickness is very slow in comparison with the diffusion processes in the direction perpendicular to  $x$ :

$$(dL/dt)\tau_{\perp} \ll L, \quad (2)$$

where  $\tau_{\perp} \approx l^2/D_o^{(ox)}$  is the characteristic diffusion time in the perpendicular direction. Generally, this inequality applies after a certain initial period of time. In the case of parabolic growth kinetics,  $L \approx kt^{1/2}$ , for instance, Eq. (2) transforms into  $t \gg \tau_{\perp}$ . It becomes valid after the initial period  $\tau_{\perp} \approx l^2/D_o^{(ox)}$ , which normally is rather short due to the microscopic scale of  $l$  (a few  $\mu\text{m}$ ).

Since the oxygen diffusion coefficient in oxide is approximately 2 orders of magnitude higher than in the  $\alpha$ -phase (in the temperature range of the FZK tests, 1200-1400 °C),  $D_o^{(ox)} \gg D_o^{(\alpha)}$ , the second term in the r.h.s of Eq. (1) can be neglected, unless oxide is far from being converted completely into the  $\alpha$ -phase (i.e.  $f$  is not too close to 1):

$$\frac{\partial}{\partial t}[c_o(x,t)f(x,t) + \rho_o(x,t)(1-f(x,t))] \approx \frac{\partial}{\partial x} \left[ D_o^{(ox)}(1-f) \frac{\partial \rho_o}{\partial x} \right]. \quad (3)$$

In accordance with the phase diagram for the binary Zr-O system, Fig. 28, the equilibrium lines separating the two-phase region ( $\text{ZrO}_2 + \alpha\text{-Zr(O)}$ ) from the tetragonal  $\text{ZrO}_2$  and  $\alpha\text{-Zr(O)}$  phases and determining the concentration distribution in the spatial two-phase zone (i.e.  $c_o(x,t)$  and  $\rho_o(x,t)$ ) can be approximated well (within a relatively narrow temperature interval of  $\sim 50$  K across the oxide layer in the FZK tests) by straight lines. Under the condition of a linear temperature profile (which is the case for the oxide layer), it therefore holds:

$$T^{(\alpha)} = T_1 - \frac{(T_1 - T_2)}{L}x = T_1 - \frac{\Delta T}{L}x, \quad (4)$$

The concentration profiles in each phase of the two-phase mixture can also be represented satisfactorily in the linear form, as shown in Fig. 30:

$$\rho_o(x,t) = \rho_o(T_1) + \frac{\Delta\rho_o}{L}x, \quad (5)$$

$$c_o(x,t) = c_o(T_1) + \frac{\Delta c_o}{L}x, \quad (6)$$

where  $L = L_2 - L_1$  is the thickness of the two-phase zone and  $L_1$  and  $L_2$  are the positions of the two-phase zone boundaries  $I_1$  and  $I_2$ , respectively.

In this approximation the r.h.s. of Eq. (3) can be further simplified:

$$\frac{\partial}{\partial t} [c_o(x,t)f(x,t) + \rho_o(x,t)(1-f(x,t))] \approx \frac{\partial}{\partial x} \left[ D_o^{(\alpha)}(1-f) \frac{\rho_o(I_2) - \rho_o(I_1)}{L} \right]. \quad (7)$$

### 3.2.1. Flux matches at the two-phase zone interfaces

Growth of the two-phase layer thickness  $L$  is determined by the relocation velocities of its two interfaces which can be obtained from the flux matching conditions at these interfaces [11].

At the boundary  $I_1$  between the two-phase ( $\alpha\text{-Zr(O)} + \text{ZrO}_2$ ) zone and the inner  $\alpha\text{-Zr(O)}$  layer, the flux matches for the oxygen and zirconium components have the form:

$$-D_o^{(\alpha)} \frac{\partial c_o}{\partial x} \Big|_{I_1} - c_o(I_1) \frac{dL_1}{dt} = [c_o(I_1)f(I_1) + \rho_o(I_1)(1-f(I_1))] \left( u_1 - \frac{dL_1}{dt} \right) - D_o^{(\alpha)}(1-f(I_1)) \frac{\Delta\rho_o}{L}, \quad (8)$$

$$-c_{Zr} \frac{dL_1}{dt} = [c_{Zr}f + \rho_{Zr}(1-f)] \left( u_1 - \frac{dL_1}{dt} \right), \quad (9)$$

where  $u_1$  is the net velocity of the two-phase zone (relative to the inner  $\alpha$ -layer).

At the boundary  $I_2$  between the two-phase ( $\alpha\text{-Zr(O)} + \text{ZrO}_2$ ) zone and the outer  $\alpha\text{-Zr(O)}$  layer, the flux matches assume the following form:

$$-D_o^{(\alpha)} \left. \frac{\partial c_o}{\partial x} \right|_{I_2} + c_o(I_2) \left( u_2 - \frac{dL_2}{dt} \right) = [c_o(I_2)f(I_2) + \rho_o(I_2)(1-f(I_2))] \left( u_1 - \frac{dL_2}{dt} \right) - D_o^{(ox)}(1-f(I_2)) \frac{\Delta \rho_o}{L}, \quad (10)$$

$$c_{Zr} \left( u_2 - \frac{dL_2}{dt} \right) = [c_{Zr}f + \rho_{Zr}(1-f)] \left( u_1 - \frac{dL_2}{dt} \right), \quad (11)$$

where  $u_2 = dL_3/dt$  is the net velocity of the  $ZrO_2$  layer (relative to the inner  $\alpha$ -layer). By inserting the solutions of the diffusion equations for the two-phase zone (i.e. Eq. (7)) and for the adjacent layers into Eqs. (8)-(11), the interface velocities  $\frac{dL_1}{dt}$  and  $\frac{dL_2}{dt}$  and the growth kinetics of the precipitates,  $f(x,t)$ , can be determined generally.

This problem can be simplified by the steady-state approximation valid for oxygen diffusion in the oxide layer, when the following condition applies:

$$(dL/dt)\tau_x \ll L, \quad (12)$$

where  $\tau_x \approx L^2/D_o^{(ox)}$  is the characteristic diffusion time in axial direction  $x$ . Normally, this condition is fulfilled for oxygen diffusion in the oxide layer (see e.g. [12]). Based on the above relationship  $D_o^{(ox)} \gg D_o^{(\alpha)}$ , the flux matches indeed result in  $\Delta c^*(dL/dt) \approx D_o^{(ox)}\Delta c/L$ , where  $\Delta c$  and  $\Delta c^*$  are concentration drops across the oxide layer and at the oxide/ $\alpha$ -Zr(O) interface, respectively. Insertion of this estimate into Eq. (12) yields the condition for the applicability of the steady-state approximation in the form of  $\Delta c^*/\Delta c \ll 1$ . Validity of this condition can be deduced simply from the equilibrium binary Zr-O phase diagram properties, Fig. 28.

In this approximation, time variation of the mean concentration at each spatial point can be neglected, i.e. the l.h.s. of Eq. (7) can be set to zero:

$$\frac{\partial}{\partial x} \left[ D_o^{(ox)}(1-f) \frac{\rho_o(I_2) - \rho_o(I_1)}{L} \right] \approx 0. \quad (13)$$

The solution of Eq. (13) has the form of:

$$f(x) = const., \quad (14)$$

which corresponds to the spatially uniform distribution of  $\alpha$ -Zr(O) precipitates in the  $ZrO_2$  matrix. This qualitative result is in fair agreement with observations made in the FZK tests. Consequently, Eqs. (14) and (5) provide a spatially uniform oxygen flux in the oxide layer:

$$J_{ox} \approx D_o^{(ox)}(1-f)\frac{\Delta\rho_o}{L}, \quad (15)$$

which simplifies flux matches at the interfaces  $I_1$  and  $I_2$ .

### 3.2.2. Mass balances

Mass balances for the oxygen and zirconium atoms in the oxide layer have the form:

$$D_o^{(\alpha)} \frac{\partial c_o}{\partial x} \Big|_{I_2} + c_o(I_2) \left( \frac{dL_2}{dt} - u_2 \right) - D_o^{(\alpha)} \frac{\partial c_o}{\partial x} \Big|_{I_1} - c_o(I_1) \frac{dL_1}{dt} = \frac{d}{dt} \left[ (L_2 - L_1) \left( \frac{\rho_o(I_1) + \rho_o(I_2)}{2} (1-f) + \frac{c_o(I_1) + c_o(I_2)}{2} f \right) \right], \quad (16)$$

$$- \tilde{n}_{Zr} \frac{dL_1}{dt} + c_{Zr} \left( \frac{dL_2}{dt} - u_2 \right) = \frac{d}{dt} [(L_2 - L_1) (\rho_{Zr} (1-f) + c_{Zr} f)], \quad (17)$$

where  $c_{Zr}$  and  $\rho_{Zr}$  are molar densities of Zr in the  $\alpha$ -Zr(O) and ZrO<sub>2</sub> phases, respectively.

As explained in Section 1, the oxygen profile in the outer  $\alpha$ -layer is flat in the inert atmosphere and, thus, the term  $D_o^{(\alpha)} \frac{\partial c_o}{\partial x} \Big|_{I_2}$  in Eqs. (9) and (16) turns to zero.

### 3.3. Analysis of $\alpha$ -Zr(O) growth kinetics

When neglecting the influence of the  $\alpha$ -Zr(O) precipitates on the mass transfer through the oxide layer, the system of Eqs. (8)-(17) yields the growth rate of the outer  $\alpha$ -layer thickness  $\delta_\alpha^{(out)}$ :

$$\frac{d\delta_\alpha^{(out)}}{dt} \approx \frac{D_o^{(ox)}}{L} \Delta\rho_o \left( c_{Zr} \frac{\rho_2}{\rho_{Zr}} - c_2 \right)^{-1}, \quad (18)$$

where  $\rho_2 \equiv \rho_o(I_2)$ ,  $c_2 \equiv c_o(I_2)$ . In accordance with the phase diagram in Fig. 28, the value of  $\Delta\rho_o$  for the estimated temperature drop  $\Delta T \approx 50$  K in the FZK tests is rather small with  $\leq 0.1$  at.%. It results in a *slow* growth of the outer  $\alpha$ -layer despite a large value of the oxygen diffusion coefficient  $D_o^{(ox)}$ .

The growth rate of  $\alpha$ -Zr(O) precipitates in the oxide layer can be evaluated from the same system of equations:

$$\frac{d(Lf)}{dt} \approx \frac{1}{2} \frac{\Delta\rho_o}{(\bar{\rho}c_{Zr}/\rho_{Zr} - \bar{c})} \left( \frac{d\delta_\alpha^{(in)}}{dt} + \frac{d\delta_\alpha^{(out)}}{dt} \right), \quad (19)$$

where  $\delta_\alpha^{(in)}$  is the inner  $\alpha$ -layer thickness,  $\bar{\rho} = 0.5(\rho_1 + \rho_2)$ ,  $\bar{c} = 0.5(c_1 + c_2)$ . Due to the extremely small value of  $\Delta\rho_o$ , the growth rate of the precipitates is negligibly small in comparison with that of the inner and outer  $\alpha$ -layers. This is in apparent contradiction with the test observations. Hence, formation and quick growth of precipitates is supposed to be due to some additional reasons.

It is presumed that the main reason for the enhanced formation of precipitates during annealing might be compressive stresses induced in the oxide layer by the inner  $\alpha$ -phase layer during oxidation. These stresses emerge due to the volumetric expansion of the oxide phase that induces a mismatch between the two layers at the  $\alpha$ -Zr(O)/oxide interface. The outer  $\alpha$ -phase layer induces additional stresses in the oxide for the same reason. In contrast to this, formation of the metallic  $\alpha$ -phase precipitates in the oxide reduces the volumetric expansion of the oxide layer and, thus, the stresses in oxide. This makes local conversion of oxide into the  $\alpha$ -Zr(O) phase precipitates *energetically favourable*.

In this case, precipitate growth takes place at the expense of the outer  $\alpha$ -layer. In first approximation, it can be described by an equation similar to Eq. (18):

$$\frac{d(Lf)}{dt} \approx \frac{D_o^{(ox)}}{L} \Delta\rho_o \left( c_{Zr} \frac{\rho_2}{\rho_{Zr}} - c_2 \right)^{-1}. \quad (20)$$

This growth continues until the compressive stresses in the oxide decrease to some ultimate value. After this, the volume fraction of precipitates does no longer increase.

During the initial stage of annealing, the growth of the outer  $\alpha$ -layer will therefore be suppressed due to an enhanced growth of the precipitates (as can be deduced from the mass balance equations). Then, after reaching a stable value of the volume fraction of precipitates  $f^*$ , it increases according to the following relationship:

$$\frac{d\delta_\alpha^{(out)}}{dt} = \frac{D_o^{(ox)}(1-f^*)}{L} \Delta\rho_o \left( c_{Zr} \frac{\rho_2(1-f^*) + c_2 f^*}{\rho_{Zr}(1-f^*) + c_{Zr} f^*} - c_2 \right)^{-1}. \quad (21)$$

Due to a relatively small value of  $f^* \approx 0.1-0.2$  attained in the tests, this expression does not significantly differ from Eq. (16), which neglects the influence of precipitates.

Such a behaviour of the  $\alpha$ -phase is obvious from the comparison of the top photos in Figs. 22 and 26 with the bottom photos in the same figures displaying the post-test appearance of the oxidised Zry tube before and after annealing.

The growth rate of the inner  $\alpha$ -Zr layer obeys the following relationship:

$$\frac{d\delta_{\alpha}^{(in)}}{dt} = \left( D_o^{(\alpha)} \frac{\partial c_o}{\partial x} \Big|_{l_1} - \frac{D_o^{(ox)}(1-f^*)\Delta\rho_o}{L} \right) \left( c_{Zr} \frac{\rho_1(1-f^*) + c_1 f^*}{\rho_{Zr}(1-f^*) + c_{Zr} f^*} - c_1 \right)^{-1}. \quad (21)$$

During some initial period when the oxygen diffusion flux in the inner  $\alpha$ -layer significantly exceeds the flux in the oxide layer, behaviour of the inner layer is very similar to a standard one calculated in the absence of the temperature gradient. After the “saturation” of the inner  $\alpha$ -Zr phase, however, when the first flux in the r.h.s. of Eq. (21) becomes very small, the growth of the inner  $\alpha$ -layer ceases and turns to its reduction. Such a reduction of the inner  $\alpha$ -layer was observed in some of the tests at least.

During this late stage, the reduction rate of the inner  $\alpha$ -layer is very close to the growth rate of the outer  $\alpha$ -layer, as can be seen from the comparison of Eqs. (19) and (20).

### 3.4. Conclusions with respect to model development

1. Analysis of the new FZK tests relating to the oxidised Zry cladding behaviour under steam starvation conditions shows that the bulk precipitation of the  $\alpha$ -Zr(O) phase and growth of the outer  $\alpha$ -Zr(O) layer observed can be associated with a significant temperature gradient across the ZrO<sub>2</sub> layer that is attained under induction heating in the QUENCH facility.
2. Evolution of the oxide layer thickness and kinetics of the  $\alpha$ -Zr(O) phase growth (inner, outer  $\alpha$ -layers and precipitates in the oxide layer) may be described by the new model based on the general Flemings' approach to the modelling of mass transfer through a two-phase zone in a temperature gradient. Some additional factors, which provide for an enhanced growth of the precipitates (e.g. compressive stresses in oxide), are considered qualitatively.
3. Analysis of the system of equations obtained reveals qualitatively correct predictions concerning the formation and growth of the outer  $\alpha$ -Zr(O) layer, initial growth and subsequent reduction of the inner  $\alpha$ -Zr(O) layer, and evolution of the  $\alpha$ -Zr(O) precipitates in oxide observed in the tests.
4. More accurate solutions of the model will require more detailed experimental data on the kinetics of oxide and  $\alpha$ -Zr(O) layers growth and  $\alpha$ -Zr(O) precipitates evolution.

## 4. Experiments with small tube probes under quasi-isothermal conditions

Two test series were performed in 2003-2004 and 2006 with a negligible radial temperature gradient across the cladding wall.

### 4.1. Test rig and experimental procedure for isothermal tests

All isothermal tests were performed in the so-called BOX rig. This facility ([Fig. 31](#)) consists of

- a tube furnace with maximum temperatures of 1700 °C, equipped with an alumina reaction tube (inner diameter: 32 mm, length: 600 mm) and molybdenum heaters delivered by HTM Reetz GmbH Berlin;
- a gas supply system for Ar and steam (0-4 mol/h each), consisting of a gas flow controller, a liquid flow controller, and a so-called controlled evaporator-mixer unit (CEM), where the liquid water is evaporated and mixed with the non-condensable gas. The whole system is made by Bronkhorst High-Tech B.V.;
- and a quadrupole mass spectrometer (MS) Balzers GAM 300.

The mass spectrometer allows for the quantitative analysis of all gaseous reaction products, including steam. The Bronkhorst steam and gas supply system was used for steam calibration. All parts of the system are computer-controlled by a LabView program especially written for the BOX rig.

### 4.2. Results of quasi-isothermal tests

#### 4.2.1. Experimental series in 2003-2004 with single-sided oxidation

The typical time schedule of the tests is shown in [Fig. 32](#). Two samples were inserted simultaneously into the furnace: one sealed cladding segment and one massive rod, both with similar geometrical parameters (diameter 10.75 mm and height 20 mm). Three tests were performed with sample pairs ([Fig. 33](#)). The first cladding sample was welded under air atmosphere. During heating, the oxygen and nitrogen inside the sample were absorbed by Zircaloy. Consequently, the pressure difference across the cladding wall reached 1 bar. As a result, this sample collapsed at a temperature above 1200 °C due to the high ductility of Zry at this temperature. Another two

cladding samples were sealed under argon atmosphere at a pressure of about 0.5 bars. As a result of the pressure increase during heating, the samples were subject to a typical ballooning extension.

The results of post-test examinations are presented in [Table 7](#) and [Table 8](#). Metallographic investigation reveals dissolution of the initial oxide layer on the surface of the rods compared to the relatively thick residual oxide layer of tube samples ([Fig. 34](#)). A more detailed examination reveals the development of the outer  $\alpha$ -Zr(O) layer and formation of metallic precipitates inside the oxide layer ([Fig. 35](#)). These processes are more pronounced for the sample with the initially lower oxidation degree. The EDX analysis shows a complete saturation of the  $\alpha$ -Zr(O) phase ([Fig. 36](#)).

#### ***4.2.2. Experimental series in 2006 with double-sided oxidation of different cladding materials***

These test series were performed 1) to eliminate the transition processes by heating and cooling of the samples, which may cause temperature gradients inside the sample and 2) to check the influence of different kinds of cladding materials on the annealing process.

To exclude the influence of the temperature transients, the BOX rig was equipped with an air lock allowing for an exchange of specimens at reaction temperature and under defined atmosphere ([Fig. 37](#)). In the beginning of the test series, the furnace was heated to the desired temperature of 1350 °C and all auxiliary heaters for the tubing, valves, and flanges were switched on. After inserting the specimen, the air lock was connected to the furnace and flushed with argon. When the mass spectrometer indicated the removal of residual air from the furnace, the sample was slowly pushed into the hot centre of the furnace and thermally equilibrated before steam was switched on. In any case, the gas flow was changed from the oxidising gas or gas mixture to pure argon at the end of the isothermal oxidation period. The specimen was pulled into the air lock, where it quickly cooled down and could be exchanged by a new one. [Fig. 38](#) shows a time sequence of the test conduct with a first reference (only oxidised) sample, a second oxidised, and then annealed sample. Typical gas concentrations at furnace outlet during annealing are depicted in [Fig. 39](#). The rest of steam is stabilised at ~800 vppm, and rest of hydrogen is stabilised at ~180 vppm. Such small gas concentrations are quite low and these gas species have not influence on investigated samples.

Post-test appearance of three sample pairs is depicted in [Fig. 40](#). [Fig. 41](#) shows the two-sided regular oxidation of the samples with a negligible change of the oxide layer thickness after annealing. The initial pre-oxidation state reflects the absence of an initial  $\beta$ -Zr layer. The corresponding test results are summarized in [Table 9](#) and [Table 10](#). Investigation of the external oxide layer ([Fig. 42](#)) of annealed samples practically shows the absence of bulk metallic precipitates, but the outer  $\alpha$ -Zr(O) scale develops in all three kinds of cladding materials. Development of similar metallic scale was not observed on the surface of the internal oxide layer ([Fig. 43](#)). The important difference between conditions inside external and internal oxide layers is the different sign of stresses in the oxide. This difference can explain appearance of the outer  $\alpha$ -Zr(O) layer at the late stage of the tests, when the oxygen profile in oxide becomes flat and the stress gradient (rather than the temperature gradient absent in these tests) in radial direction induces oxygen flux from oxide into the internal layers, leading to formation and growth of the external  $\alpha$ -Zr(O) layer (similarly to behaviour under temperature gradient considered in Section 3). It is interesting to compare this case with other tests at significantly higher temperature. Tests relating to the dissolution of ZrO<sub>2</sub> crucibles by molten Zircaloy in an inert atmosphere [14] also revealed the formation of an  $\alpha$ -Zr(O) layer on the outer surface of the ZrO<sub>2</sub> crucible during relative short test duration ([Fig. 44](#)).

## Conclusions

1. The behaviour of the oxide layer on the cladding tube surface was investigated experimentally under steam starvation conditions at annealing temperatures between 1250 and 1500 °C. Twenty four single rod tests were performed under strongly non-isothermal conditions inside an inductively heated furnace. Six tests with short cladding tube segments were performed under isothermal conditions inside a tube furnace.
2. Evolution of the oxide layer thickness may be rather complicated: the initial decrease may turn to an increase during long annealing.
3. A two-phase structure develops inside the oxide layer during annealing under non-isothermal conditions:  $\alpha$ -Zr(O) metallic precipitates are formed inside the ceramic matrix.
4. Formation of an outer  $\alpha$ -Zr(O) metallic layer is observed under both conditions with a strong temperature gradient across the oxide layer and isothermal conditions.
5. A new model following the general Flemings' approach to modelling mass transfer through a two-phase zone in a temperature gradient has been developed to describe the phenomena observed.
6. Analysis of the tests shows that the observed phenomena can be associated with a significant temperature gradient across the ZrO<sub>2</sub> layer. Other important factor which provide for an enhanced growth of the metallic precipitates, is presence of mechanical stresses in oxide.

## Acknowledgement

The authors thank Mrs. U. Stegmaier and Mr. A. Meier for the preparation of the test rigs and test conduct. We are very grateful to Dr. M. Steinbrück for the support of this work and to Dr. A. Boldyrev (IBRAE) for valuable discussions. We wish to thank Mrs. M. Schröder for the careful English review of this paper.

The main modelling work was performed during stay of one of the authors (M.V.) at FZK as the Guest Scientist. The IMF authorities are highly acknowledged for support of this visit.

## References

1. G. Schanz. "Recommendations and supporting information on the choice of zirconium oxidation models in severe accident codes". Wissenschaftliche Berichte, Report FZKA-6827, Karlsruhe, March 2003.
2. P. Hofmann, V. Noack, M.S. Veshchunov, A.V. Berdyshev, A.V. Boldyrev, L.W. Matveev, A.V. Palagin, V.E. Shestak. "Physico-chemical Behavior of Zircaloy Fuel Rod Cladding Tubes during LWR Severe Accident Reflood". Report FZKA 5846, Karlsruhe, May 1997.
3. J. Stuckert, U. Stegmaier. "Degradation of the cladding oxide layer under steam starvation conditions". 8<sup>th</sup> Internat. Quench Workshop, Karlsruhe, Oct. 29-31, 2002.
4. J. Stuckert, U. Stegmaier. "Behaviour of the cladding oxide layer under steam starvation conditions". 9<sup>th</sup> Internat. QUENCH Workshop, Karlsruhe, October 13-15, 2003. Proc. on CD-ROM.
5. J. Stuckert, U. Stegmaier. "Behaviour of oxide layer on Zircaloy cladding tube under steam starvation conditions. Tests at temperatures between 1250°C and 1450°C". 10<sup>th</sup> Internat. QUENCH Workshop, Karlsruhe, October 26-28, 2004. Proc. on CD-ROM.
6. J. Stuckert, M. Steinbrück, U. Stegmaier, A.V. Palagin. „On the thermo-physical properties of Zircaloy-4 and ZrO<sub>2</sub> at high temperatures". Report FZKA-6739, Karlsruhe, October 2002.
7. A.V. Palagin, J. Stuckert. Internal Report PSF 3392. Forschungszentrum Karlsruhe, June 2003.
8. R. Ruh and H.J. Garret, J. Am. Ceram. Soc. 50 (1967) 257.
9. M.C. Flemings, Solidification Processing. McGraw-Hill, New York, 1974.
10. T.F. Bowe, H.D. Brody, and M.C. Flemings, Trans.AIME. 227 (1963) 374.
11. M.S. Veshchunov, P. Hofmann, Modelling of the interactions between B<sub>4</sub>C and stainless steel at high temperatures. J. Nucl. Mater., 236 (1995) 72-91.
12. A.V. Berdyshev, L.V. Matveev, M.S. Veshchunov. "Development of the data base for the kinetic model of the Zircaloy4/steam oxidation at high temperatures (1000°C ≤ T ≤ 1825°C)". Preprint IBRAE-97-05, Moscow, 1997.
13. J. Stuckert, M. Steinbrück, U. Stegmaier. "Development of the metallic layer on the surface of oxidised Zry-cladding under steam starvation conditions". ISTC/WTZ Progress Meeting, Moscow, July 3-6, 2006. Proc. on CD-ROM.
14. P. Hofmann, J. Stuckert, A. Miassoedov, M.S. Veshchunov, A.V. Berdyshev, A.V. Boldyrev. "ZrO<sub>2</sub> dissolution by molten Zircaloy and cladding oxide shell failure. New experimental results and modelling". Report FZKA-6383, Karlsruhe, December 1999.

| Measured parameters |                                  |                                  |                             |                            |                                    | Calculated parameters           |                     |                       |
|---------------------|----------------------------------|----------------------------------|-----------------------------|----------------------------|------------------------------------|---------------------------------|---------------------|-----------------------|
| Test                | Oxidation duration at ~1450°C, s | Annealing duration at ~1450°C, s | Probe weight before test, g | Probe weight after test, g | H <sub>2</sub> measured with MS, g | Oxygen content in the sample, g | Oxygen content, wt% | Hydrogen absorbed, mg |
| 021009a             | 249                              | 0                                | 26.847                      | 27.887                     | 0.1225                             | 1.032                           | <b>3.7</b>          | 6.6                   |
| 021009b             | 242                              | 10800                            | 26.872                      | 27.903                     | 0.1273                             | 1.029                           | <b>3.7</b>          | 1.4                   |
| 021009c             | 755                              | 0                                | 26.859                      | 28.558                     | 0.2035                             | 1.690                           | <b>5.9</b>          | 7.8                   |
| 021010a             | 750                              | 10800                            | 26.862                      | 28.532                     | 0.2061                             | 1.667                           | <b>5.9</b>          | 2.4                   |
| 021010b             | 1816                             | 0                                | 26.823                      | 29.312                     | 0.3030                             | 2.481                           | <b>8.5</b>          | 7.1                   |
| 021010c             | 1994                             | 10800                            | 26.83                       | 29.537                     | 0.3355                             | 2.704                           | <b>9.2</b>          | 2.6                   |

Table 1. 2002 experiments in the Quench test rig at ~1450°C with an annealing duration of ~3h: test parameters and some measurement results.

| Test    | $\beta$ -Zr $\mu\text{m}$ | $\alpha$ -Zr(O) $\mu\text{m}$ | ZrO <sub>2</sub> $\mu\text{m}$ | Total cladding thickness, $\mu\text{m}$ | Metal precipitates in oxide layer, % |
|---------|---------------------------|-------------------------------|--------------------------------|---|--------------------------------------|
| 021009a | 431                       | 182                           | <b>134</b>                     | 747                                     |                                      |
| 02109b  | 0                         | 733                           | <b>0</b>                       | 733                                     |                                      |
| 02109c  | 177                       | 397                           | <b>228</b>                     | 802                                     |                                      |
| 021010a | 0                         | 602                           | <b>186</b>                     | 788                                     | <b>24</b>                            |
| 021010b | 0                         | 463                           | <b>412</b>                     | 875                                     |                                      |
| 021010c | 0                         | 324                           | <b>549</b>                     | 873                                     | <b>18</b>                            |

Table 2. 2002 experiments in the Quench test rig at ~1450°C with an annealing duration of ~3h: results of metallographic investigations.

| Test    | Oxidation duration at ~1450°C, s | Annealing duration at ~1450°C, s | $\beta$ -Zr $\mu\text{m}$ | $\alpha$ -Zr(O) $\mu\text{m}$ | ZrO <sub>2</sub> $\mu\text{m}$ | Total cladding thickness, $\mu\text{m}$ | Metal precipitates in oxide layer, % |
|---------|----------------------------------|----------------------------------|---------------------------|-------------------------------|--------------------------------|---|--------------------------------------|
| 030317b | 660                              | 600                              | 0                         | 586                           | <b>182</b>                     | 768                                     | <b>12</b>                            |
| 30416c  | 660                              | 1200                             | 0                         | 575                           | <b>191</b>                     | 766                                     | <b>21</b>                            |
| 30416a  | 660                              | 1800                             | 0                         | 616                           | <b>134</b>                     | 750                                     | <b>16</b>                            |
| 030318a | 640                              | 1821                             | 0                         | 537                           | <b>236</b>                     | 773                                     | <b>17</b>                            |
| 30416d  | 660                              | 3600                             | 0                         | 544                           | <b>215</b>                     | 759                                     | <b>19</b>                            |
| 030318b | 660                              | 5400                             | 0                         | 538                           | <b>230</b>                     | 767                                     | <b>22</b>                            |

Table 3. 2003 experiments in the Quench test rig at ~1450°C with a pre-oxidation duration of ~660 s: results of metallographic investigations.

| Test    | Oxidation duration at ~1450°C, s | Annealing duration at ~1450°C, s | $\beta$ -Zr $\mu\text{m}$ | $\alpha$ -Zr(O) $\mu\text{m}$ | ZrO <sub>2</sub> $\mu\text{m}$ | Total cladding thickness, $\mu\text{m}$ | Metallic precipitates in oxide layer, % |
|---------|----------------------------------|----------------------------------|---------------------------|-------------------------------|--------------------------------|---|---|
| 030319a | 1080                             | 300                              | 0                         | 497                           | <b>307</b>                     | 804                                     | <b>6</b>                                |
| 30422a  | 1080                             | 1200                             | 0                         | 515                           | <b>268</b>                     | 783                                     | <b>13</b>                               |
| 030319b | 1080                             | 1800                             | 0                         | 481                           | <b>338</b>                     | 819                                     | <b>15</b>                               |
| 30422b  | 1080                             | 2400                             | 0                         | 499                           | <b>299</b>                     | 798                                     | <b>24</b>                               |
| 030319c | 1080                             | 3600                             | 0                         | 428                           | <b>407</b>                     | 834                                     | <b>19</b>                               |
| 30416b  | 1080                             | 5400                             | 0                         | 434                           | <b>371</b>                     | 805                                     | <b>18</b>                               |

Table 4. 2003 experiments in the Quench test rig at ~1450°C with a pre-oxidation duration of ~1080 s: results of metallographic investigations.

| Test   | Oxidation phase    | Cladding layer thickness |                           |                |                  |              |                   |                   |
|--------|--------------------|--------------------------|---------------------------|----------------|------------------|--------------|-------------------|-------------------|
|        | Starvation phase   |                          | Start of starvation phase |                |                  | Final status |                   |                   |
|        | Duration, min.     |                          | $\beta$ -Zr               | $\alpha$ Zr(O) | ZrO <sub>2</sub> | $\beta$ -Zr  | $\alpha$ -Zr(O)   | ZrO <sub>2</sub>  |
| 30416c | 13.5               | Experimental data        | --                        | --             | --               | 0            | <b>575</b>        | <b>191</b>        |
|        | 19.5               | Calculation (TCi data)   | 181                       | 385            | 249              | 0            | <b>614</b>        | <b>184</b>        |
| 30416a | 13.5               | Experimental data        | --                        | --             | --               | 0            | <b>616</b>        | <b>134</b>        |
|        | 29.5               | Calculation (TCi data)   | 195                       | 372            | 246              | 0            | <b>629</b>        | <b>161</b>        |
| 30416d | 13.5               | Experimental data        | --                        | --             | --               | 0            | <b><u>544</u></b> | <b><u>215</u></b> |
|        | <b><u>59.5</u></b> | Calculation (TCi data)   | 164                       | 397            | 256              | 0            | <b><u>629</u></b> | <b><u>161</u></b> |
| 30422a | 20.5               | Experimental data        | --                        | --             | --               | 0            | <b>515</b>        | <b>268</b>        |
|        | 19.5               | Calculation (TCi data)   | 9                         | 511            | 315              | 0            | <b>554</b>        | <b>275</b>        |
| 30422b | 20.5               | Experimental data        | --                        | --             | --               | 0            | <b>499</b>        | <b>299</b>        |
|        | 39.5               | Calculation (TCi data)   | 0                         | 513            | 325              | 0            | <b>551</b>        | <b>279</b>        |
| 30416b | 20.5               | Experimental data        | --                        | --             | --               | 0            | <b><u>434</u></b> | <b><u>371</u></b> |
|        | <b><u>89.5</u></b> | Calculation (TCi data)   | 0                         | 514            | 324              | 0            | <b><u>558</u></b> | <b><u>261</u></b> |

Table 5. Comparison of the SVECHA calculation results with experimental data.

| Test parameters |                       |                       | Sample weighing              |                             |                                 | Metallographic post-test investigation |                                |                                  |                                  |  |
|-----------------|-----------------------|-----------------------|------------------------------|-----------------------------|---------------------------------|--|--------------------------------|----------------------------------|----------------------------------|--|
| Test            | Oxidation duration, s | Annealing duration, s | Sample weight before test, g | Sample weight after test, g | $\Delta m$ (~oxygen content), % | $\beta$ -Zr, $\mu\text{m}$             | $\alpha$ -Zr(O), $\mu\text{m}$ | ZrO <sub>2</sub> , $\mu\text{m}$ | Cladding thickness $\mu\text{m}$ | Metallic precipitates in ZrO <sub>2</sub> , area % |
| 040908a         | 700                   | 0                     | 26.6849                      | 27.6146                     | <b>3.4</b>                      | 438                                    | 170                            | <b>180</b>                       | 788                              |  |
| 040906a         | 624                   | 2470                  | 26.7193                      | 27.677                      | <b>3.5</b>                      | 216                                    | 453                            | <b>96</b>                        | 765                              | <b>5</b>   |
| 040907b         | 720                   | 5400                  | 26.6717                      | 27.6963                     | <b>3.7</b>                      | 0                                      | 665                            | <b>80</b>                        | 745                              | <b>14</b>  |
| 040907a         | 720                   | 9000                  | 26.666                       | 27.7148                     | <b>3.8</b>                      | 0                                      | 654                            | <b>75</b>                        | 729                              | <b>10</b>  |
| 040909b         | 1180                  | 0                     | 26.6849                      | 27.8963                     | <b>4.3</b>                      | 354                                    | 223                            | <b>240</b>                       | 817                              |  |
| 040908d         | 1188                  | 2407                  | 26.7759                      | 28.1076                     | <b>4.7</b>                      | 0                                      | 620                            | <b>181</b>                       | 801                              | <b>4</b>   |
| 040908b         | 1186                  | 5410                  | 26.6973                      | 27.8853                     | <b>4.3</b>                      | 0                                      | 645                            | <b>118</b>                       | 763                              | <b>4</b>   |
| 040909a         | 1190                  | 9006                  | 26.8061                      | 28.1296                     | <b>4.7</b>                      | 0                                      | 606                            | <b>155</b>                       | 761                              | <b>8</b>   |

Table 6. Two series of 2004 experiments in the Quench test rig at 1270 °C...1320 °C.

| Measured parameters |                      |                      |                              |                             | Calculated parameters           |                     |
|---------------------|----------------------|----------------------|------------------------------|-----------------------------|---------------------------------|---------------------|
| Test                | Oxidation duration s | Annealing duration s | Sample weight before test, g | Sample weight after test, g | Oxygen content in the sample, g | Oxygen content, wt% |
| 030912 rod          | 660                  | 5400                 | 12.4968                      | 12.8611                     | 0.3643                          | <b>2.8</b>          |
| 030912 tube         | 660                  | 5400                 | 6.9778                       | 7.3363                      | 0.3585                          | <b>4.9</b>          |
| 040513 rod          | 1080                 | 5400                 | 11.8529                      | 12.248                      | 0.3951                          | <b>3.2</b>          |
| 040513 tube         | 1080                 | 5400                 | 6.9902                       | 7.6392                      | 0.649                           | <b>8.5</b>          |
| 040517 rod          | 1080                 | 1200                 | 11.8251                      | 12.2506                     | 0.4255                          | <b>3.5</b>          |
| 040517 tube         | 1080                 | 1200                 | 6.976                        | 7.5868                      | 0.6108                          | <b>8.1</b>          |

Table 7. 2003 and 2004 BOX experiments at 1400°C and 1450 °C, respectively, with different oxidation and annealing durations.

| Test    | $\beta$ -Zr $\mu\text{m}$ | $\alpha$ -Zr(O) $\mu\text{m}$ | ZrO <sub>2</sub> $\mu\text{m}$ | Outer metal surface layer, $\mu\text{m}$ |
|---------|---------------------------|-------------------------------|--------------------------------|--|
| 030912r | 4182                      | 943                           | 0                              |  |
| 030912t | 0                         | 685                           | 96                             | <b>16</b>                                |
| 040513r | 3720                      | 1405                          | 0                              |  |
| 040513t | 0                         | 378                           | 356                            | <b>7</b>                                 |
| 040517r | 4333                      | 637                           | 155                            |  |
| 040517t | 0                         | 284                           | 375                            |  |

Table 8. 2003 and 2004 BOX experiments at 1400°C and 1450 °C, respectively: results of metallographic investigations.

| Measured parameters |          |                                 |                                  |                              |                             | Calculated parameters           |                     |
|---------------------|----------|---------------------------------|----------------------------------|------------------------------|-----------------------------|---------------------------------|---------------------|
| Test                | Material | Oxidation duration at 1350°C, s | Annealing duration at ~1350°C, s | Sample weight before test, g | Sample weight after test, g | Oxygen content in the sample, g | Oxygen content, wt% |
| 060125b1            | Zry-4    | 720                             | 0                                | 2.9899                       | 3.4016                      | 0.4117                          | <b>12.1</b>         |
| 060125b2            | Zry-4    | 750                             | 9000                             | 2.9958                       | 3.4234                      | 0.4276                          | <b>12.5</b>         |
| 060124c1            | Duplex   | 720                             | 0                                | 3.0518                       | 3.4474                      | 0.3956                          | <b>11.5</b>         |
| 060124c2            | Duplex   | 720                             | 9000                             | 3.0333                       | 3.4375                      | 0.4042                          | <b>11.8</b>         |
| 060125a1            | E-110    | 720                             | 0                                | 2.3531                       | 2.7055                      | 0.3524                          | <b>13.0</b>         |
| 060125a2            | E-110    | 720                             | 9000                             | 2.3512                       | 2.7066                      | 0.3554                          | <b>13.1</b>         |

Table 9. 2006 isothermal BOX experiments at 1350 °C with an oxidation of ~12 min in steam (60 g/h) and annealing of 150 min in argon (50 l/h).

| Test     | Material | Outer ZrO <sub>2</sub> μm | α-Zr(O) μm | Internal ZrO <sub>2</sub> μm | Outer metal surface layer, μm |
|----------|----------|---------------------------|------------|------------------------------|-------------------------------|
| 060125b1 | Zry-4    | 142                       | 544        | 137                          |                               |
| 060125b2 | Zry-4    | 150                       | 553        | 110                          | <b>13</b>                     |
| 060124c1 | Duplex   | 149                       | 566        | 132                          |                               |
| 060124c2 | Duplex   | 109                       | 582        | 108                          | <b>8</b>                      |
| 060125a1 | E-110    | 170                       | 487        | 132                          |                               |
| 060125a2 | E-110    | 161                       | 485        | 115                          | <b>9</b>                      |

Table 10. 2006 isothermal BOX experiments at 1350 °C: results of metallographic investigations.

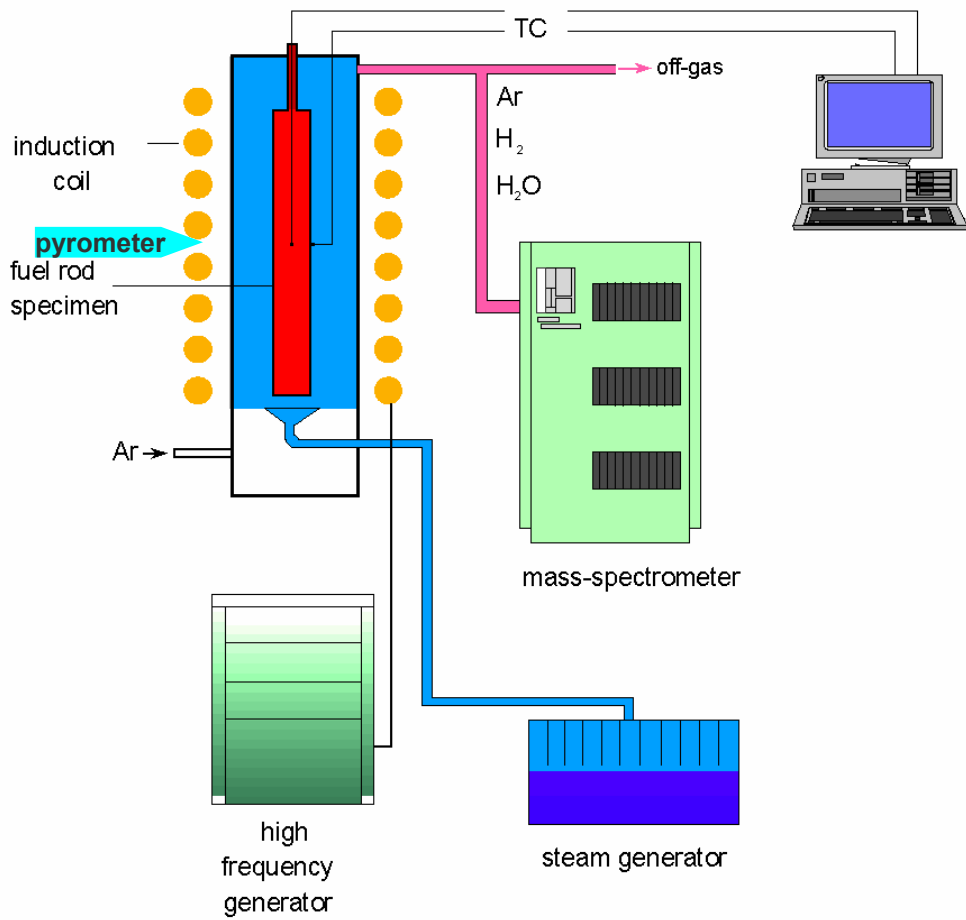


Fig. 1. Schematic representation of the QUENCH-SR test rig.

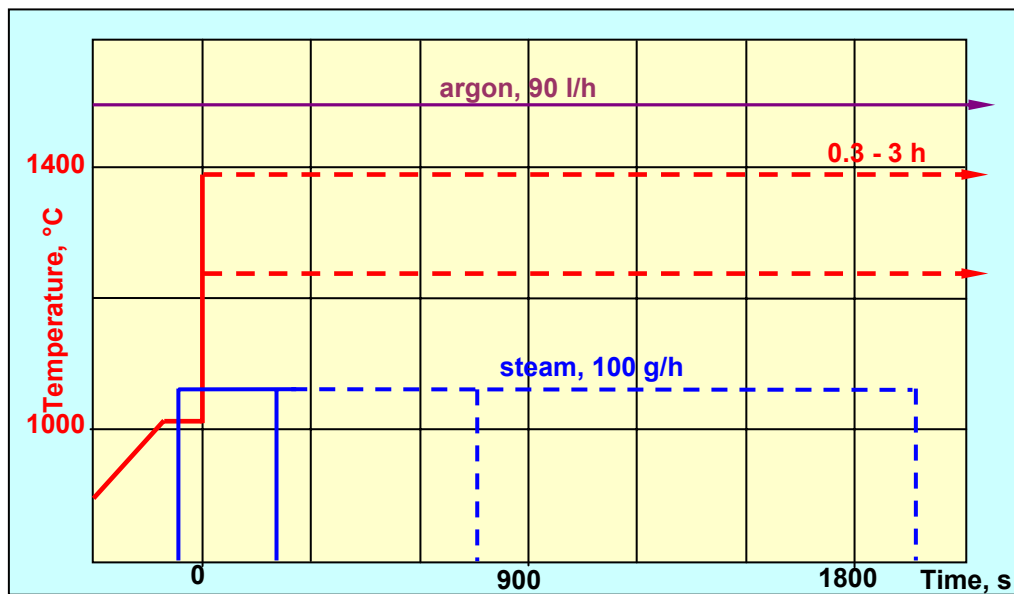


Fig. 2. Typical test conduct.

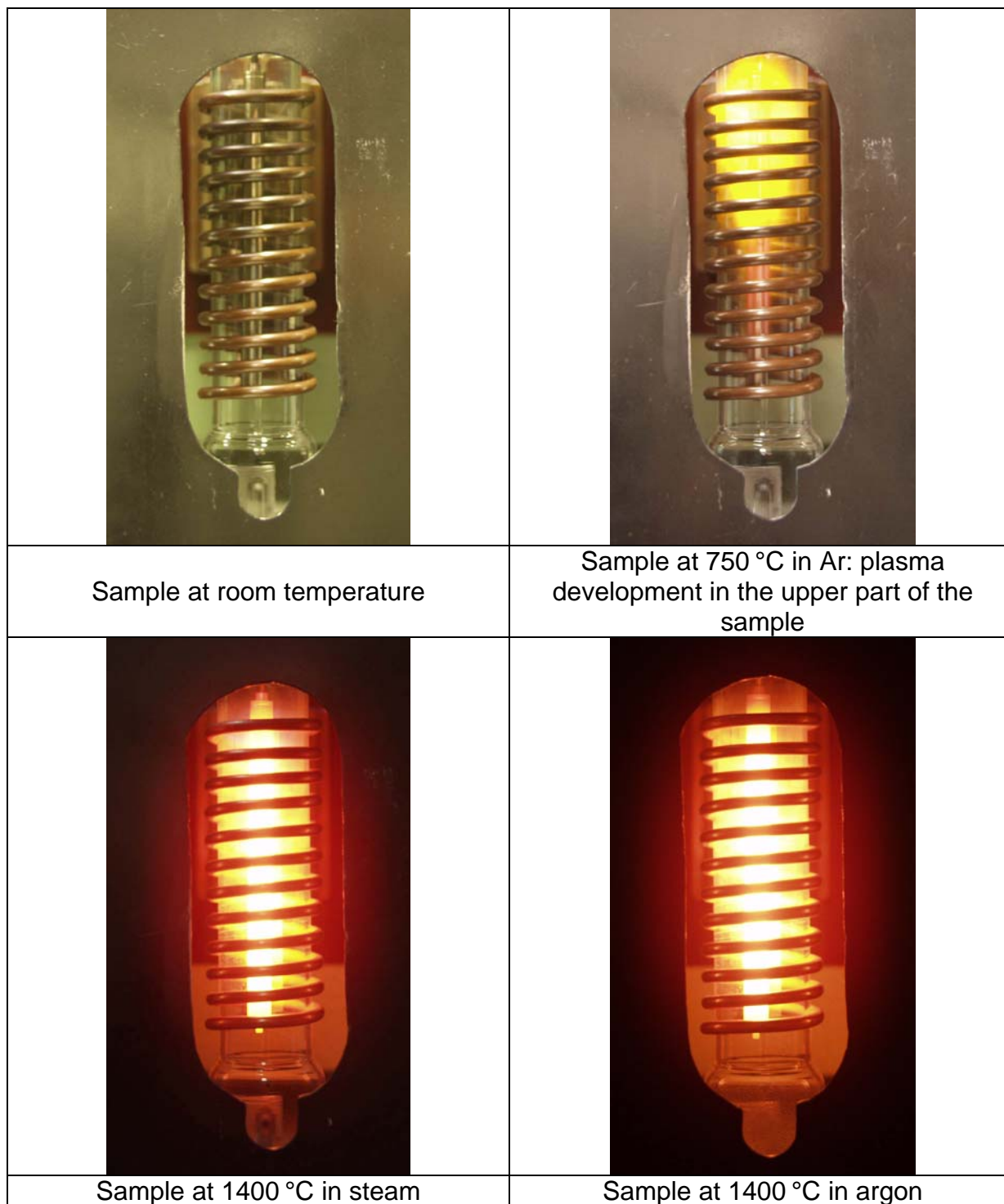


Fig. 3. Sample in the inductive furnace at different temperatures.

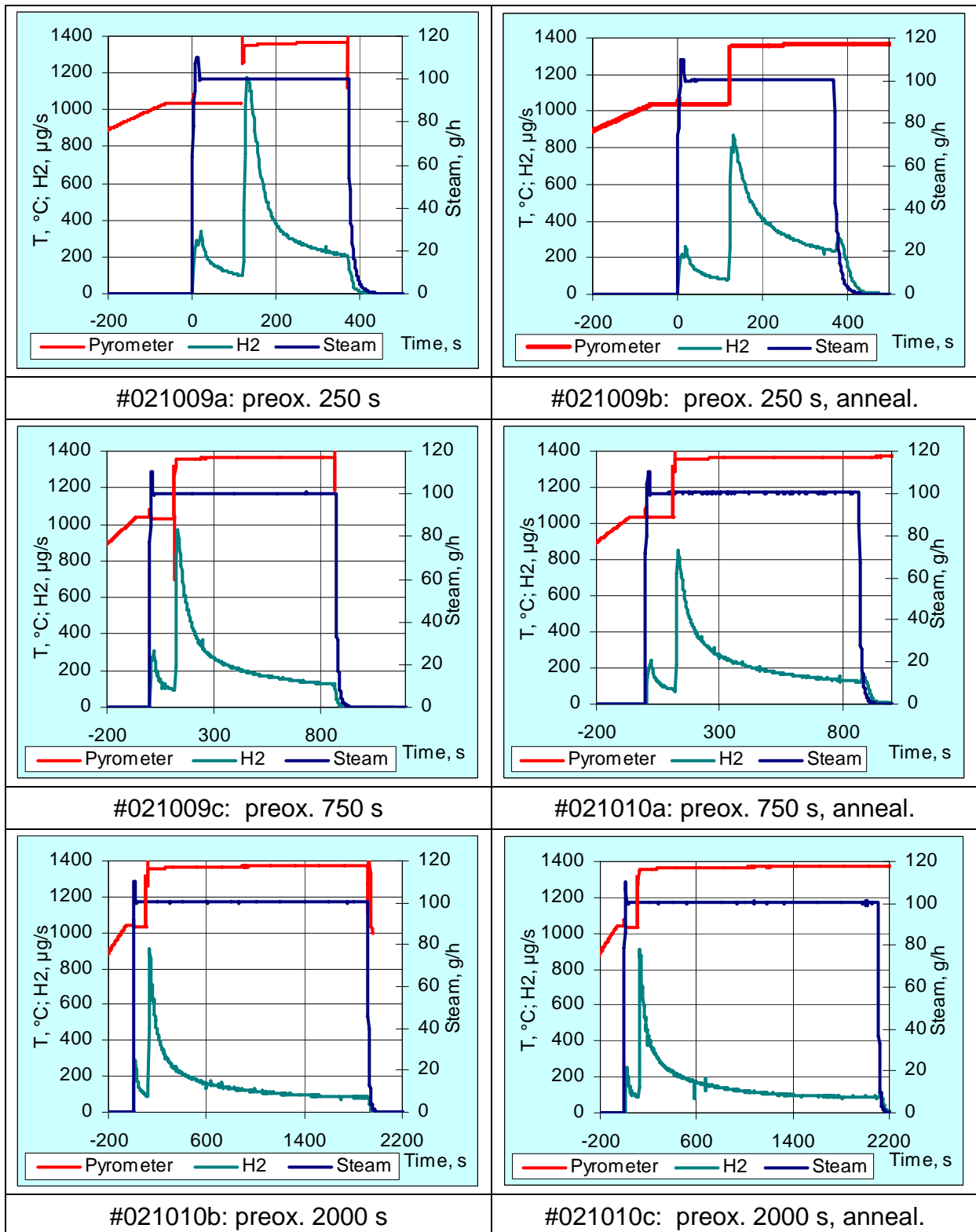
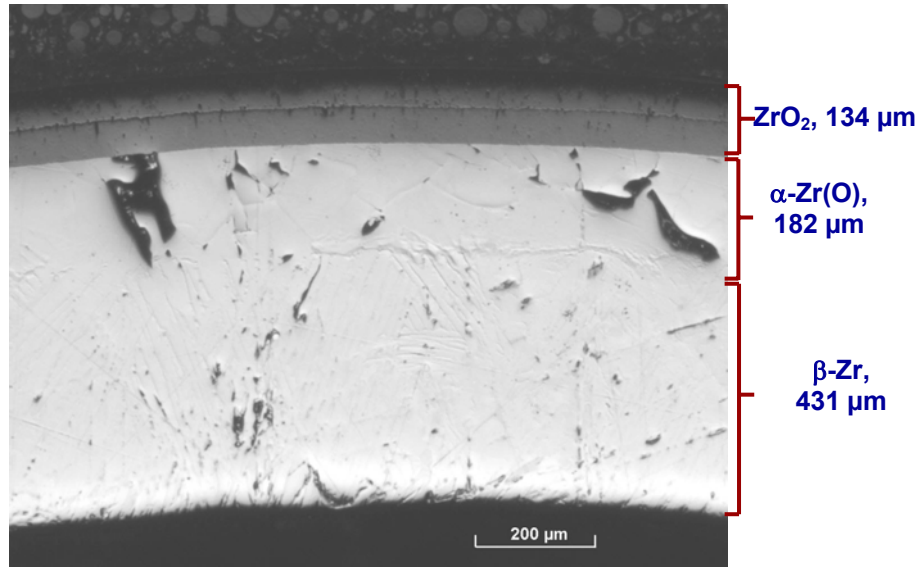


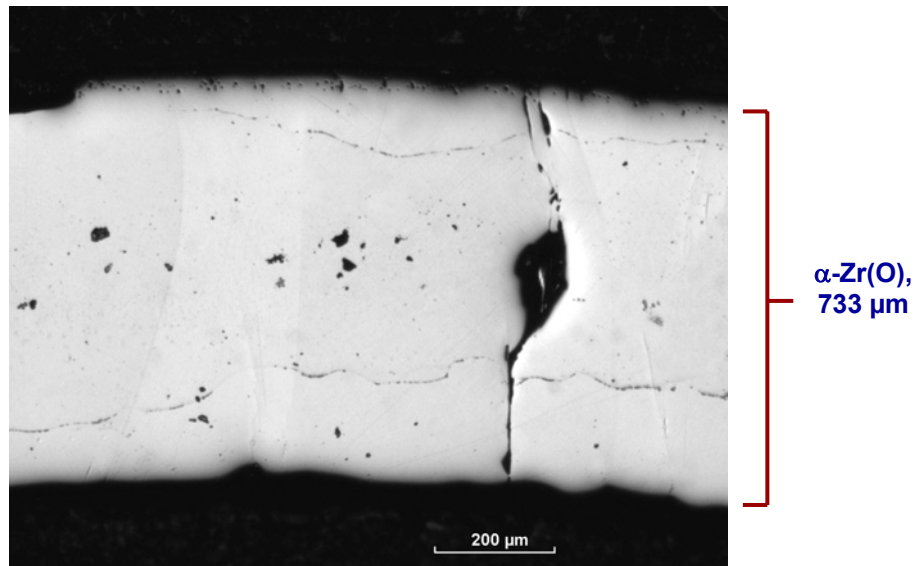
Fig. 4. 2002 experiments in the Quench test rig with different pre-oxidation durations and an annealing time of ~3 h: pyrometer ( $\epsilon=0.7$ ), steam supply, and hydrogen release diagrams (mass spectrometer data)



Fig. 5. 2002 experiments in the Quench test rig with different pre-oxidation durations and an annealing time of ~3 h: external view of the Zry-4 claddings pre-oxidised in steam and then annealed in argon at a temperature of ~1475 °C measured with a pyrometer on the cladding surface.

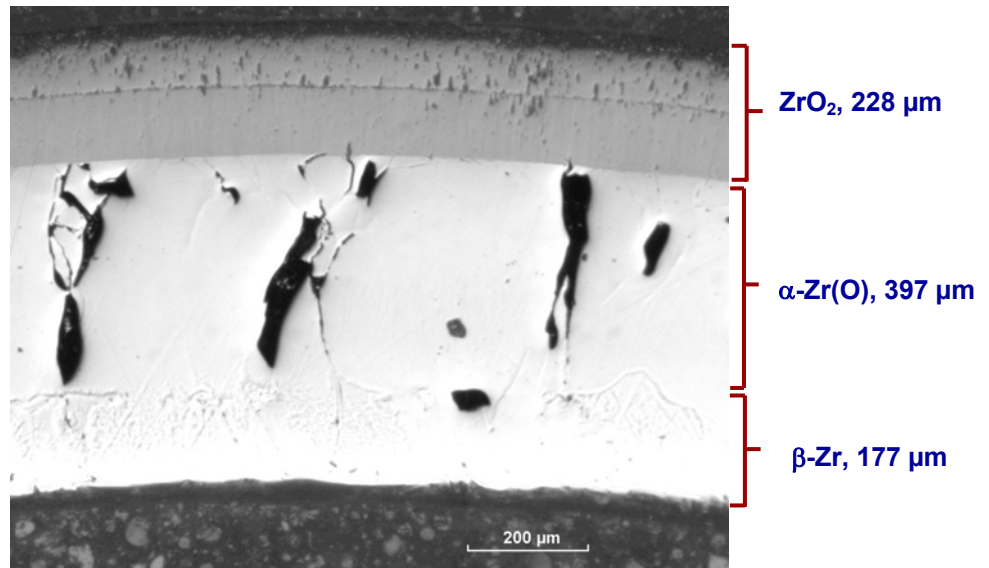


reference sample: conventional oxide layer on the outer surface

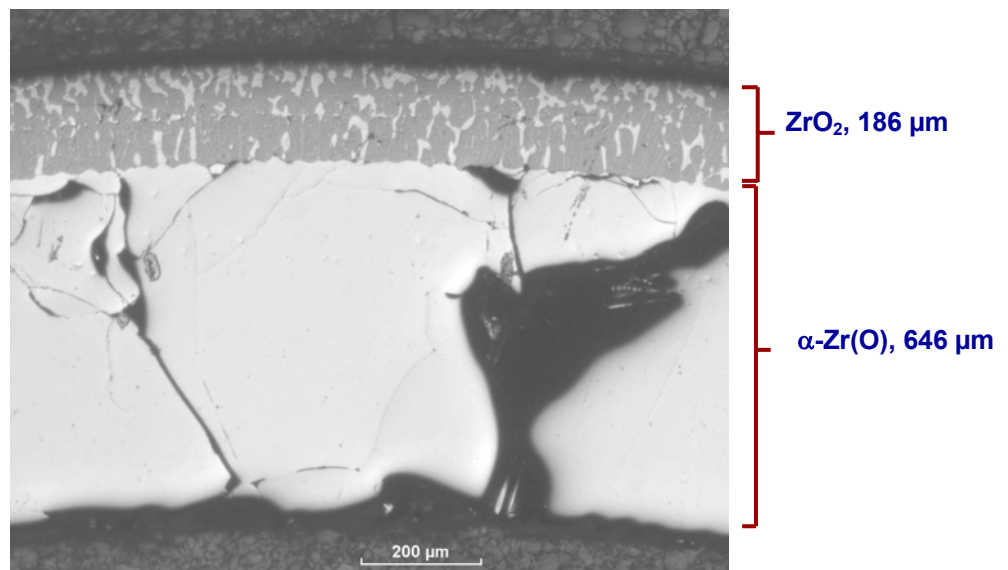


annealed sample: homogenisation of the  $\alpha$ -layer during dissolution of the oxide layer

Fig. 6. Cross-sections at middle elevation of the Zry-4 specimens pre-oxidised at  $\sim 1475$  °C for 250 s (upper photo) and pre-oxidised at  $\sim 1475$  °C for 250 s and then annealed at  $\sim 1475$  °C for 10800 s (lower photo).

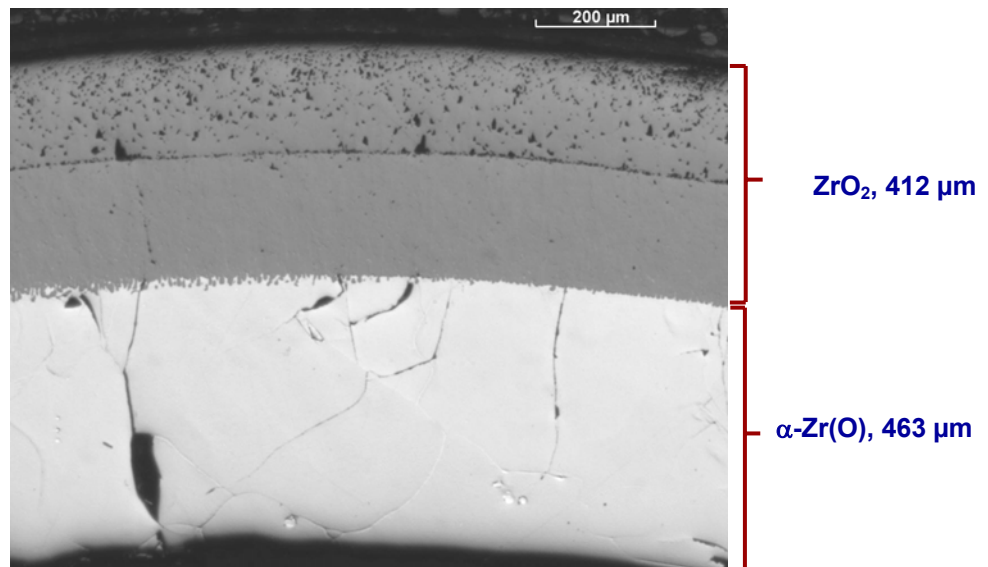


reference sample: oxide layer without metallic precipitates

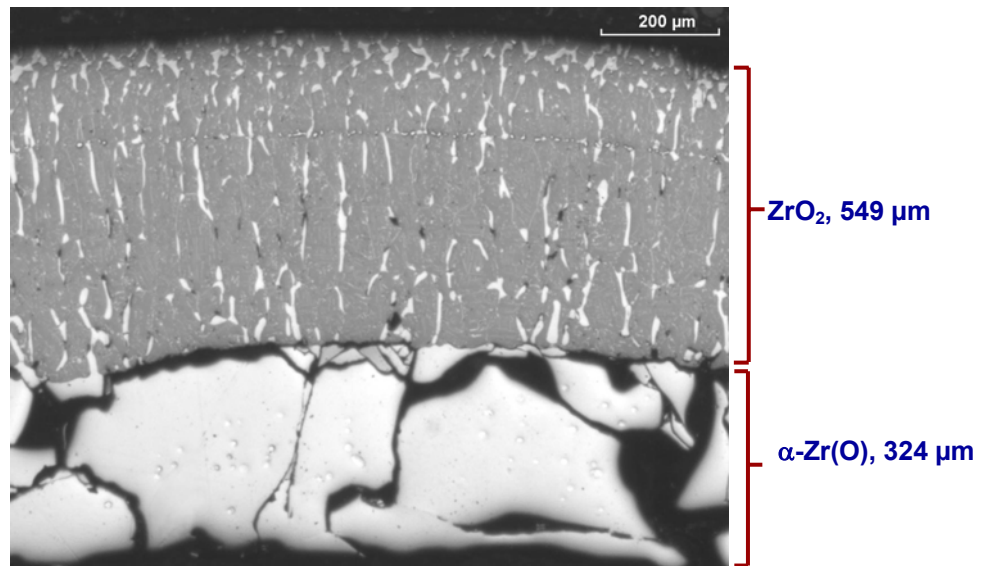


annealed sample: development of α-Zr(O) precipitates inside the thinning oxide layer

Fig. 7. Cross-sections at middle elevation of the Zry-4 specimens pre-oxidised at ~1475 °C for 750 s (upper photo) and pre-oxidised at ~1475 °C for 750 s and then annealed at ~1475 °C for 10800 s (lower photo).



reference sample: oxide layer without metallic precipitates



annealed sample: development of α-Zr(O) precipitates inside the thinning oxide layer

Fig. 8. Cross-sections at middle elevation of the Zry-4 specimens pre-oxidised at ~1475 °C for 2000 s (upper photo) and pre-oxidised at ~1475 °C for 2000 s and then annealed at ~1475 °C for 10800 s (lower photo).

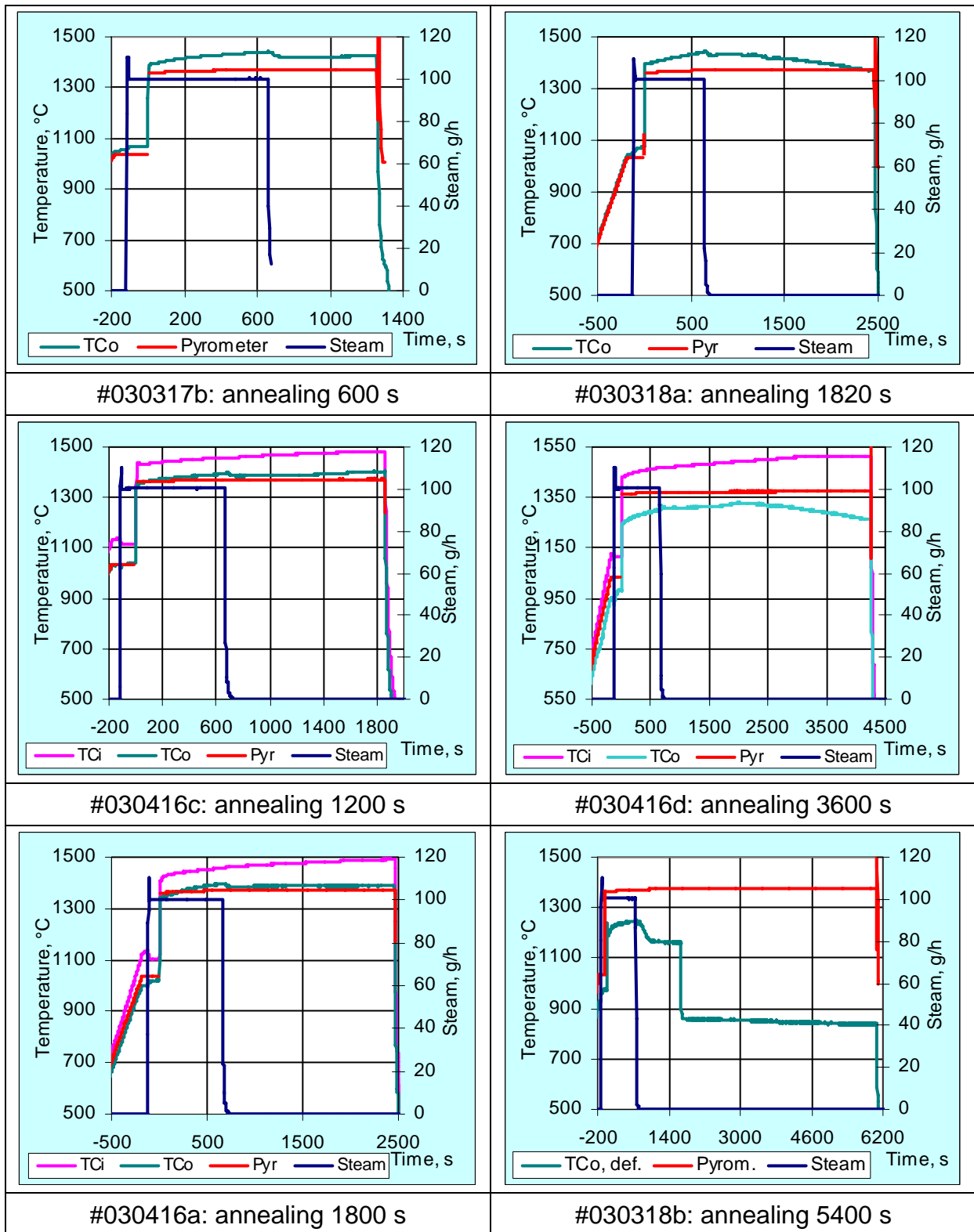


Fig. 9. 2003 experiments in the Quench test rig with a pre-oxidation duration of 660 s and different annealing durations: pyrometer ( $\epsilon=0.65$ ), middle thermocouples (inside TCi and outside TCo), and steam supply diagrams.

pre-oxidation duration: 660 s (initial  $ZrO_2$  ~250  $\mu m$ )

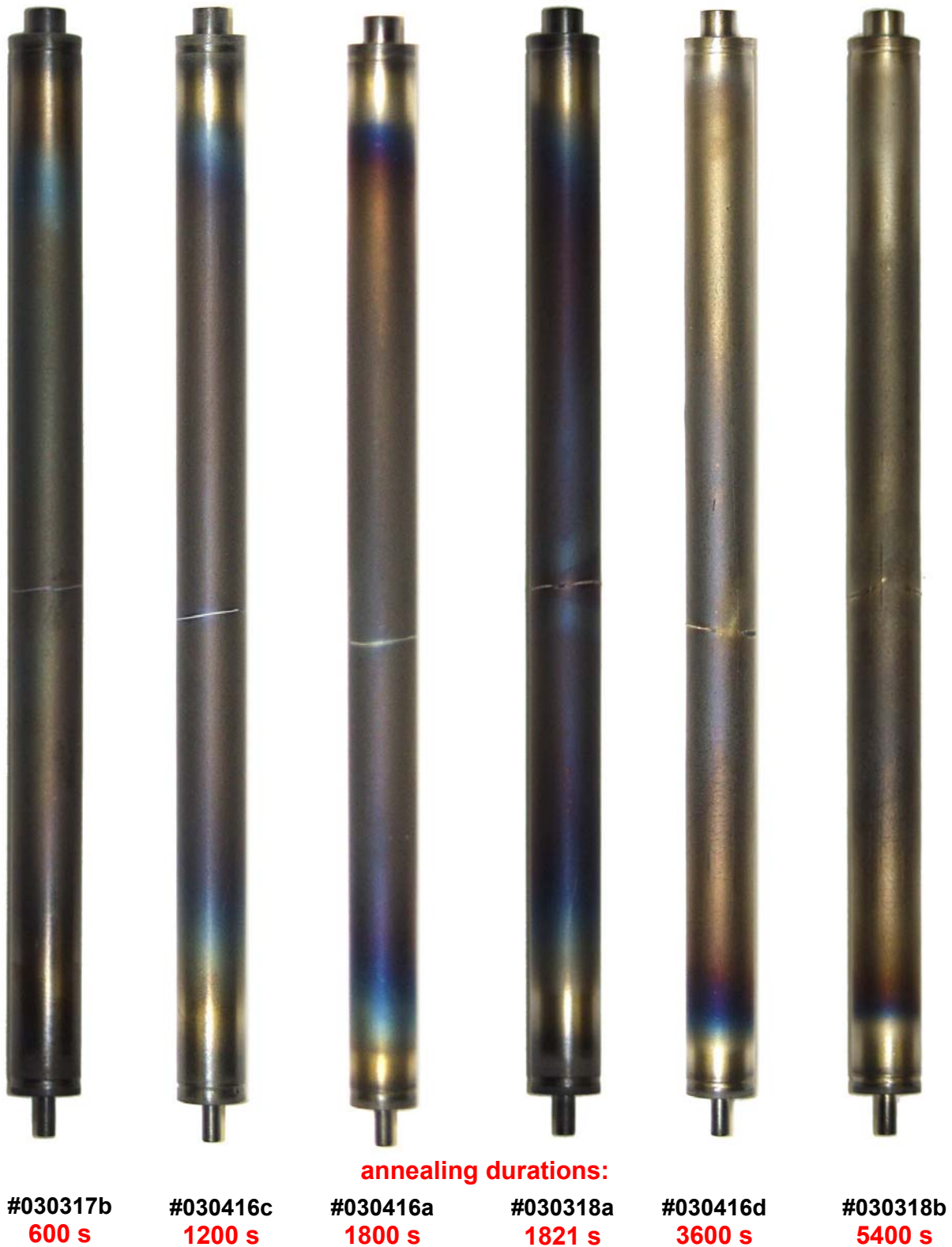


Fig. 10. 2003 experiments in the Quench test rig with a pre-oxidation of ~11 min. and different annealing durations: outer view of the Zry-4 claddings pre-oxidised in steam and then annealed in argon at a temperature of ~1475 °C measured with a TC fixed to the cladding.

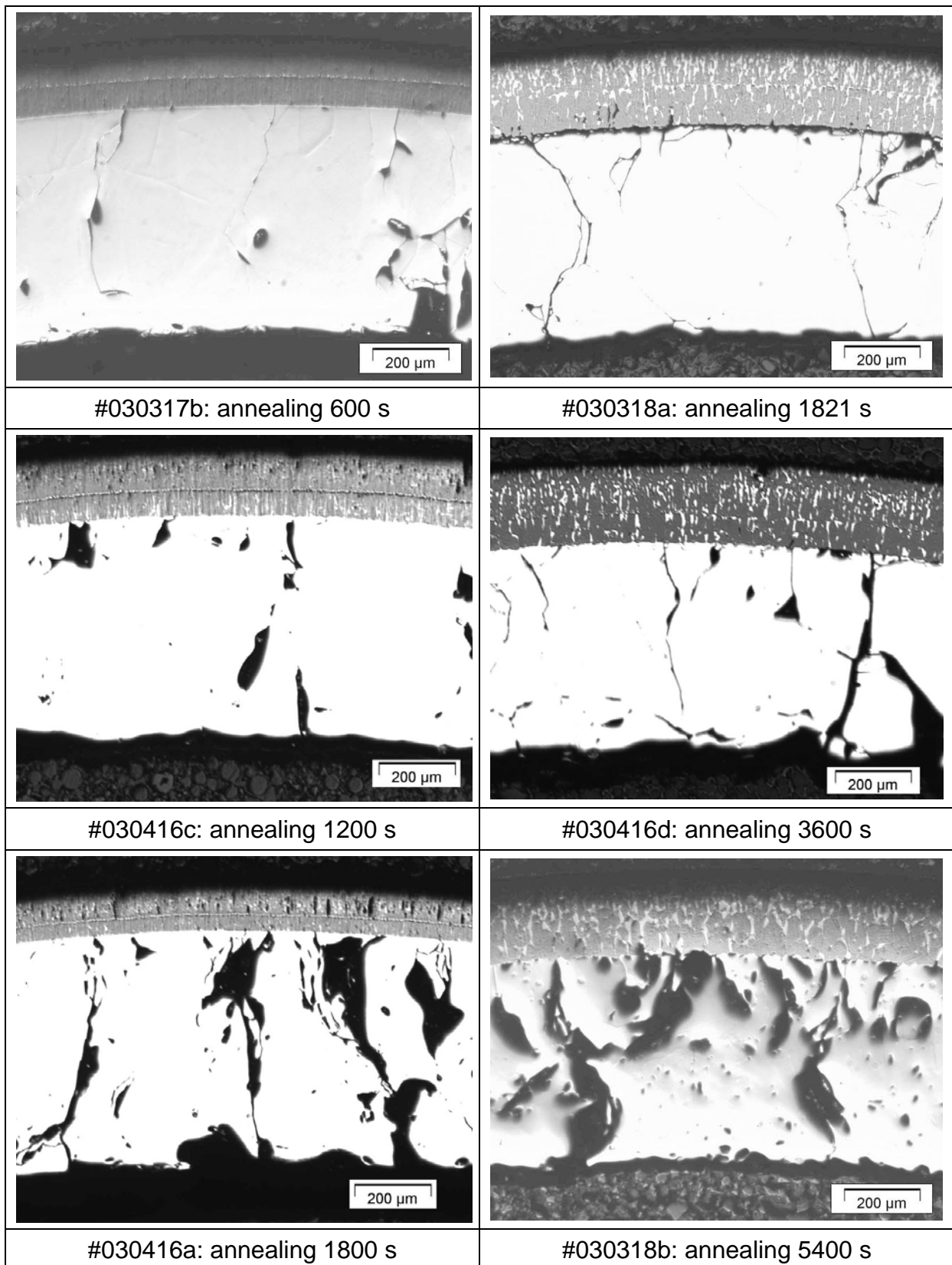


Fig. 11. 2003 experiments in the Quench test rig with a pre-oxidation of ~11 min. and different annealing durations: cladding cross-section.

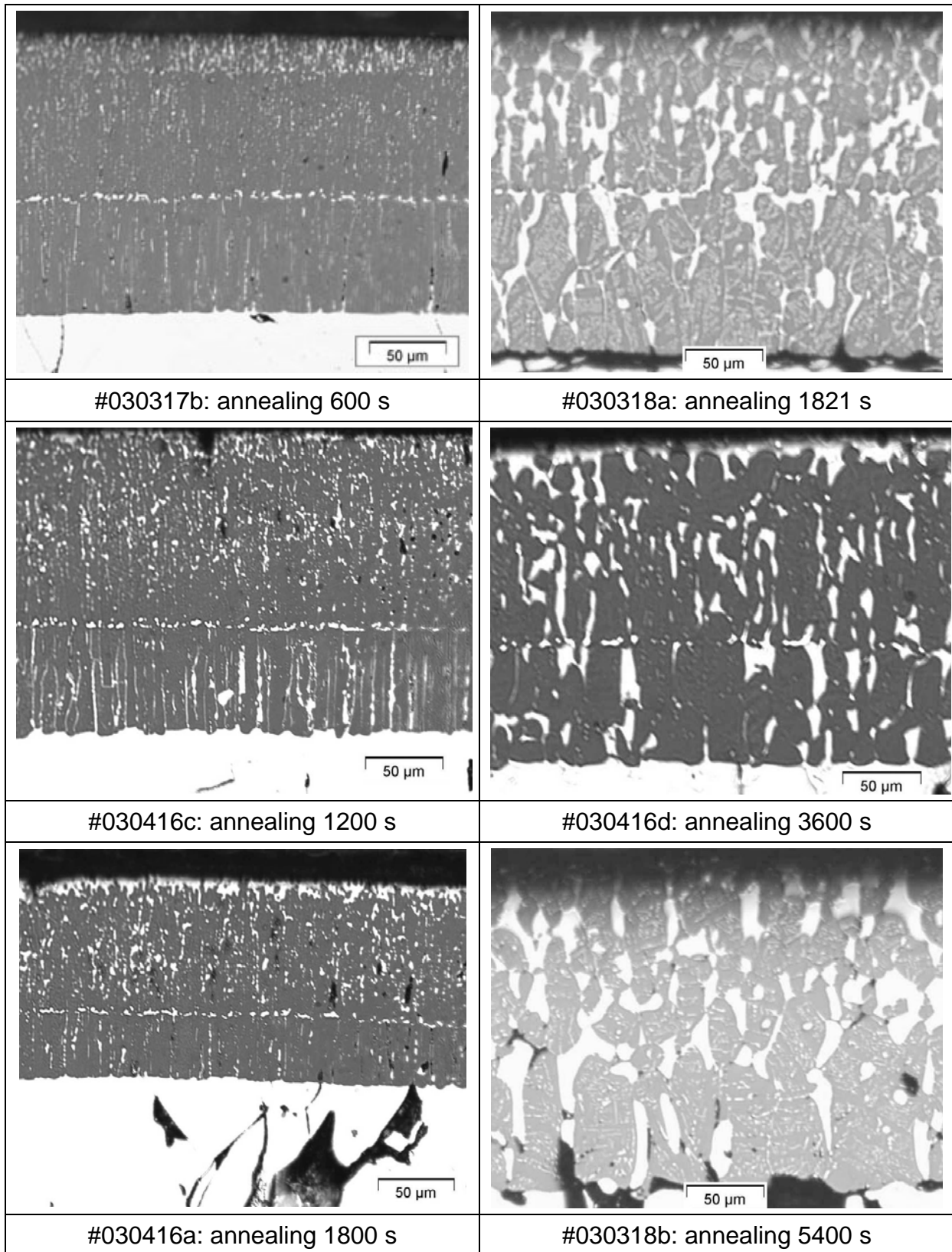
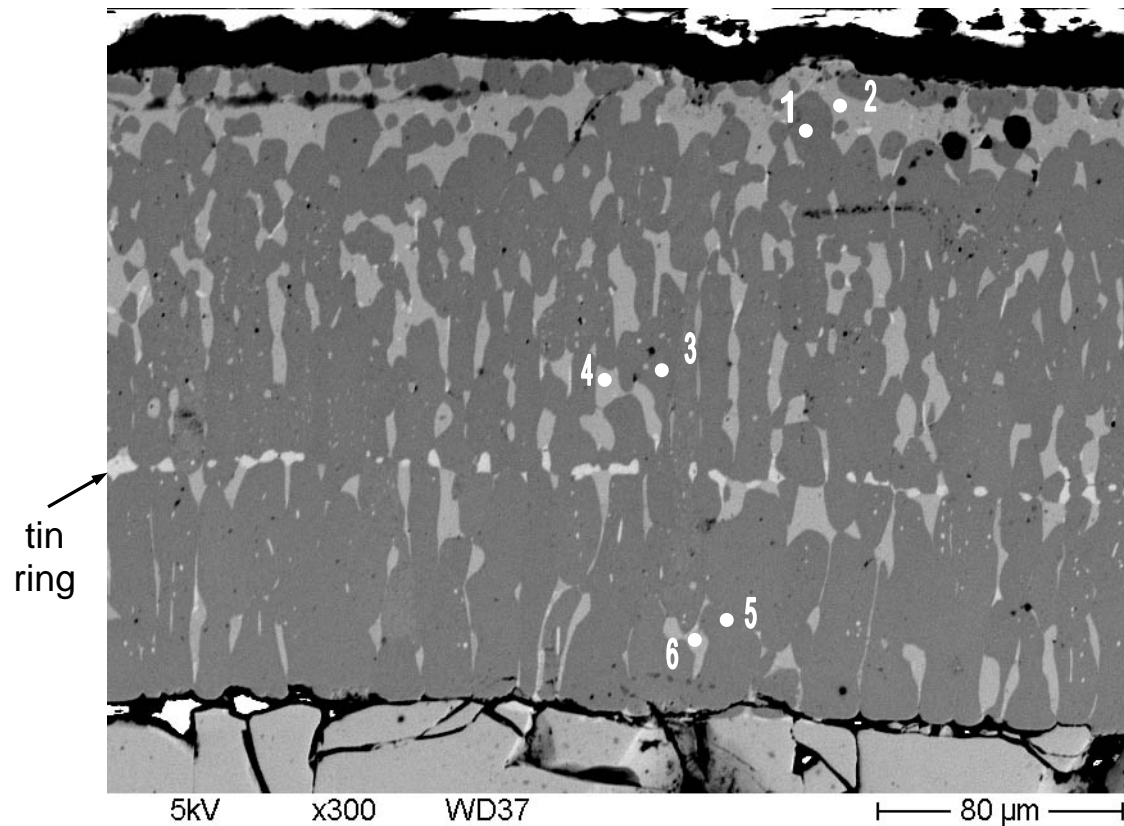


Fig. 12. 2003 experiments in the Quench test rig with a pre-oxidation of ~11 min. and different annealing durations: oxide layer structure. Coagulation of  $\alpha$ -Zr(O) precipitates and formation of the outer  $\alpha$ -Zr(O) surface layer.



| Position | Zr     | Oxygen |                    |
|----------|--------|--------|--------------------|
| Index    | Atom % | Atom % |                    |
| 1        | 34     | 66     | ZrO <sub>2-x</sub> |
| 2        | 75     | 25     | α-Zr(O)            |
| 3        | 36     | 64     | ZrO <sub>2-x</sub> |
| 4        | 72     | 28     | α-Zr(O)            |
| 5        | 37     | 63     | ZrO <sub>2-x</sub> |
| 6        | 69     | 31     | α-Zr(O)            |

Fig. 13. 2003 experiments in the Quench test rig: test with an annealing duration of 3600 s and an initial oxide layer of ~200 μm. EDX analysis of outer layers on the cladding.

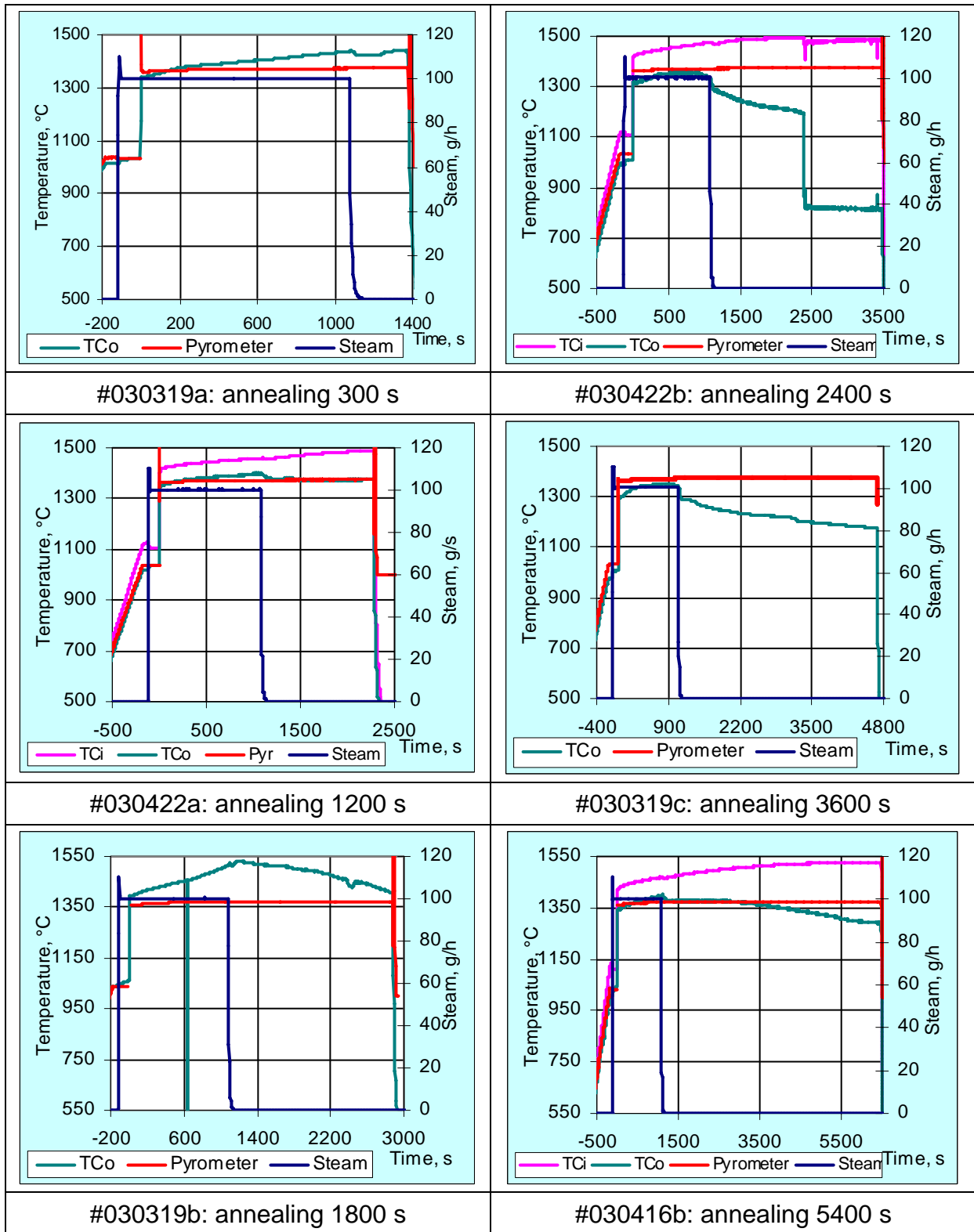


Fig. 14. 2003 experiments in the Quench test rig with a pre-oxidation duration of 1080 s and different annealing durations: pyrometer ( $\epsilon=0.65$ ), middle thermocouples (inside TCi and outside TCo), and steam supply diagrams

pre-oxidation duration: 1080 s (initial  $ZrO_2$  ~320  $\mu m$ )

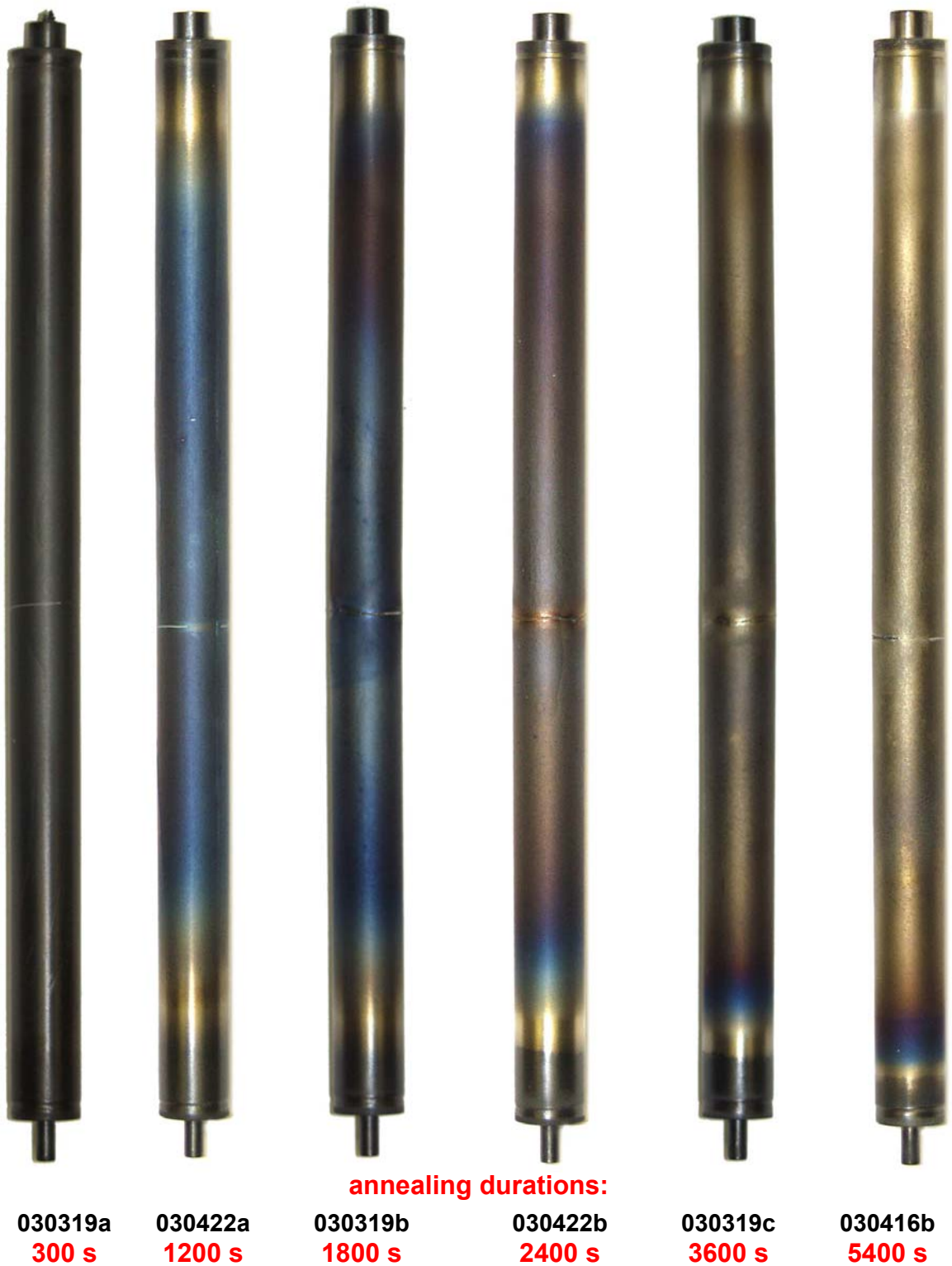


Fig. 15. 2003 experiments in the Quench test rig with a pre-oxidation of ~18 min. and different annealing durations: outer view of the Zry-4 claddings pre-oxidised in steam and then annealed in argon at a temperature of ~1475 °C measured with a TC fixed to the cladding.

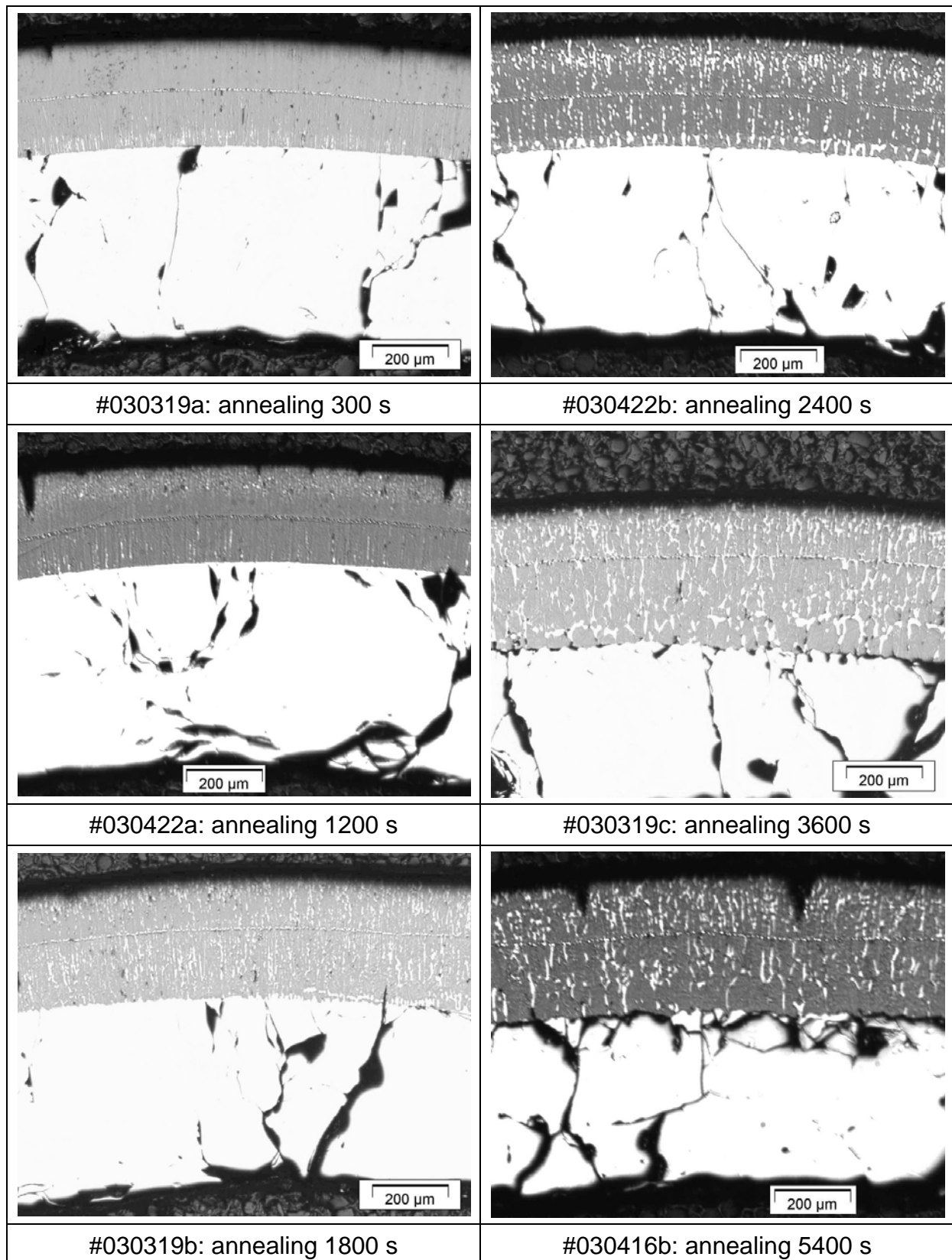


Fig. 16. 2003 experiments in the Quench test rig with a pre-oxidation of ~18 min. and different annealing durations: cladding cross-section.

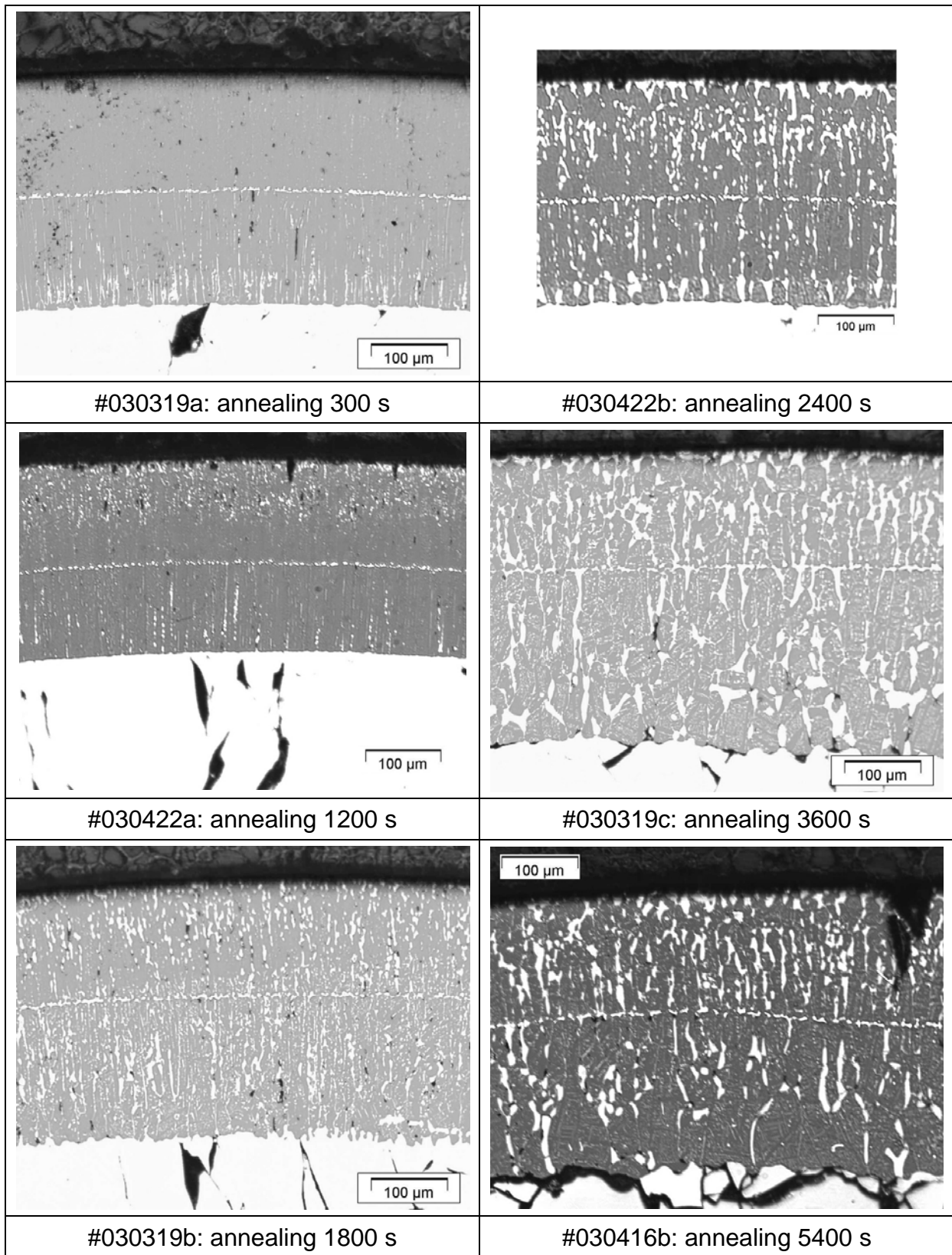


Fig. 17. 2003 experiments in the Quench test rig with a pre-oxidation of ~18 min. and different annealing durations: oxide layer structure. Coagulation of  $\alpha$ -Zr(O) precipitates.

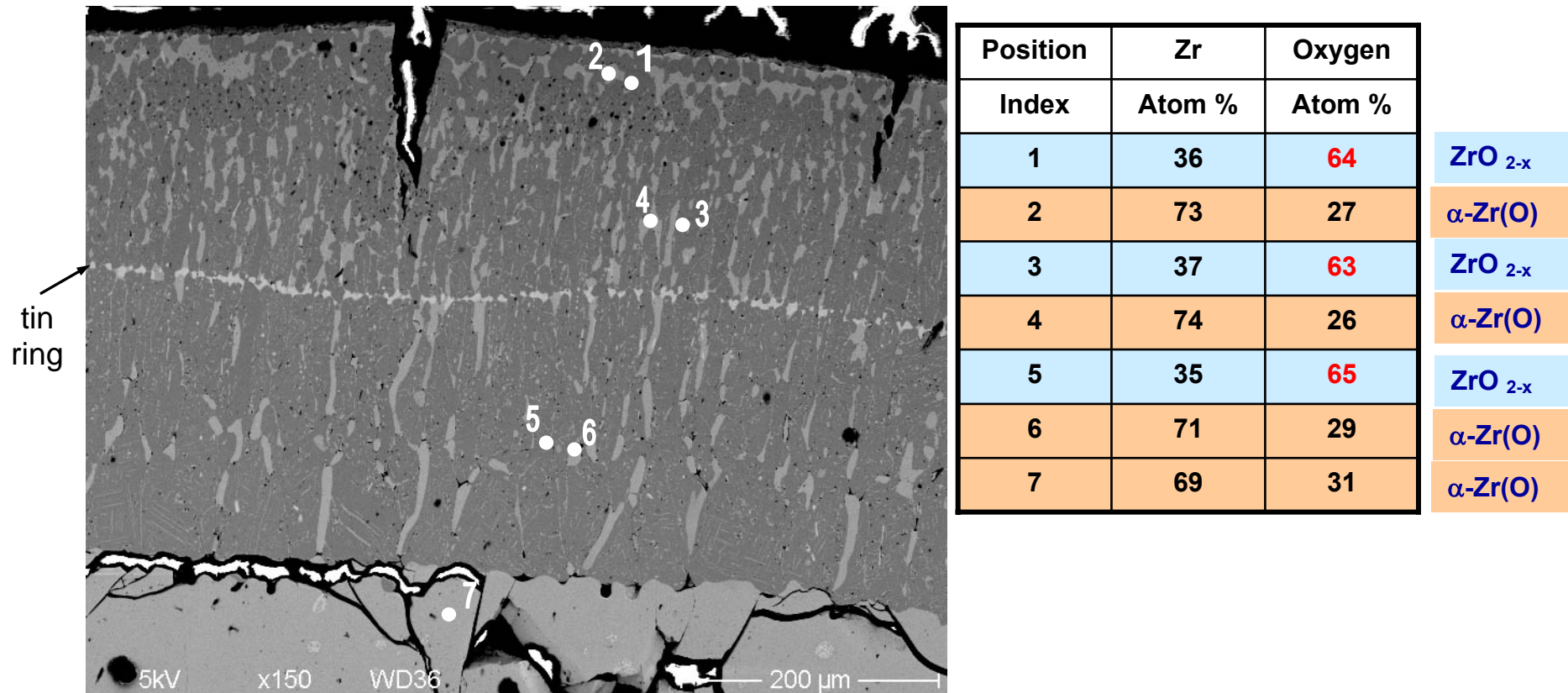


Fig. 18. 2003 experiments in the Quench test rig: test with an annealing duration of 5400 s and an initial oxide layer of ~320 μm. EDX analysis of outer layers on the cladding.

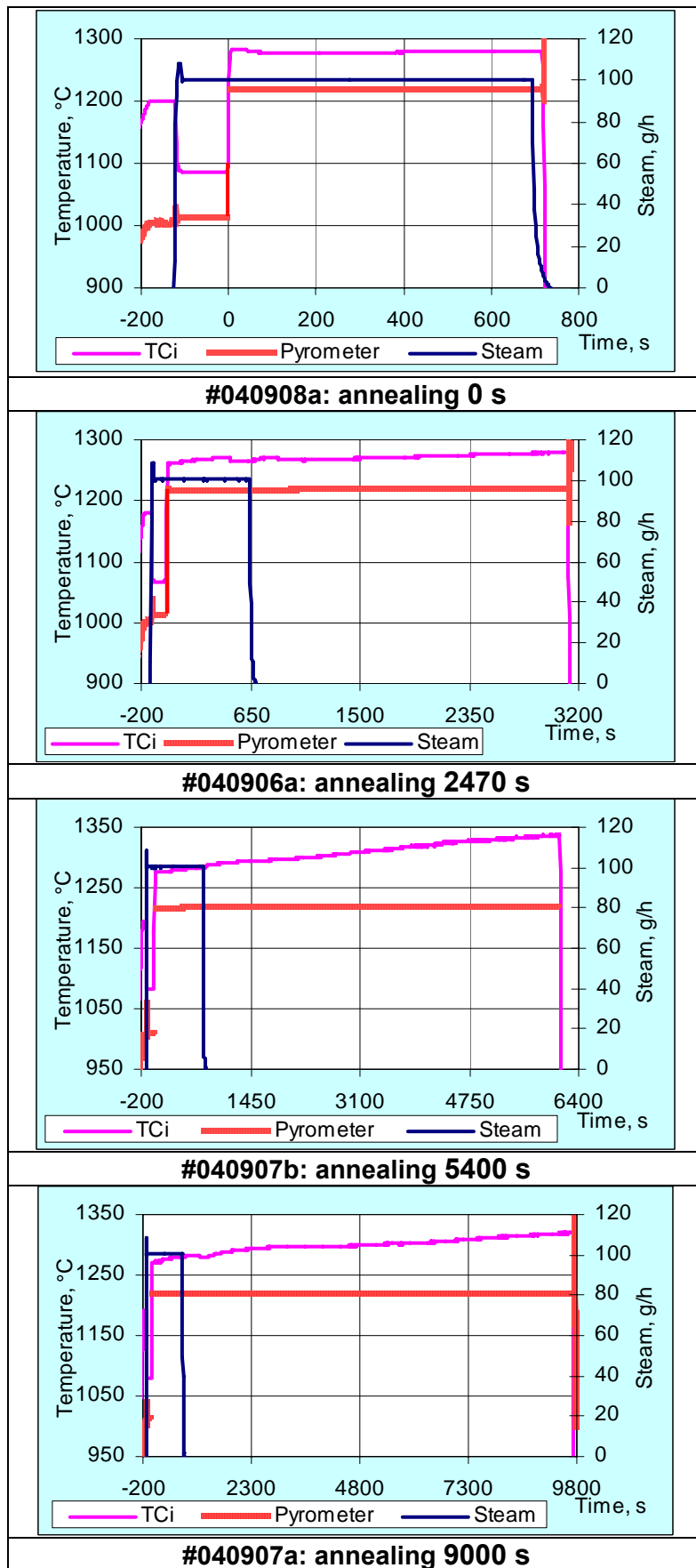


Fig. 19. 2004 experiments in the Quench test rig with a pre-oxidation duration of 720 s and different annealing durations: pyrometer ( $\epsilon=0.7$ ), middle thermocouples (inside of sample), and steam supply diagrams.

pre-oxidation duration: ~ 720 s (initial ZrO<sub>2</sub> ~180 μm)

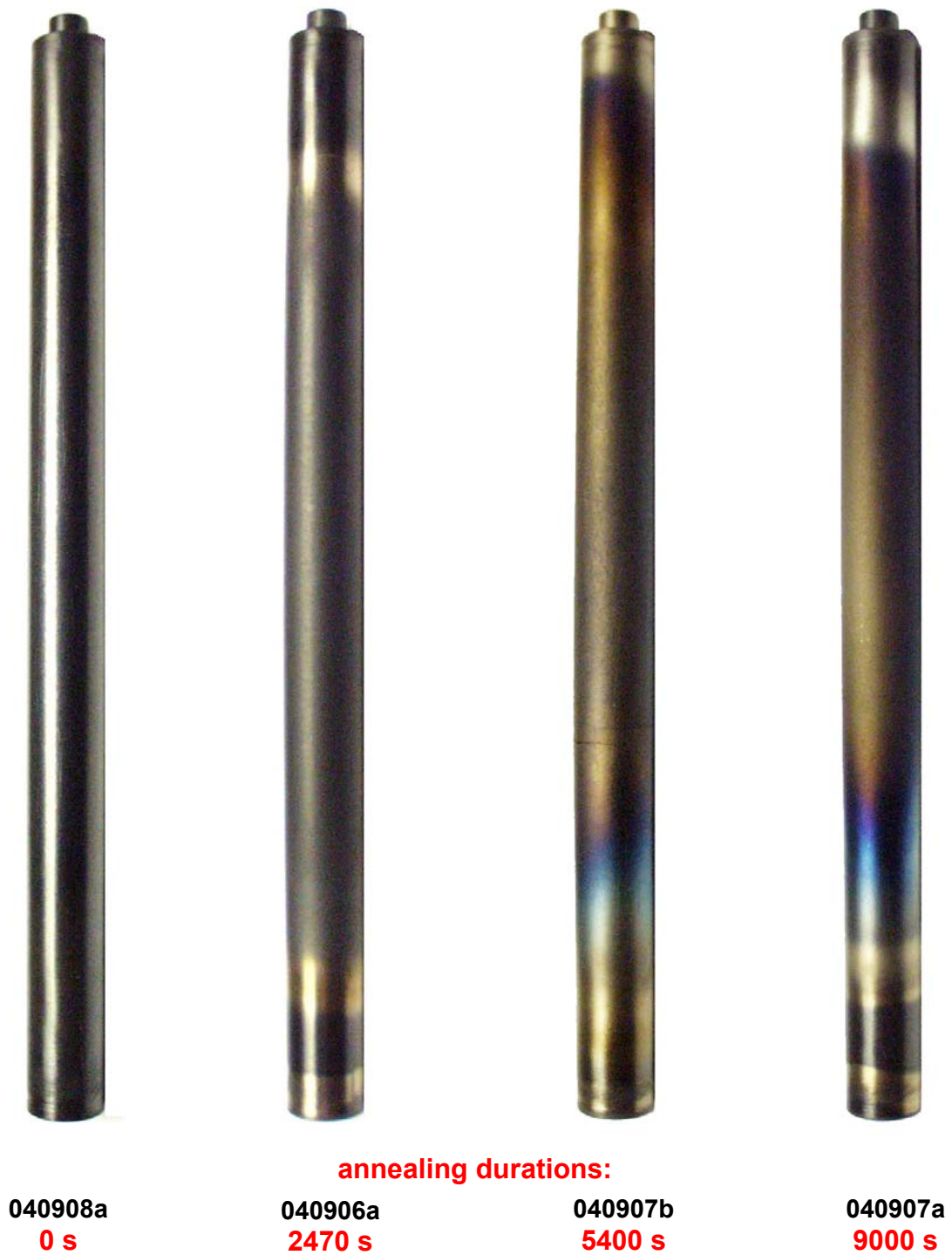


Fig. 20. 2004 experiments in the Quench test rig with a pre-oxidation of ~12 min. and different annealing durations: outer view of the Zry-4 claddings pre-oxidised in steam and then annealed in argon at a temperature of ~1300 °C measured with the internal centre TC located inside the specimen at the middle elevation.

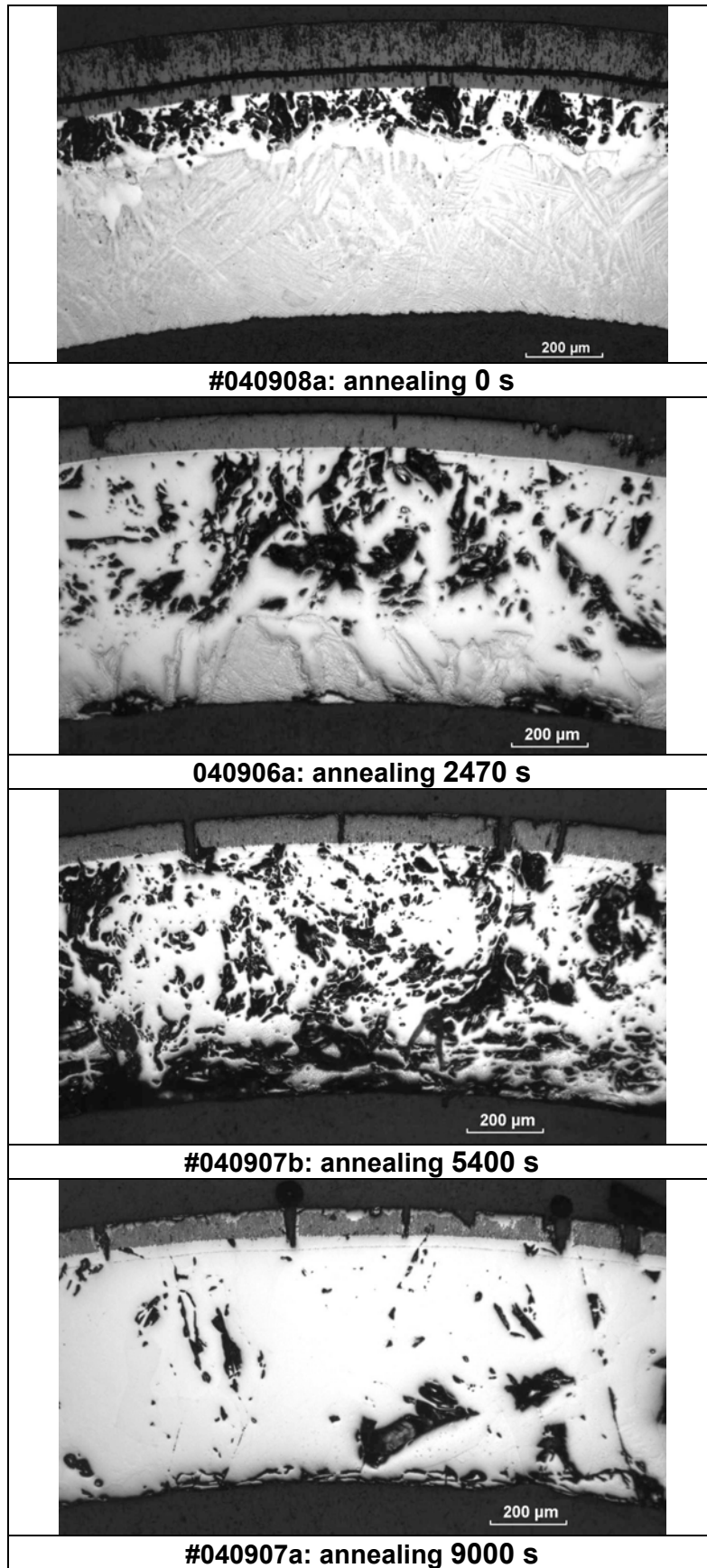


Fig. 21. 2004 experiments in the Quench test rig with a pre-oxidation of ~12 min. and different annealing durations at ~1300 °C: cladding cross-section.

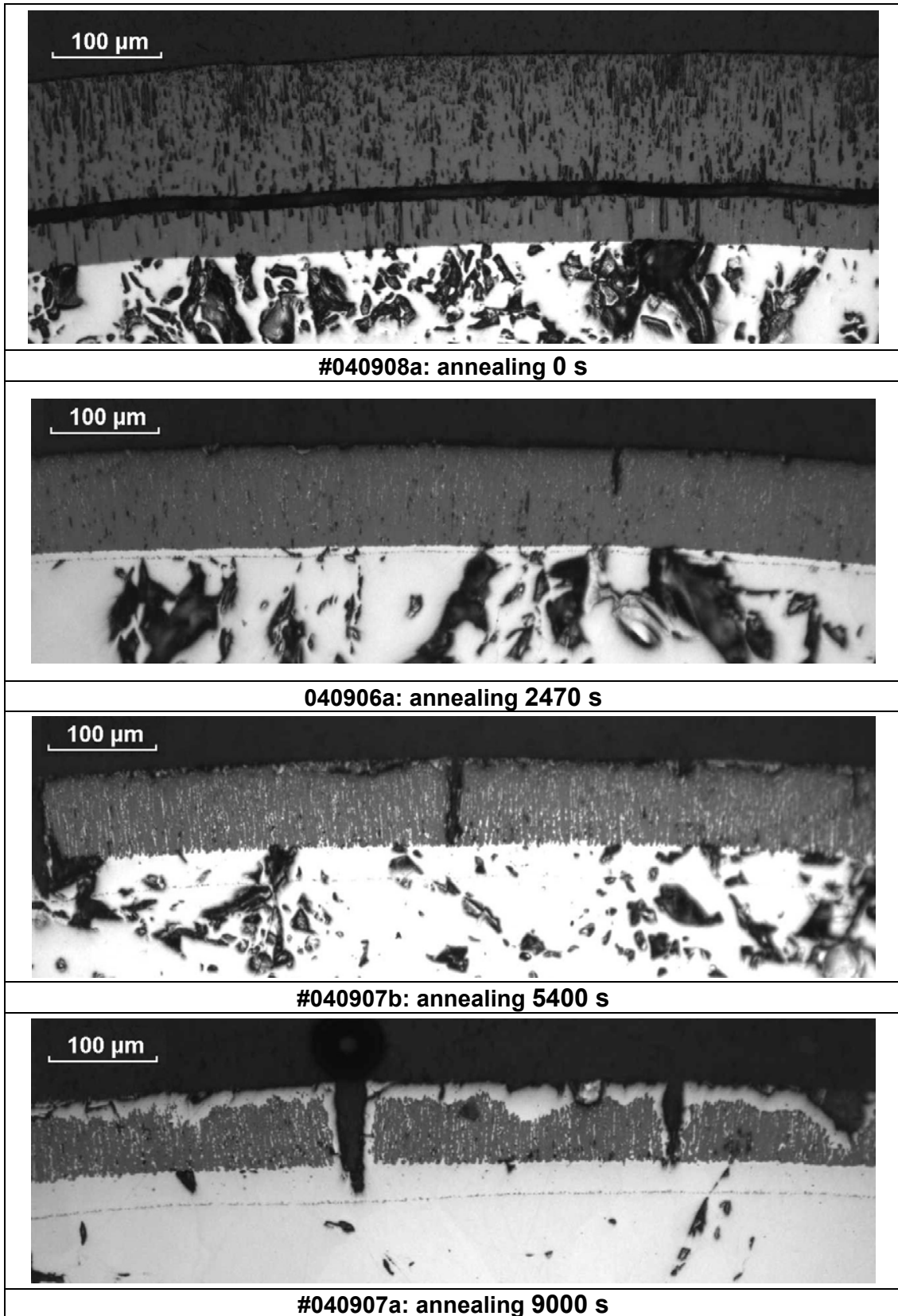


Fig. 22. 2004 experiments in the Quench test rig with a pre-oxidation of ~12 min. and different annealing durations at ~1300 °C: oxide layer structure. Development of  $\alpha$ -Zr(O) precipitates and formation of the outer  $\alpha$ -Zr(O) surface layer.

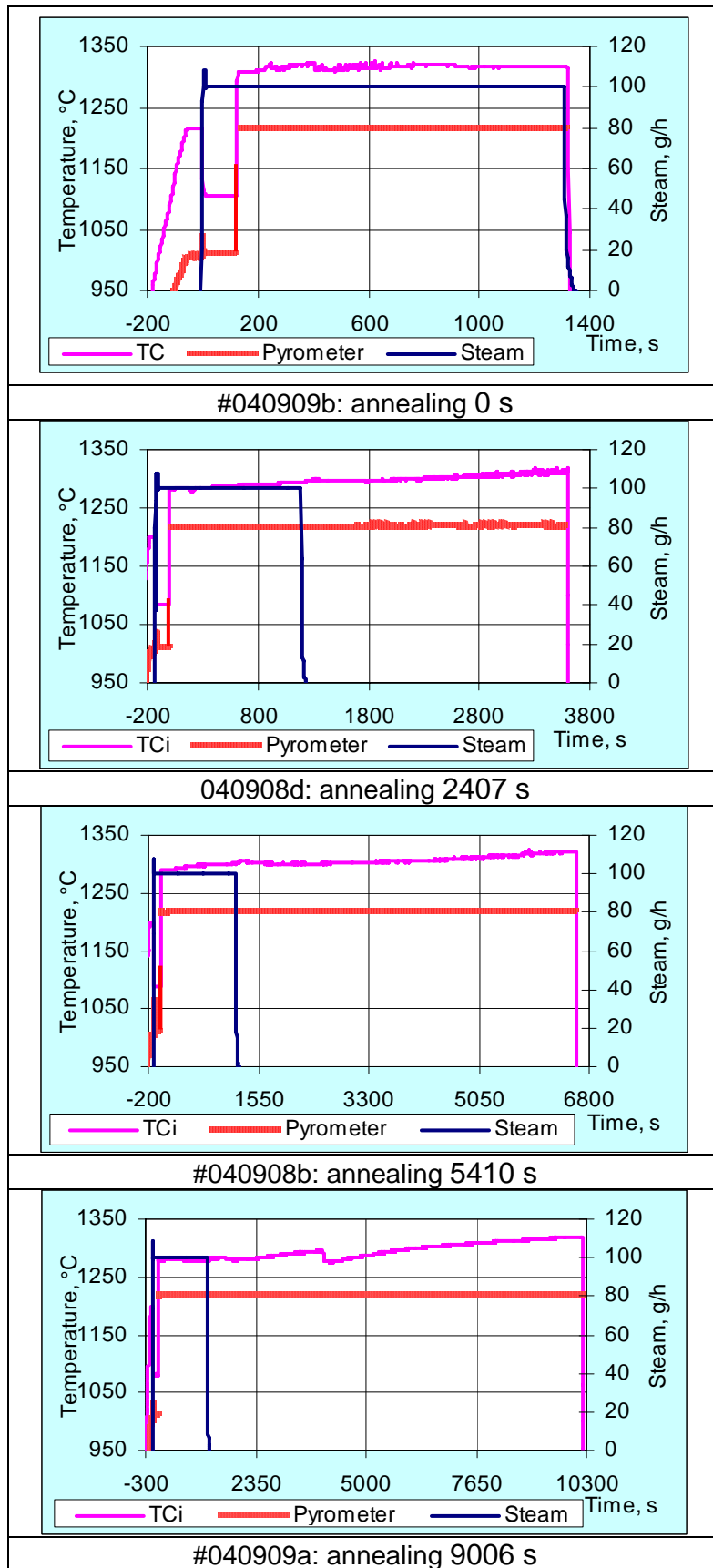


Fig. 23. 2004 experiments in the Quench test rig with a pre-oxidation duration of 20 min. and different annealing durations: pyrometer ( $\epsilon=0.7$ ), middle thermocouples (inside of sample), and steam supply diagrams.

pre-oxidation duration: ~ 1180 s (initial ZrO<sub>2</sub> ~240 μm)

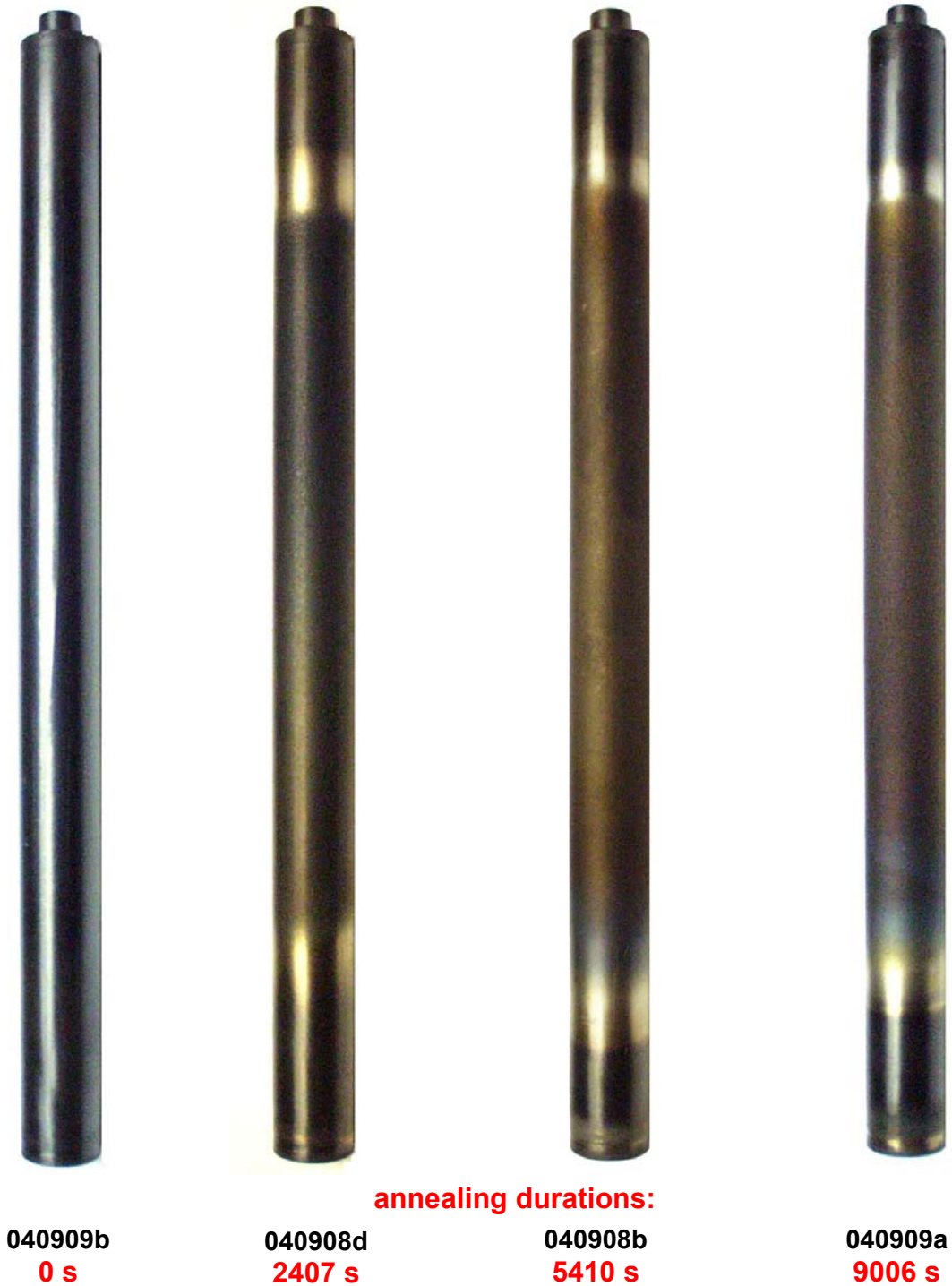


Fig. 24. 2004 experiments in the Quench test rig with a pre-oxidation of ~20 min. and different annealing durations: outer view of the Zry-4 claddings pre-oxidised in steam and then annealed in argon at a temperature of ~1300 °C measured with the internal centre TC located in the specimen at the middle elevation.

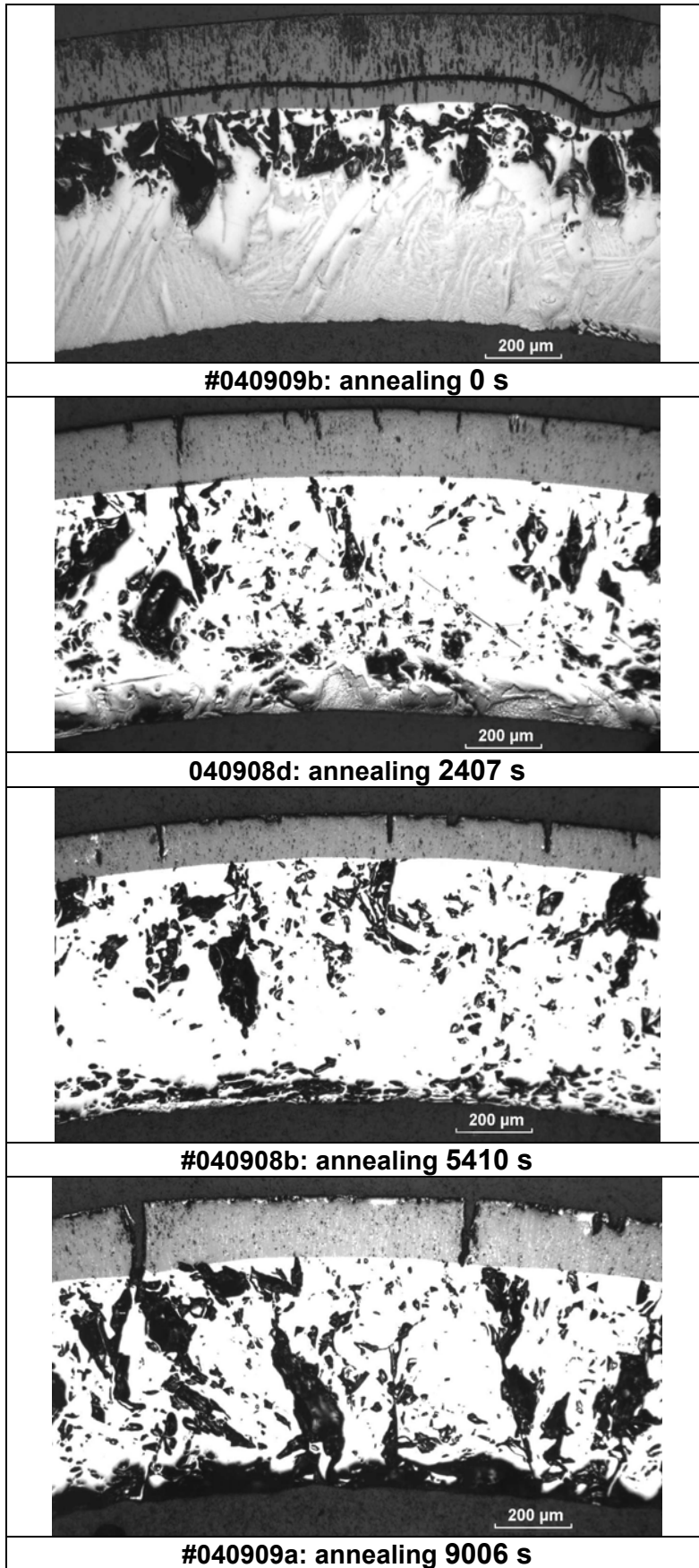


Fig. 25. 2004 experiments in the Quench test rig with a pre-oxidation of ~20 min. and different annealing durations at ~1300 °C: cladding cross-section.

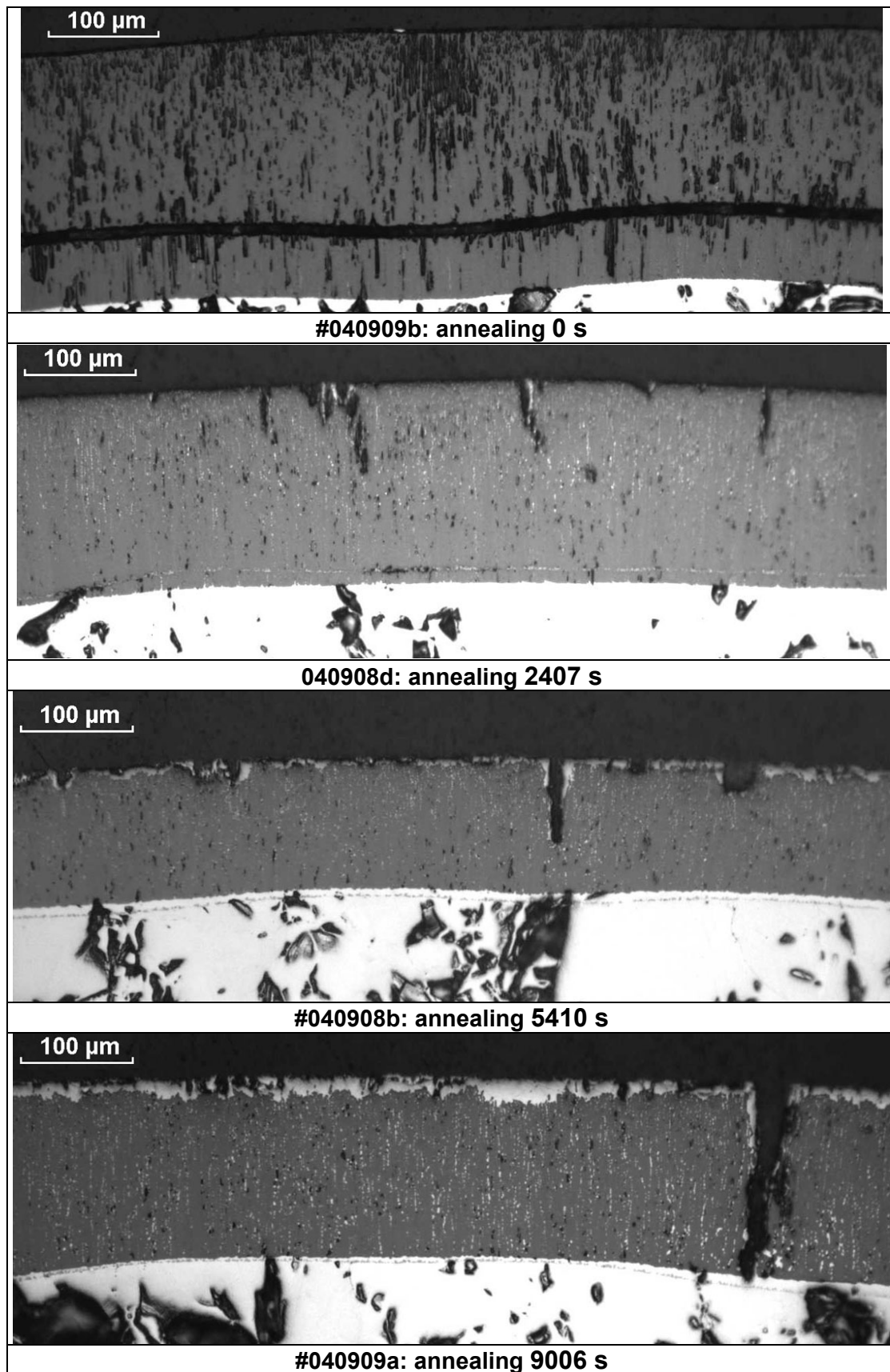


Fig. 26. 2004 experiments in the Quench test rig with a pre-oxidation of ~20 min. and different annealing durations at ~1300 °C: oxide layer structure. Development of  $\alpha$ -Zr(O) precipitates and formation of the outer  $\alpha$ -Zr(O) surface layer.

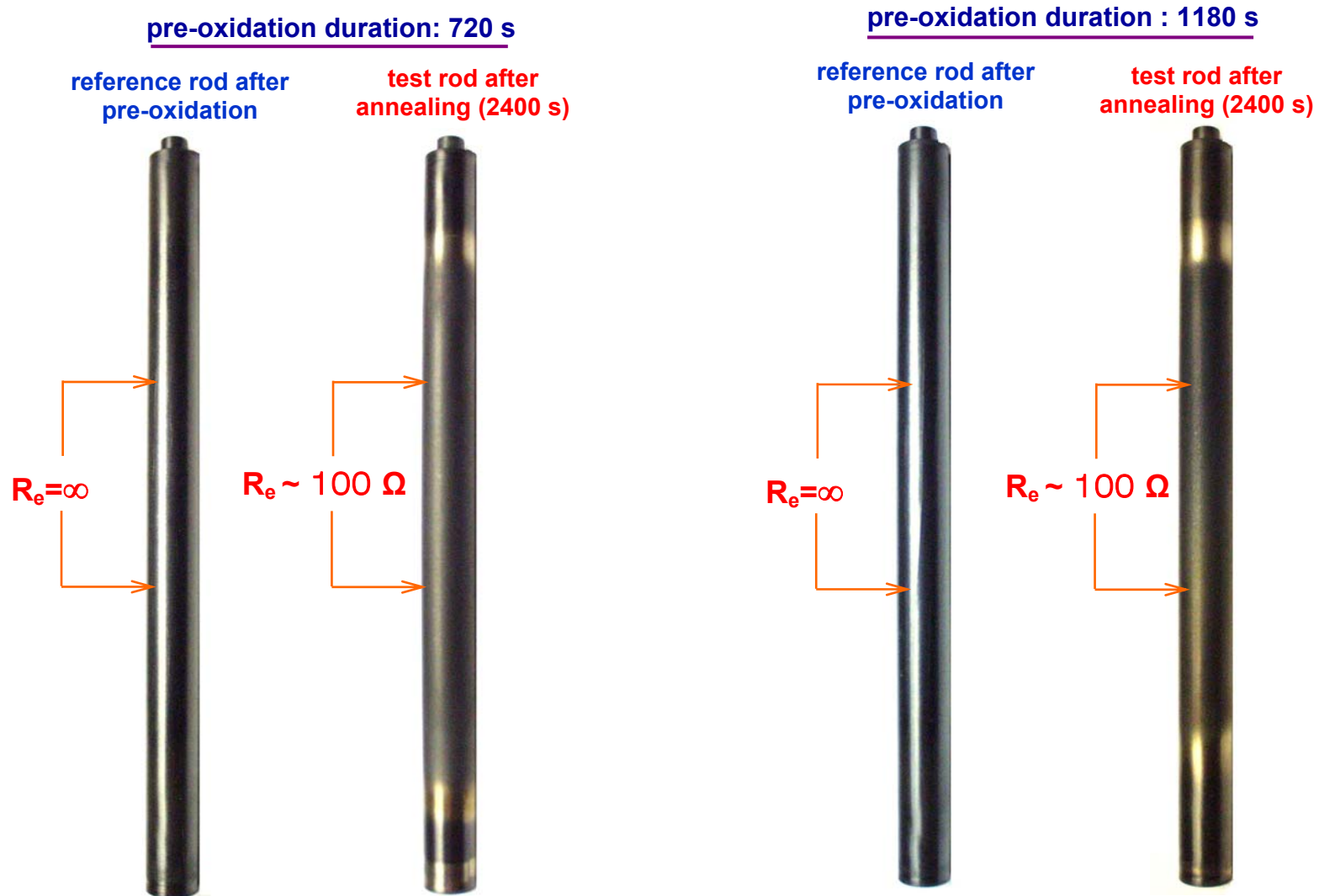


Fig. 27. Measurement of the surface's electrical resistance demonstrates the presence of a metallic surface layer after a relatively short duration of annealing.

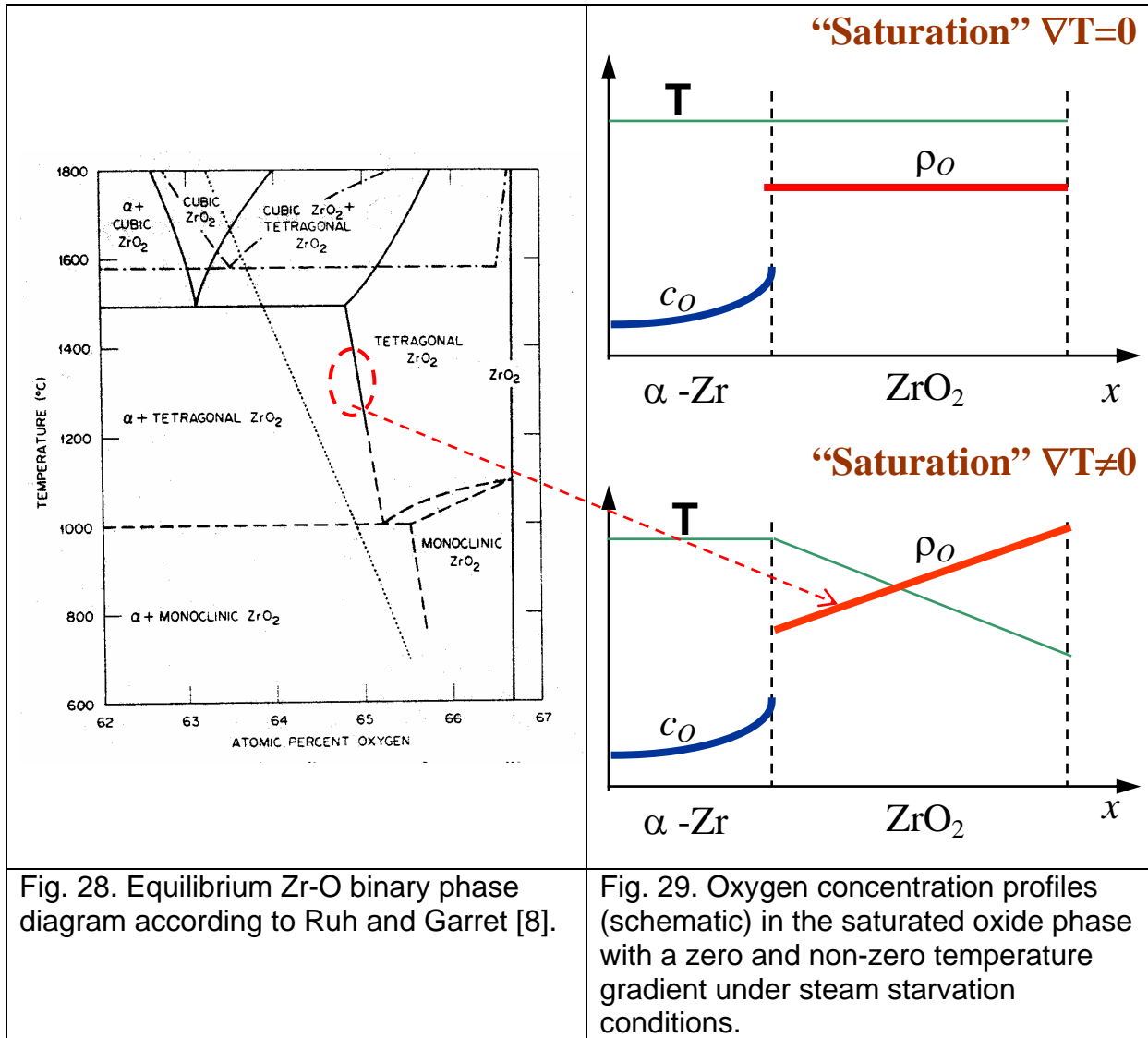


Fig. 28. Equilibrium Zr-O binary phase diagram according to Ruh and Garret [8].

Fig. 29. Oxygen concentration profiles (schematic) in the saturated oxide phase with a zero and non-zero temperature gradient under steam starvation conditions.

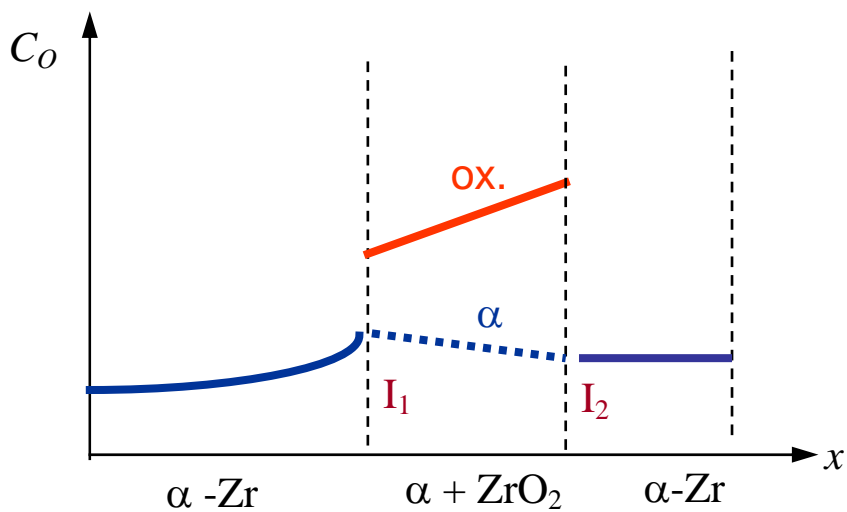


Fig. 30. Oxygen concentration profiles (schematic) in different layers of the oxidised Zry cladding after saturation (equilibration) of the oxide phase under steam starvation conditions.

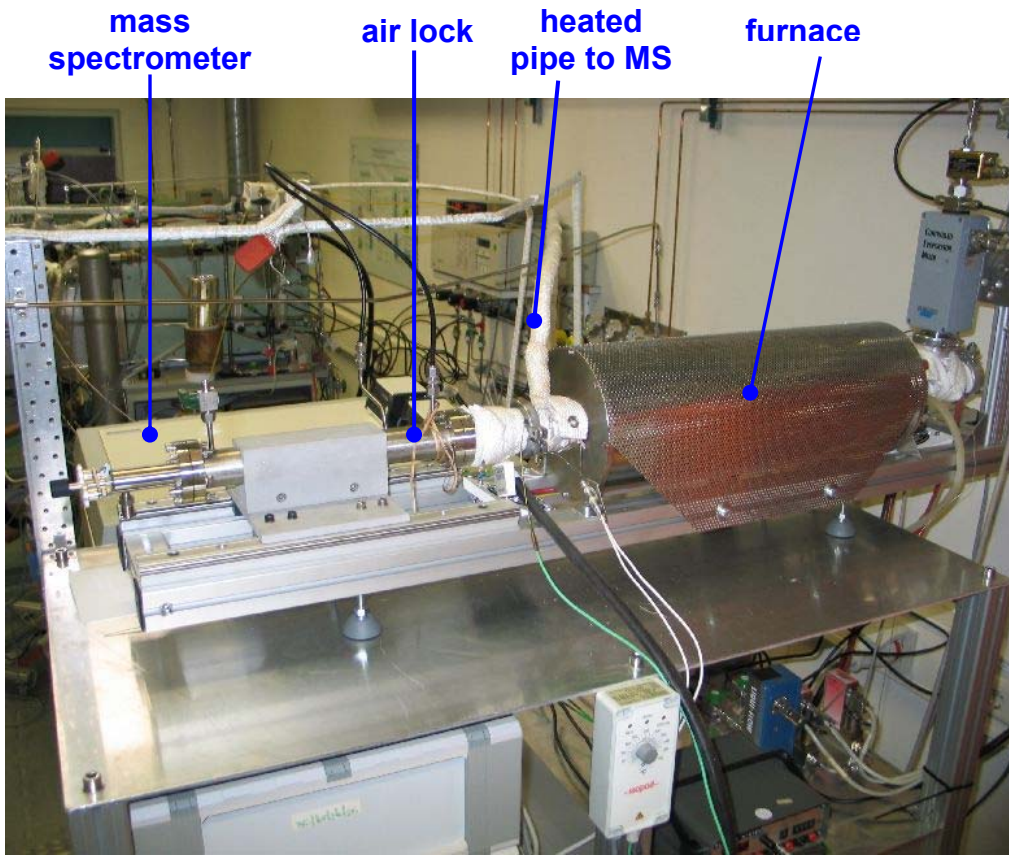


Fig. 31. BOX rig for oxidation experiments under quasi-isothermal conditions.

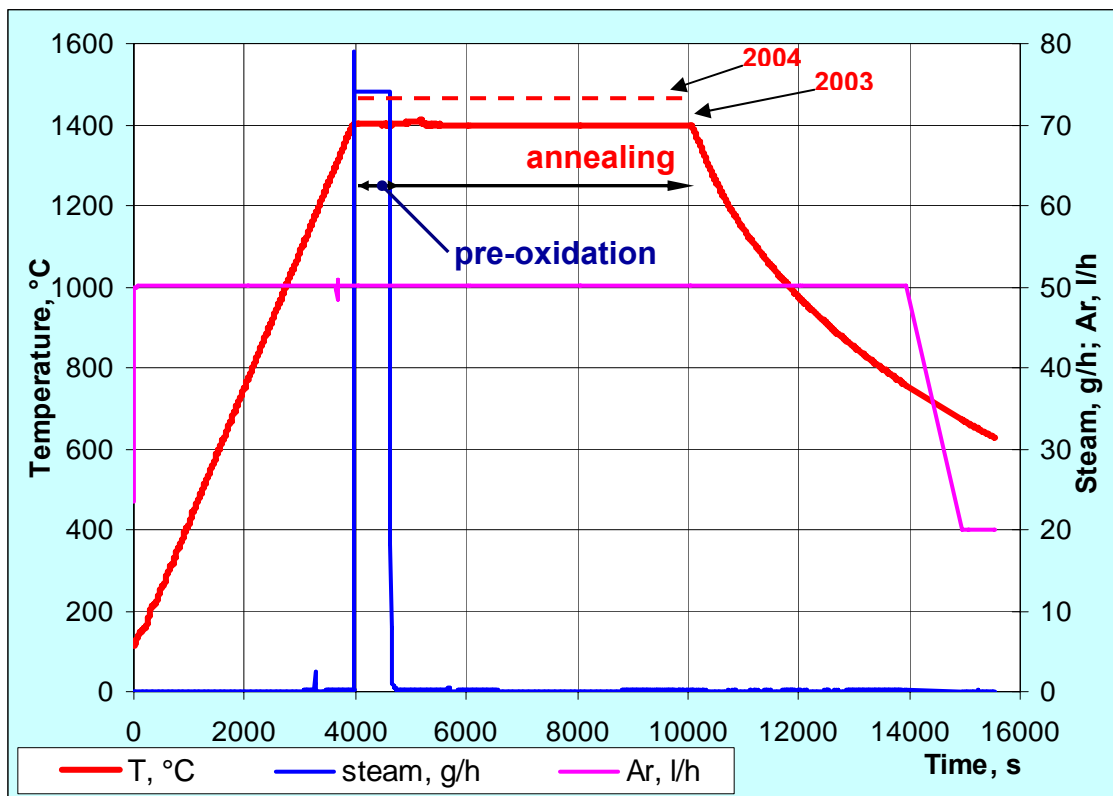


Fig. 32. Time schedule of the BOX tests in 2003..2004 with rods and sealed tubes.

|  |   |
|--|---|
|       |                     |
| <p>#030912r: massive <b>rod</b>; T=1400 °C; pre-oxidation 660 s; annealing 5400 s</p>  | <p>#030912t: <b>sealed tube</b> filled with air; T=1400 °C; pre-oxidation 660 s; annealing 5400 s</p> |
|      |                    |
| <p>#040513r: T=1450 °C; massive <b>rod</b>; pre-oxidation 1080 s; annealing 5400 s</p> | <p>#040513t: <b>sealed tube</b> filled with Ar; T=1450 °C; pre-oxidation 1080 s; annealing 5400 s</p> |
|     |                   |
| <p>#040517r: massive <b>rod</b>; T=1450 °C; pre-oxidation 1080 s; annealing 1200 s</p> | <p>#040517t: <b>sealed tube</b> filled with Ar; T=1450 °C; pre-oxidation 1080 s; annealing 1200 s</p> |

Fig. 33. Overview of samples after the BOX tests with Zry-4 rods and Zry-4 sealed tubes filled with air (1st tube) or argon (2nd and 3rd tubes).

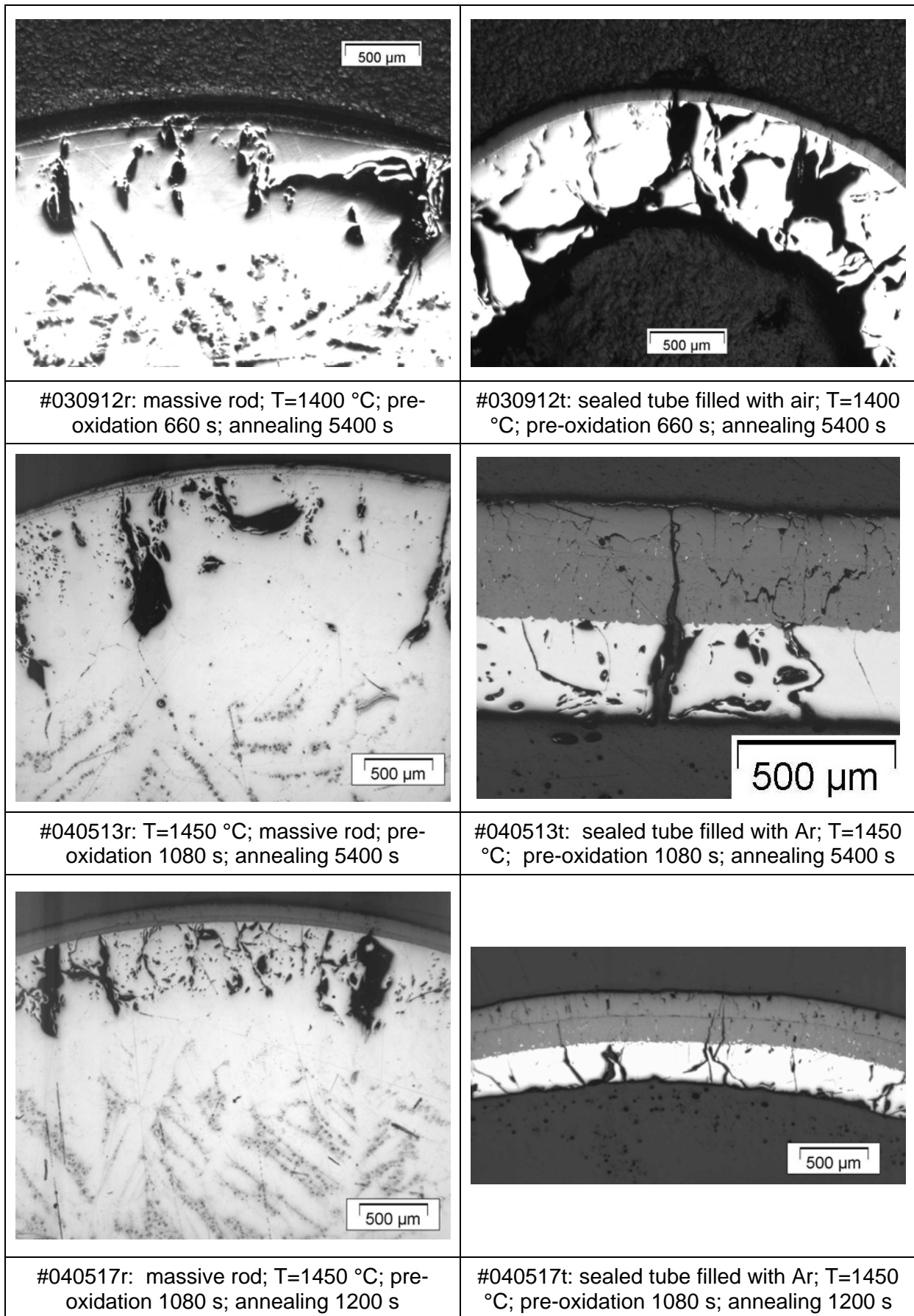


Fig. 34. BOX tests in 2003..2004: layer structure.

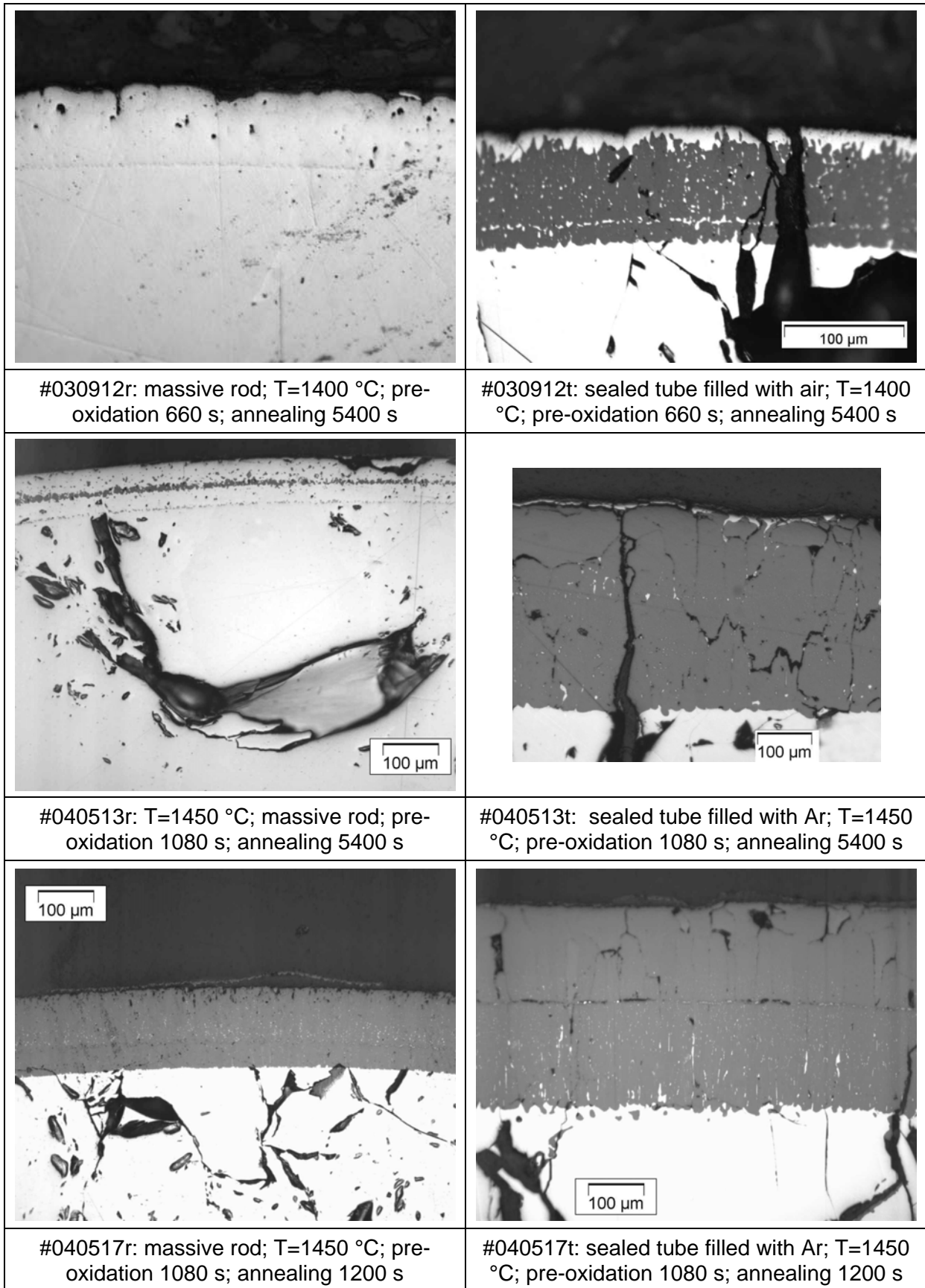


Fig. 35. BOX tests in 2003..2004: structure of outer oxide layer

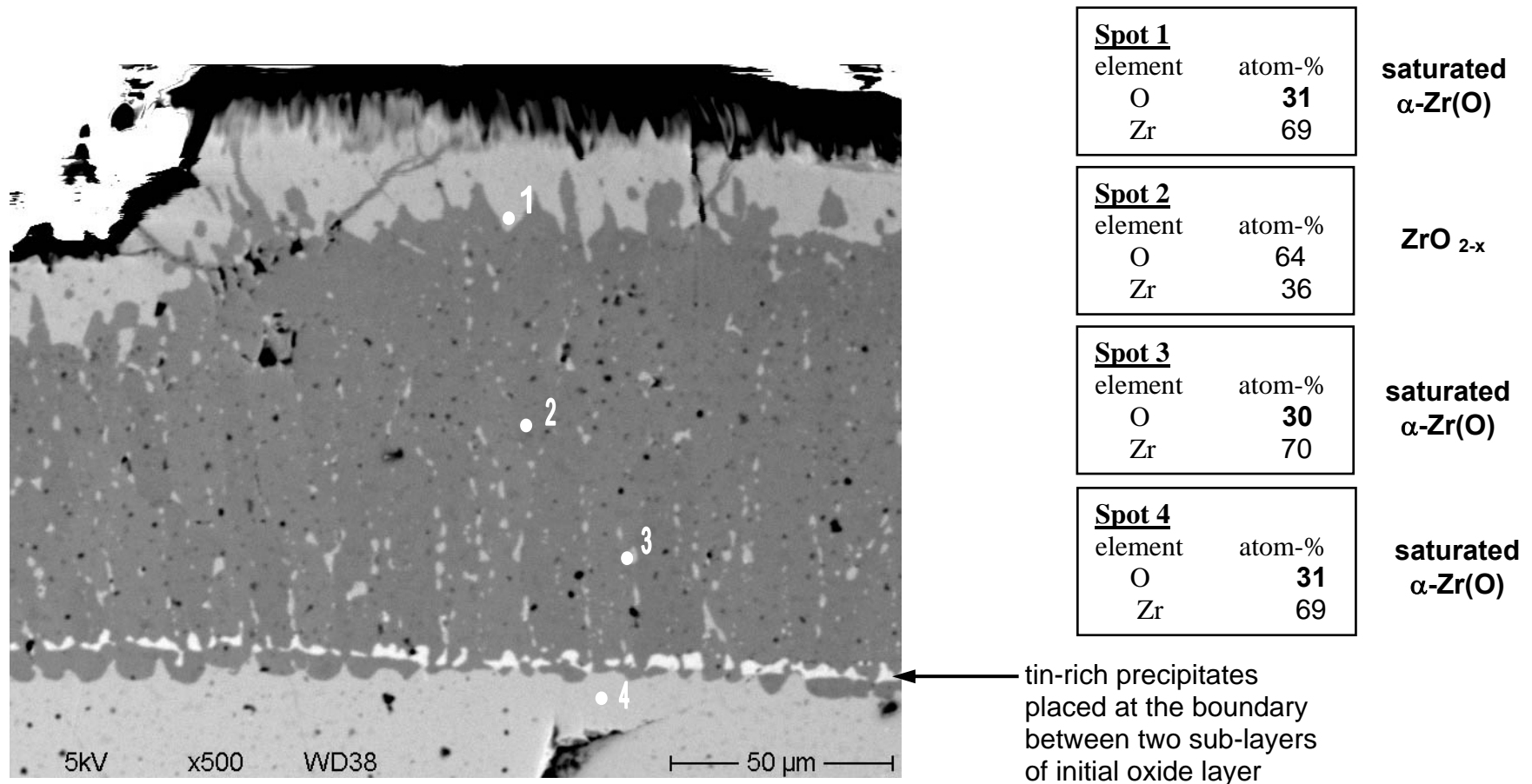


Fig. 36. Isothermal BOX test: EDX analysis of the outer layers on the surface of a sample pre-oxidised at 1400°C for 660 s and annealed for 5400 s.

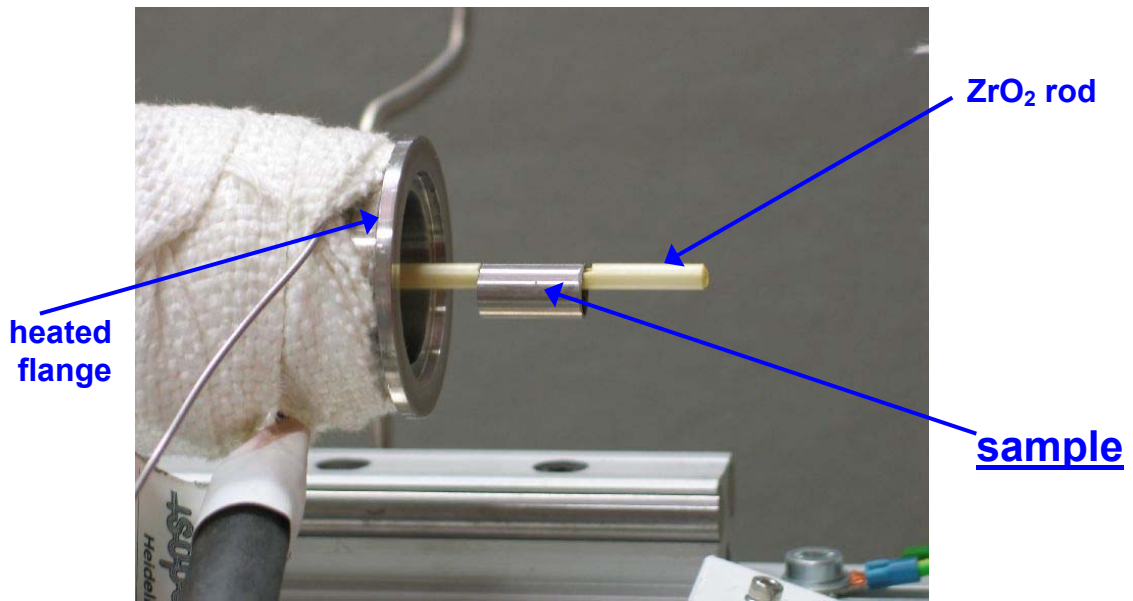


Fig. 37. BOX rig: movable sample holder allows for the fast sample positioning in the furnace and the fast sample removal from the furnace.

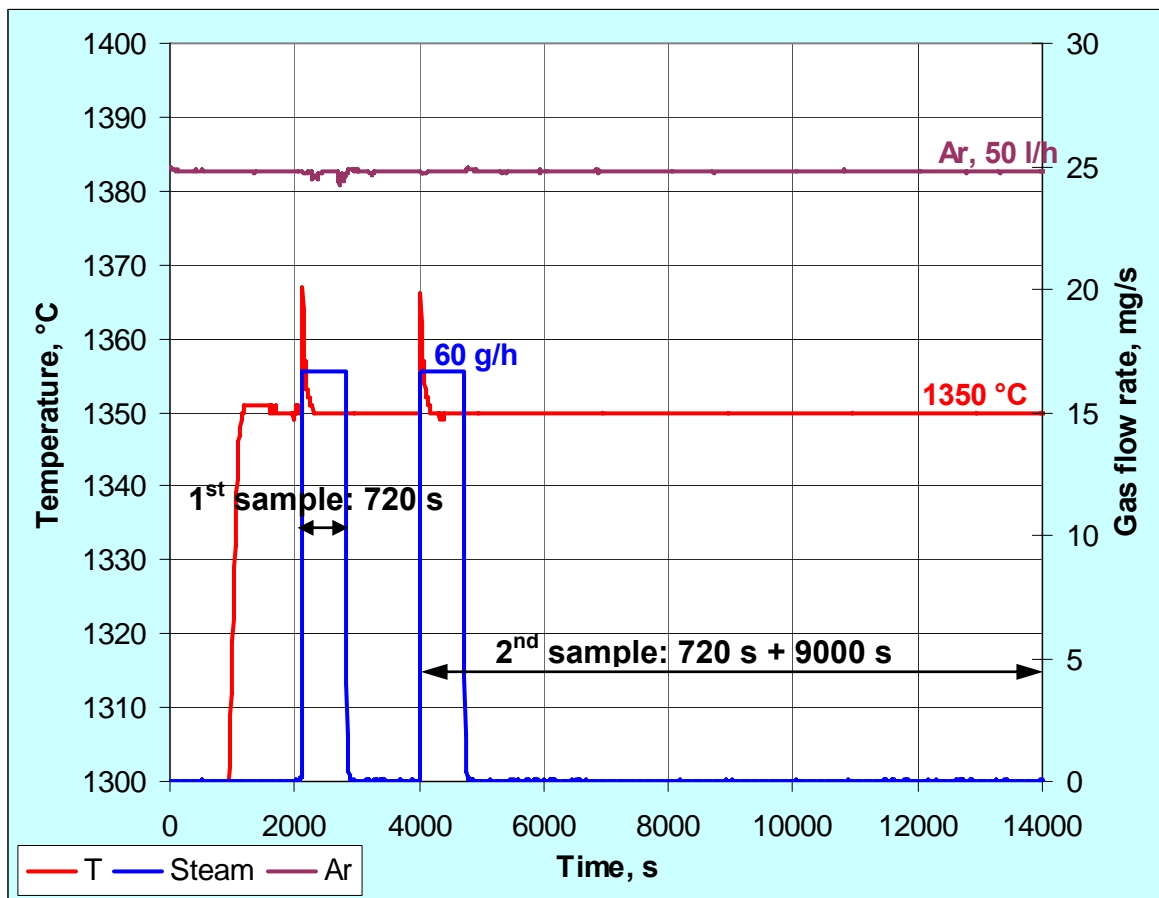


Fig. 38. Time schedule of the 2006 isothermal BOX tests with open tubes inserted into the furnace and withdrawn from the furnace at work temperature

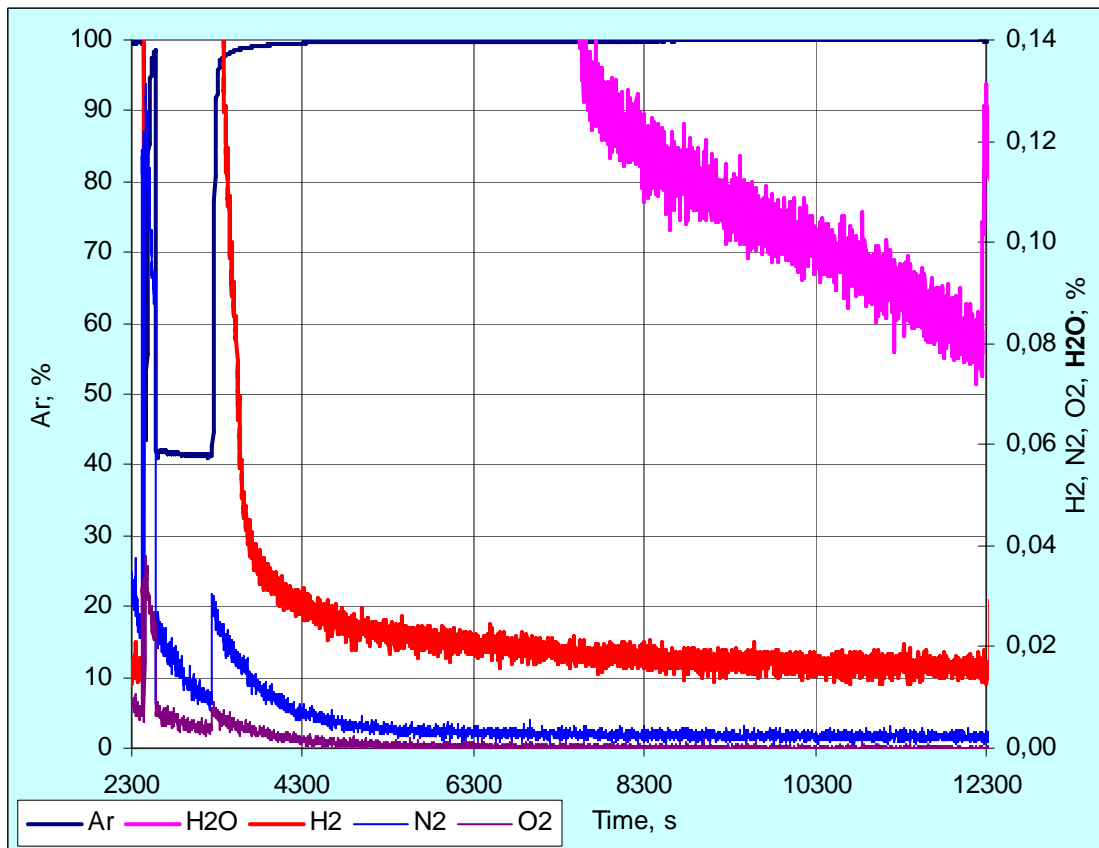
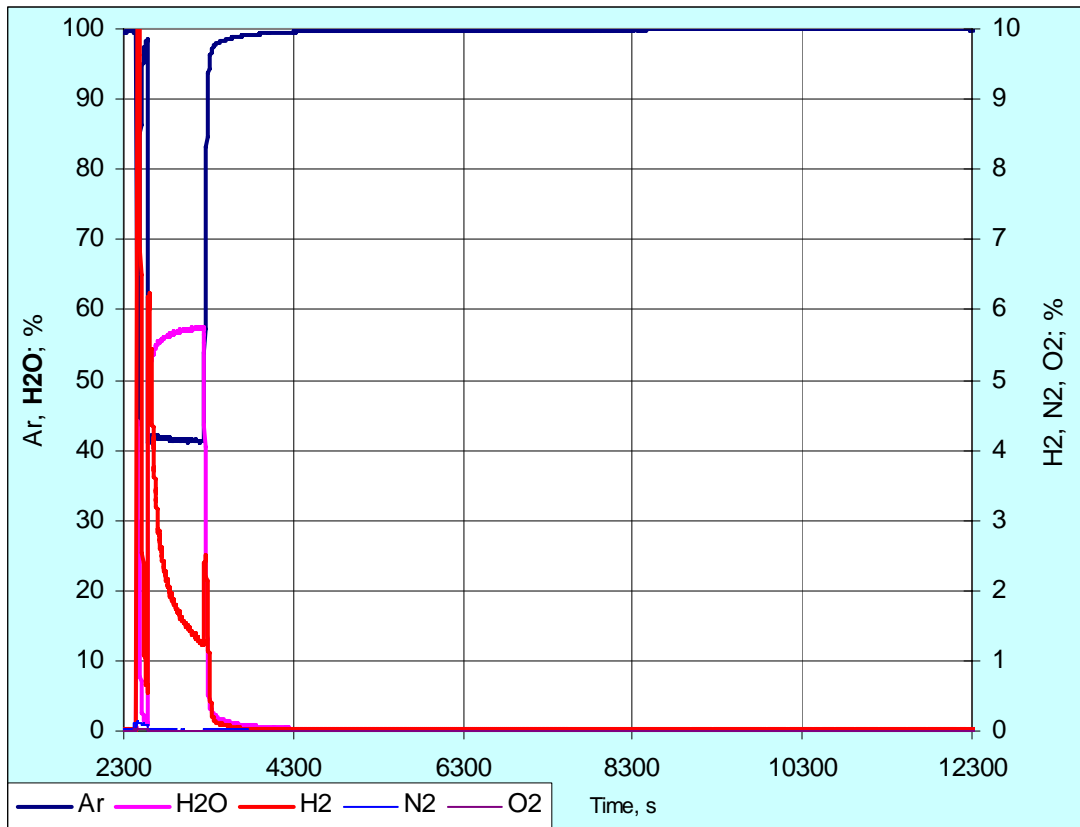


Fig. 39. Annealing series 2006; mass-spectrometer measurements of gas concentrations during annealing of the Zry-4 sample.

|   |  |
|---|--|
|    |    |
| <p>#060125b1: oxidised Zry-4 sample</p>   | <p>#060125b2: oxidised &amp; annealed Zry-4 sample</p>                               |
|   |   |
| <p>#060124c1: oxidised Duplex sample</p>  | <p>#060124c2: oxidised and annealed Duplex sample</p>                                |
|  |  |
| <p>#060125a1: oxidised E110 sample</p>  | <p>#060125a2: oxidised and annealed E110 sample</p>                                  |

Fig. 40. Isothermal BOX tests in 2006 with different cladding materials: overview of samples oxidised in steam for 720 s without annealing (left column) and with annealing for 9000 s in argon at 1350 °C (right column).

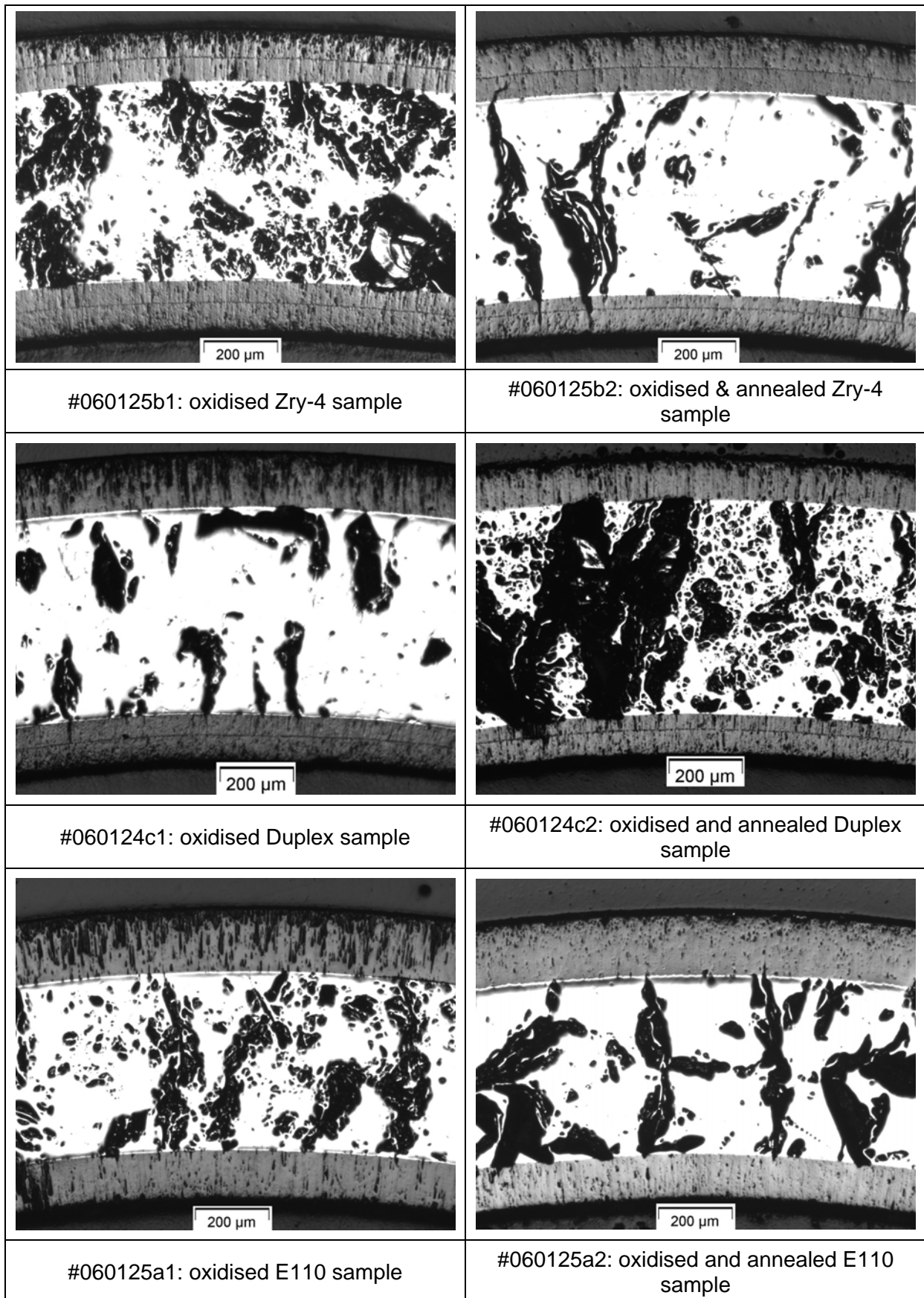


Fig. 41. Isothermal BOX tests in 2006 (1350 °C) with different cladding materials: cladding cross-sections.

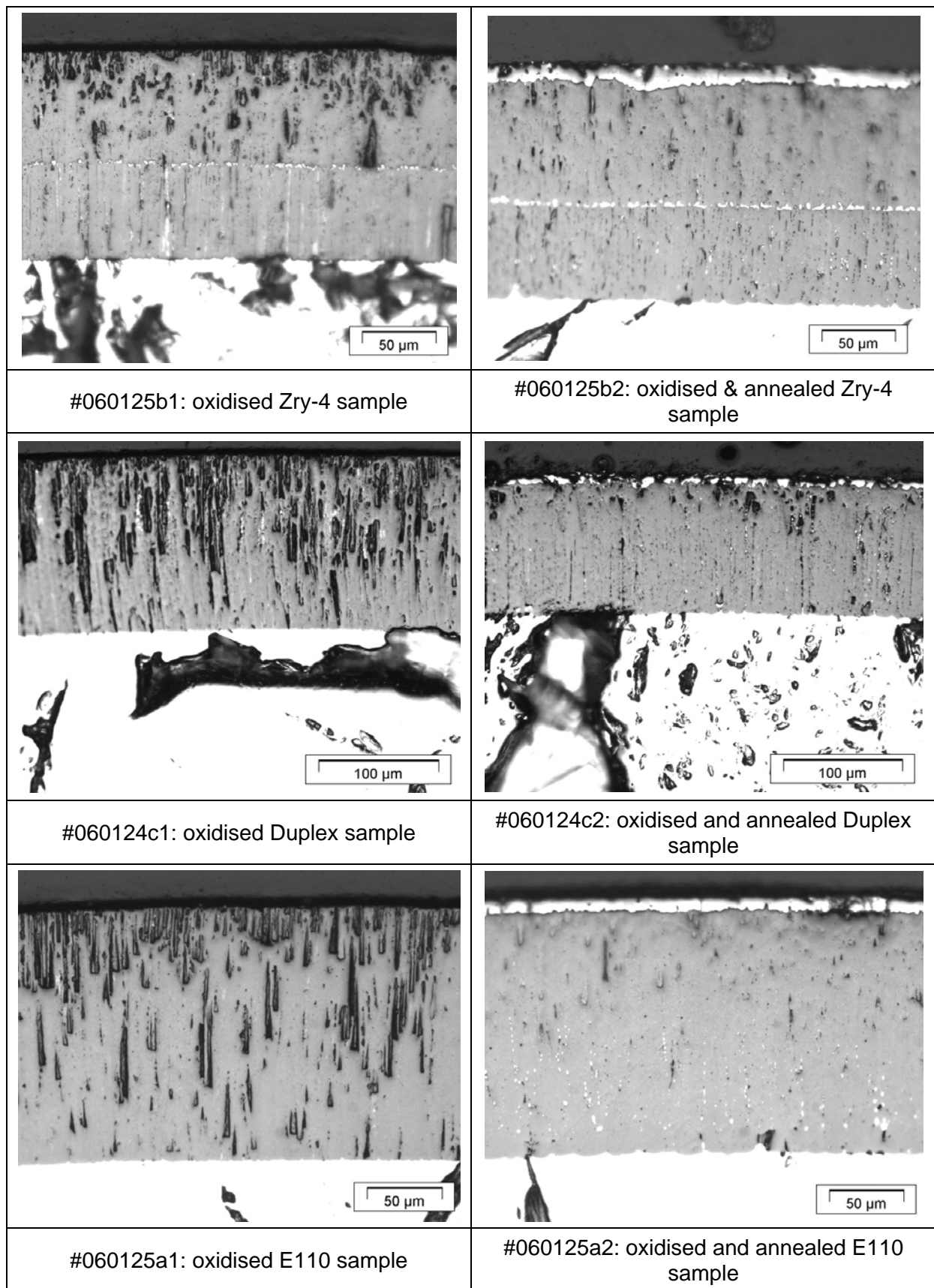


Fig. 42. Isothermal BOX tests in 2006 (1350 °C): cracked structure of oxide layer without annealing (left column) and development of outer metallic scale on surface of annealed samples (right column)

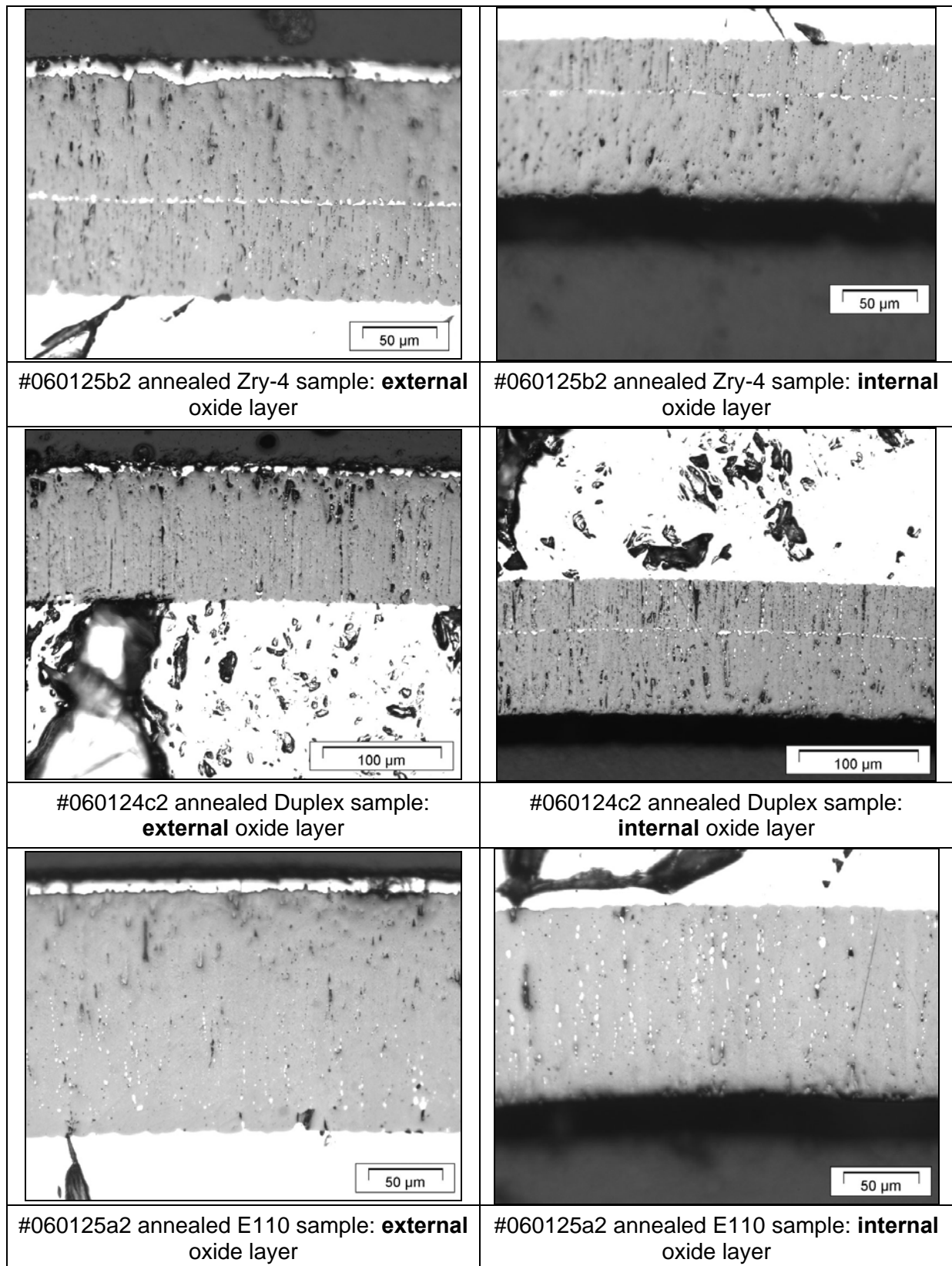


Fig. 43. Isothermal BOX tests 2006 (1350 °C): development of  $\alpha$ -Zr(O) film at surface of external oxide layer (left column) and absence of  $\alpha$ -Zr(O) film at surface of internal oxide layer (right column)

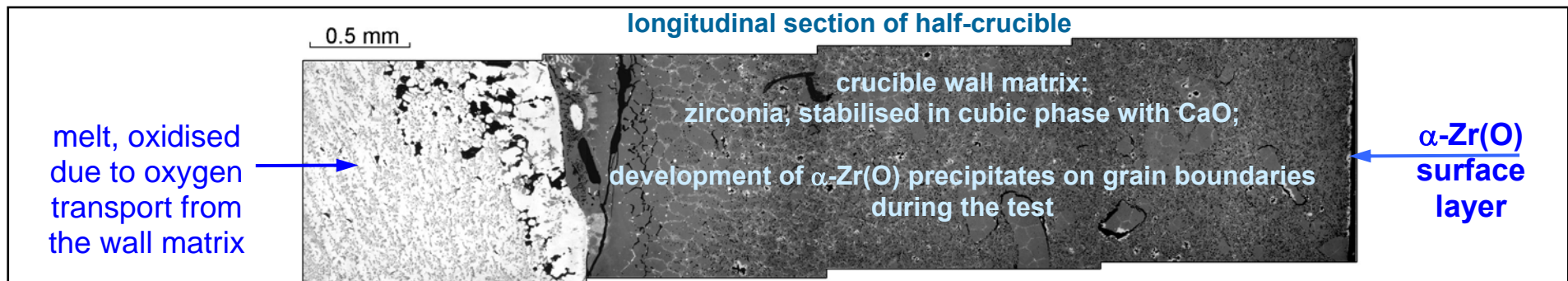
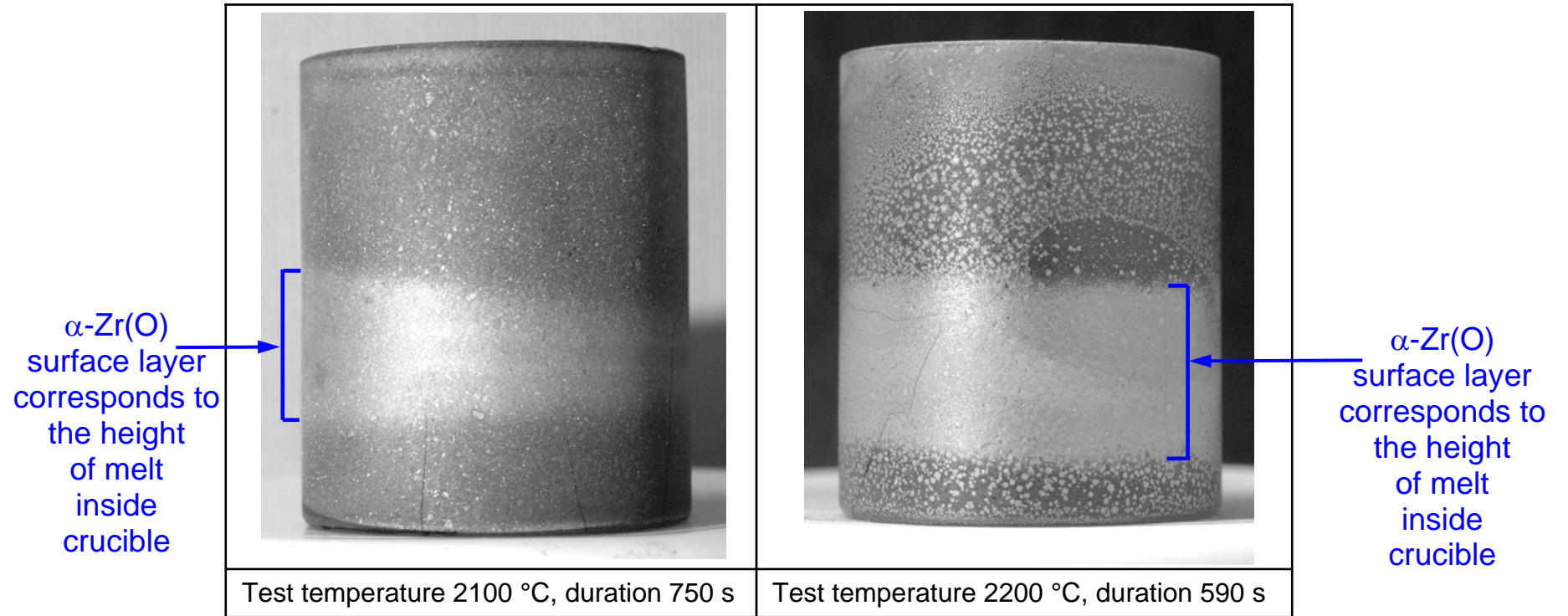


Fig. 44. Outer view of ZrO<sub>2</sub> crucibles used for the tests relating to the dissolution of ZrO<sub>2</sub> with molten Zircaloy under Ar: formation of an  $\alpha$ -Zr(O) metallic strip with the height corresponding to the melt height inside the crucible.